Abstract

Title of Dissertation: Investigation into the Driving Force Dependence of Excess Electron Transport in DNA

Neil Peter Campbell

Doctor of Philosophy, 2009

Dissertation Directed by: Professor Steven E. Rokita

Department of Chemistry and Biochemistry

The purpose of this dissertation is to investigate the driving force dependence of excess electron transport in deoxyribonucleic acid (DNA) using napthyl amines as electron donors.

The ability of DNA to act as a pathway for the migration of charge was first proposed in 1963 by Elgy and Spivey. Since then, investigation of two complementary processes, hole transport and excess electron transport, have been studied. Of these processes research has focused mostly on hole transport.

Hole transport has been studied for several decades. As such, the four fundamental parameters affecting the processes have been elucidated: the distance dependence has been found to be weak, G/C sequences have been found to allow for

more efficient hole transport, migration from the 3' to 5' direction is more efficient, and a driving force dependence on the efficiency of hole transport has been found.

Only recently has attention turned to the determination of the fundamental parameters affecting excess electron transport. Investigations to date have determined that there is a weak distance dependence on excess electron transport, A/T sequences allow more efficient transport, and excess electron transport is more efficient when migrating from the 5' to 3' end of DNA. The one parameter affecting excess electron transport that has not been investigated is the driving force dependence.

To test for driving force dependence, napthyl amines were screened for their ability to initiate charge transfer by reductive electron donation using an assay based on the photoinduced reduction and subsequent scission of duplex DNA containing a 5-bromo-2'-deoxyuridine (^{Br}U) residue and an abasic site. Each compound had varying reducing potentials (driving forces), which allowed investigation into the driving force dependence of excess electron transport. Six compounds (1,5-diaminonapthalene, N1-methyl-1,5-diaminonathalene, N1,N5-dimethyl-1,5-diaminonapthalene, N1,N1-dimethyl-1,5-diaminonapthalene, N1,N1,N5-trimethyl-1,5-diaminonapthalene, N1,N1,N5,N5-tetramethyl-1,5-daiminonapthalene) were screened under both aerobic and anaerobic conditions, and found to initiate charge transfer. No correlation between the reduction potential of the compounds (driving force) and the rate of strand scission was seen.

Subsequently, the oligonucleotide conjugates of two of the compounds, 1,5-diaminonapthalene and N1,N1,N5,N5-tetramethyl-1,5-diaminonapthalene, were prepared and studied to determine if a driving force dependence on excess electron transport exists when the compounds are covalently attached to the DNA. 1,5-diaminonapthalene and

N1,N1,N5,N5-tetramethyl-1,5-diaminonapthalene were chosen as they showed the greatest difference in their reducing potentials. The conjugates showed no difference in the rate of excess electron transport, thus indicating there is not a driving force dependence on excess electron transport in DNA, at least using these compounds and in this system.

Investigation into the Driving Force Dependence of Excess Electron Transport in Duplex DNA

By

Neil Peter Campbell

Dissertation submitted to the Faculty of the Graduate School of the

University of Maryland, College Park, in partial fulfillment

of the requirements for the degree of

Doctor of Philosophy

2009

Advisory Committee:

Professor Steven E. Rokita, Chair
Professor Philip DeShong
Professor Daniel E. Falvey
Assistant Professor T. Ashton Cropp
Professor Peter Kofinas

Lay Abstract

Most of us have seen the double helix – the twisted column of genetic code – that comprises DNA. While it is often depicted as hollow, DNA actually has a core running through the center of it. This core is thought to be able to conduct electricity based on how the DNA is stacked and what it is made of. It is hypothesized that harmful UV rays from the sun hit the cell, which contains DNA, sending a charge through the DNA that causes damage that potentially leads to cell mutations and skin cancer. Since DNA is hypothesized to be able to send a harmful charge, it is conversely thought to be able to send a controlled charge. This would mean that DNA could potentially act as a "wire," sending and receiving electronic pulses similar to those in current electronic devices that indicate time, send messages, receive Internet signals, turn on lights, etc. – only on a much smaller scale.

The study of what is known as excess electron transport in DNA could enable us to better understand – and therefore combat – skin cancer. It also could enable us to further shrink the size of electronics. When the first computer was introduced, it was the size of an entire floor in an office building. Today, we have personal computers that are the size of brief cases. In the future, we could have a personal computer that fits on our wrist and does 10 times what our current computers do.

There are two main ways that DNA can act as a carrier of an electrical charge. These are known as hole transport and excess electron transport. In hole transport, an electronic hole is created at a specific site in the DNA. Like dominos falling one into another, this hole is then filled by the neighboring site in the DNA, which creates another

hole which is then filled by a neighbor. This process continues until the hole can no longer move down the DNA strand.

In excess electron transport, the domino effect is somewhat similar. Here, however, an excited electron is injected into the DNA, which is then passed down the DNA until it can no longer move further down the strand.

There are four main factors that affect the efficiency of both hole transport and excess electron transport. They are (1) the distance between the starting and end points of the transfers, (2) what stands between the starting and the end point, (3) the direction in which the charge travels along the DNA, and (4) how strong the charge was to begin with.

Regarding the distance between the starting and end points of the transfer, there is weak distance dependence in both hole transport and excess electron transport. This means that the distance along which the charge has to travel doesn't significantly affect the efficiency of either process.

What stands between the starting and the end point, known as sequence dependence, also is important. DNA is made up of four bases: adenosine, guanine, cytosine and thymine. For hole transport, guanine and cytosine allow for efficient transport. For excess electron transport, adenosine and thymine allow for a more efficient passing of the charge.

The direction in which the charge travels along the DNA has been found to be important to both hole transport and excess electron transport, but the directions that are most efficient are opposites. For hole transport the charge goes from the 3' to the 5' end

of the DNA. While migration from the 5' to the 3' end is more efficient for excess electron transport.

How strong the initial charge is and its effect on the efficiency of the process has only been investigated in hole transport. It has been found that the stronger the charge (driving force) the more efficient the rate of hole transport. The studies carried out in this dissertation investigate the possibility that a relationship on the driving force exists for excess electron transport.

Before we can test to see which strength of charge is the most efficient, we first have to establish whether or not a driving force dependence even exists in excess electron transport. To test this, we conducted studies using a series of compounds that had different driving forces. The compounds were first prepared and fully characterized so that their physical properties were known. The compounds were then screened in an experiment where the compounds **were not attached** to the DNA to see if a driving force dependence existed. No driving force dependence using this test was found.

Subsequently, two of the compounds were attached to the DNA to see if a driving force dependence existed. The compounds **were attached** to the DNA to force the process to take place. Again, no driving force dependence on the rate of excess electron transport was found – at least not with these compounds and under these test conditions.

Dedication

For Susannah and Baby Campbell

Acknowledgements

First and foremost, I would like to thank Dr. Steven Rokita for being a wonderful advisor. You have given me the chance to learn new techniques and fostered my growth as a scientist in innumerable ways. While at the University of Maryland, you supported my directions and decisions, all the while gently (and sometimes not so gently) correcting my growth.

I would like to thank my committee, Professors DeShong, Falvey, Cropp and Kofinas. Your thoughts and guidance on my project and progress toward my degree are greatly appreciated.

I would also like to thank the Rokita lab. The support provided over the years has made the entire process manageable. I have learned a great deal from each of you and hopefully taught you each a little, too. I wish you all the best of luck on your projects and futures.

Dr. Amy Finch, without the oxidation potentials, this project would never have fully taken shape. I would still be trying to determine the values myself. I am indebted to you. Also, thank you for teaching me how to run gels and getting me started on my DNA work. I would also like to thank you for being a great friend and mentor.

Patrick McTamney, you are a crazy, sugar loaded biochemist. But if I ever needed something or someone to bounce an idea off of, you were always there. There will be many stories to be shared and many more Red Dress Runs to be had. When in doubt, Naja Naja!

Jen Adler, thank you for listening to so many talks and catching all of Dr. Rokita's remarks in those talks. Without those notes it would have been hard to make sense of his scribbling.

Dr. Matt Servinsky, you friendship is one I will cherish. We are so much alike, in so many ways. The conversations about lab work between games of squash were some of the most insightful, if not sweatiest I've had. I look forward to playing many more games of squash throughout the years and staying in close contact.

Jim Watson and Emily Weinert, combined you two were a force of nature. Always prepared with pithy remarks, but always willing to help as much as possible. Your insights into your Boss proved to be valuable, even if I didn't think so at the time.

To the rest of the Wing 5 cohorts, including Kelly Daggett, William Shadrick, Melissa Resto and Brian Williams, you all kept me sane and listened to much grumbling. You all were there for me for practice talks and seminars. Should you need something, just let me know.

I would also like to thank the graduate students from my year. You were always there when I needed a compound or advice. I would especially like to thank Will Harrell, Brian Borak and Krupa Shukla for all the help that you have given me over the years.

I would be remiss if I did not thank the rest of the Department of Chemistry and Biochemistry. Through the years, the paperwork, orders and requests were taken care. I thank you for that. I would especially like to thank Linda Zappazodi, without you the labs wouldn't work.

I would also like to thank the Smoot Family, your support has made this journey manageable. I would especially like to thank Jeanne Smoot, Frank Canty and their

wonderful kids, Frank and Sophie, for allowing me to stay with them and feeding me. Additionally, I would like to thank Daniel Smoot for all the photographs and support. Finally, I would like to thank Dr. Jeanne Smoot and David Smoot; you never doubted that I would finish, and your encouragement really helped when things were tough.

To my family, Anne, John and my brother Simon, thank you. Your support of my scientific mind led to this dissertation. While we might be spread across two continents and two coasts, I miss you all and love you very much.

I would like to thank my wife. It is impossible to list all the things for which I am thankful. Thank you for your support. It was very tough, nearly impossible, to live apart from you for over a year while I finished my degree. I promise, it will be worth it. Also, I would like to thank you for reading my dissertation. While you might think that mere grammatical corrections might be minor changes, I am a scientist, not an English major, and it showed. Finally, your involvement in the process of my degree from inception of the idea to completion and graduation is more than I could have hoped or asked for.

Table of Contents

Table of Figures

Table of Tables

Table of Equations

List of Abbreviations

±-BINAP	racemic 2,2'-bis(diphenylphosphino)-1,1'-binaphthyl
A	adenosine
AC	alternatic current voltametry
Ac_2O	acetic anhydride
BOC_2O	ditertbutyl dicarbamate
Br_2	bromine
^{Br}U	5-bromo-2'-deoxyuridine
C	cytosine
CaH	calcium hydride
CCl_4	carbon tetrachloride
$CDCl_3$	dueterated chloroform
CH_2Cl_2	methylene chloride
cm	centimeter
Cs_2CO_3	cesium carbonate
CuBr	copper bromide
CV	cyclic voltametry
DAN	1,5-diaminonapthalene
ddH_2O	double distilled water
DMAP	dimethyaminopyridine
DNA	deoxyribonuclic acid
dpm	decays per minute
EET	excess electron transport

E_{00}	singlet energy
E_{ox}	oxidation potential
E_{ox}^{*}	excited state oxidation potential
ESI-MS	electrospray ionization mass spectrometry
EtOH	ethanol
FA	fluorescence anisotropy
$FeCl_3$	iron trichloride
Fmoc	9-fluorenylmethyl functionality
Fmoc-Cl	9-fluorenylmethyl chloride
Fmoc-Su	9-fluorenylmethyl succinate
G	guanine
H_2O	water
H_2SO_4	sulfuric acid
HBr	hydrobromic acid
HCl	hydrochloric acid
HOMO	highest occupied molecular orbital
HPLC	high performance liquid chromatography
hr	hour
HT	hole transport
K_2CO_3	potassium carbonate
kcal	kilocalaries
KI	potassium iodide
KX	potassium halide

LUMO	lowest unoccupied molecular orbital
MALDI-TOF	matrix assisted laser desorption/ionization time of flight mass spectrometry
mCi	milliCuries
MeOH	methanol
mg	milligram
MHz	megahertz
min.	minutes
mL	milliliter
mM	millimolar
mmol	millimols
mW	milliwatts
Na_2CO_3	sodium carbonate
$NaBH_4$	sodium borohydride
NaCl	sodium chloride
$NaHCO_3$	sodium bicaarbonate
$NaNO_2$	sodium nitrite
NaOH	sodium hydroxide
NaOt-Bu	sodium tert-butoxide
NH_2Me	methyl amine
$NH_2NH_2\,H_2O$	hydrazine monohydrate
NH_4Cl	ammonium chloride
$NHMe_2$	dimethyl amine

nm	nanomolar
NMR	nuclear magnetic resonance spectroscopy
O_2	molecular oxygen
OD	optical density
ODN	oligodeoxynucleotide
$Pd(OAc)_2$	palladium acetate
Pd/C	palladium on carbon
PG	protecting group
PNA	peptide nuclice acid
ppm	parts per million
S_0	singlet 0 vibrational energy level
SCE	saturated calomel electrode
S_n^*	singlet excited vibrational level
T	thymine
T^T	thymine-thymine dimer missing phosphate back bone
THF	tetrahydrofuran
TLC	thin layer chromatography
TMDN	N1,N1,N5,N5-tetramethyl-1,5-diaminonapthalene
μL	microliter
μM	micromolar
V	volt
Zn	zinc

Chapter 1
Background and Significance

1.1 Structure of DNA as it Relates to Charge Transport

One of the most important molecules in the world is deoxyribonucleic acid (DNA). DNA consists of the genetic code that defines all living creatures. DNA was first discovered by Miescher[1] in 1869. Subsequent work by Levene[2] began to elucidate its structure. In 1953 Watson and Crick first reported the structure of duplex DNA, which led to an unprecedented volume of work on this simple biomolecule.[3]

Duplex DNA is composed of two anti-parallel phosphate backbones to which are connected 2'-deoxyribose sugars, each of which has one of four nucleobases attached. The nucleobases are adenine (**A**), cytosine (**C**), guanine (**G**), and thymine (**T**), and are flat aromatic heterocycles that can undergo Watson-Crick base pairing. (**Figure 1.1**) The anti-parallel strands form a helical duplex with the phosphate backbone on the exterior and the base-paired nucleobases forming the internal core.

The most common helical form of DNA is B-form. In this form, the DNA is a right-handed that helix completes a full turn every 3.4 nm with 10 bases per turn and has a major and minor groove. When dehydrated the DNA adopts the A-form, which completes a full helical turn in 2.3 nm containing 11 bases per turn. In the A-form DNA, the major groove is larger, while the minor groove becomes smaller. DNA sequences with high **G**/**C** content assume a Z-helical form. Z-form of DNA has a highly distorted left-handed helix that zigzags and completes a full turn in 4.6 nm and is comprised of 12 base pairs. Z-form DNA consists of an extremely wide and shallow major groove with a nearly non-existent minor groove.

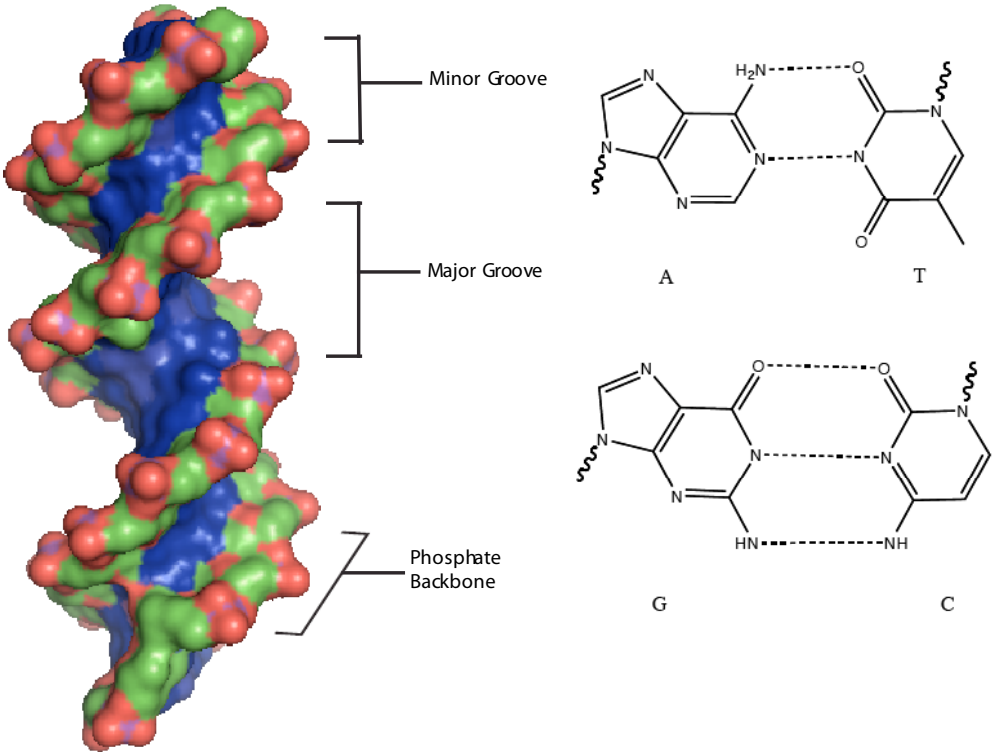

Figure 1.1: B-Helical DNA with a phosphate backbone shown in green and red and the Watson-Crick paired bases in blue. (DNA structure adapted from adna.pdb from http://chemistry.gsu.edu/glactone/PDB/DNA_RNA/)

In DNA the internal core of nucleobases is referred to as the DNA base stack. For B-form DNA, a vertical distance of 0.34 nm separates the nucleobases and a 36º twist exists between the face of one base and the adjacent base. The twist between the stacked base pairs allows the polar groups of the bases to overlap the aromatic ring of the adjacent base creating a dipole. Dipole formation in this fashion occurs in both strands with opposite directionality. The dipoles formed stabilize the DNA duplex based on the attraction of opposites.[4]

There are numerous areas of research currently being pursued with regards to DNA. A cursory Scifinder (American Chemical Society, Washington, DC) search yields 1.9 million entries when "DNA" is entered as a search term. Chemistry research on DNA ranges from incorporating unnatural nucleobases into the DNA duplex[5,6] to altering the

phosphate backbone[7-9] and ribose sugar.[10-13] Another area that is also being actively pursued is the ability of DNA to transfer charge through the DNA base stack.

Over the last 40 years, charge transport in DNA has received increasing interest. In 1962, Eley and Spivey first brought the ability for DNA to transport charge to the attention of the scientific community.[14] This led to interest in the use of DNA as a practical building block to generate wires,[15-17] nanoelectronic devices,[18] sensors,[19] insulators,[20] and conductors.[16,21]

Charge transfer is a general term to describe two processes: hole transport (HT) and excess electron transport (EET). Both processes involve the transport of an electron through the DNA stack, but the orbitals utilized differ. In hole transport, an electron is excited into the lowest unoccupied molecular orbital (LUMO) of the charge donor, generating an electron deficiency in the highest occupied molecular orbital (HOMO) of the donor, which results in the movement of an electron from the HOMO adjacent charge acceptor. This process continues through the DNA stack until the hole is trapped. In hole transfer, the trap is generally a compound that is easily reduced. In contrast, EET involves the excitation of an electron to LUMO of the donor. This excited electron then transfers to the LUMO of the neighboring acceptor until is it trapped by an easily oxidized compound. (**Figure 1.2**)

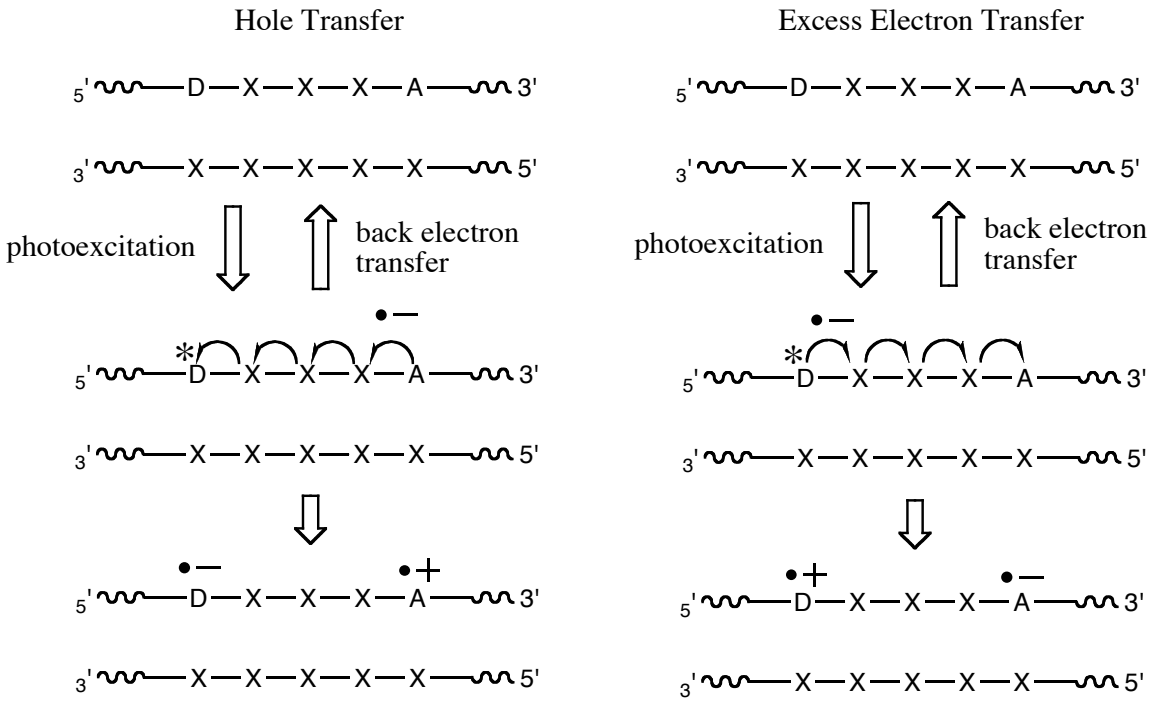

Figure 1.2: Charge transfer processes in DNA. Arrows indicate movement of electron (D=donor, D*=excited donor, A=acceptor, X=charge carrier)[22]

In both HT and EET each migration of the charge from the donor to an acceptor is an equilibrium process that is just as likely to go in reverse. This reverse process is known as back electron process. With this process incorporated into the charge transfer process, the complexity of the interpreting charge transport results becomes significantly more challenging. The competing processes of charge transfer and back electron transfer and the probability of each occurring must be taken into account when analyzing the systems used to study charge transfer in DNA.

Over the last two decades, hole transport has received more attention than EET, leading to a greater understanding of the charge transport mechanisms and DNA requirements for efficient HT. Only recently has work begun on understanding the mechanism and DNA requirements for EET.

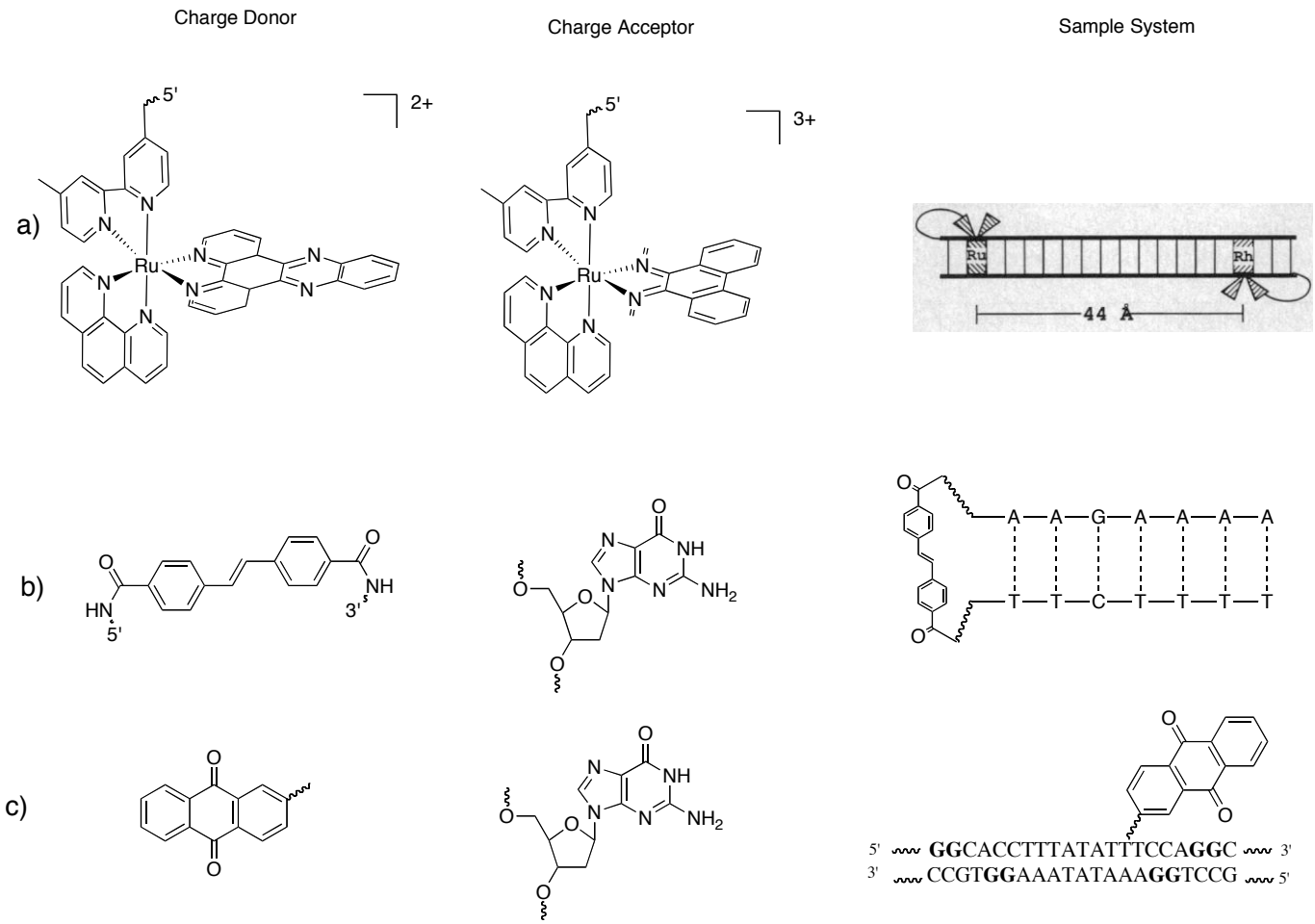

Figure 1.3: Examples of charge donor/acceptor and systems used in HT studies. (a) Ruthenium/Rhodium system used by Barton[23], (b) Stillbene-4,4'-dicarboximide used by Lewis[24] (figure adapted from Ref. 24), (c) anthraquinone/guanine system used by Schuster[25] (figure adapted from Ref. 26).

1.2 Types of charge transport in DNA

1.2.1 Hole transport

To investigate charge transfer in HT, a variety of donor/acceptor systems have been used. Examples of donor/acceptor systems range from metal intercalators used by Barton (**Figure 1.3a)**[23], small organic molecules such a stillbene-4,4'-dicarboxamide used by Lewis (**Figure 1.3b**)[24,26], and an anthraquinone used by Schuster (**Figure 1.3c**)[25] All of the donor/acceptor systems are covalently attached to the DNA and fall into one of four motifs: 1) DNA base analog, 2) capped DNA hairpins, 3) DNA base attachment, or 4) tethered intercalator. (**Figure 1.4**)

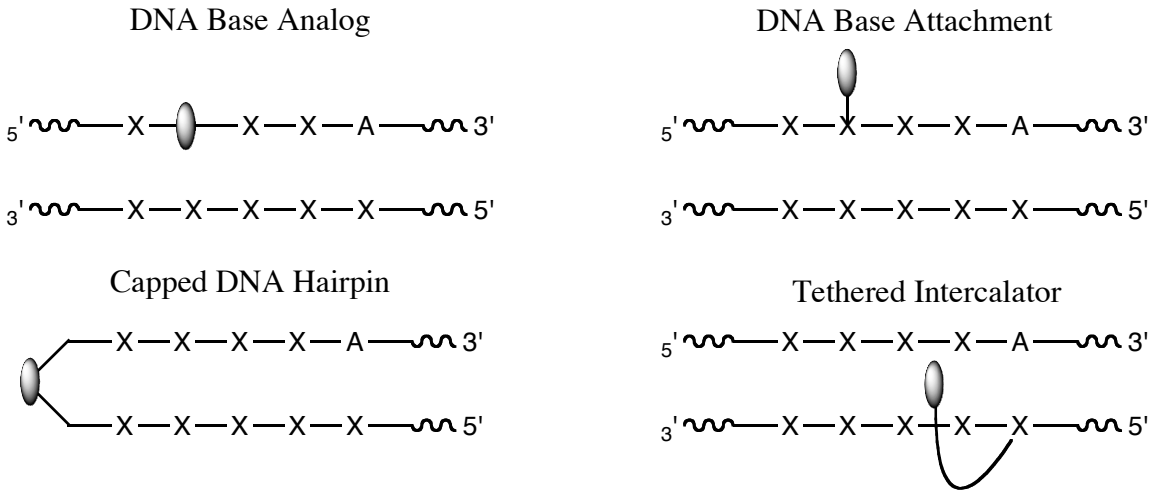

Figure 1.4: Motifs for covalently attaching HT donor acceptor systems to DNA (=donor, A=acceptor).

HT can occur are by one, or a combination of, the following mechanisms: hopping[27-29], superexchange[29,30], and polaron.[27,31-33] In the superexchange mechanism, HT occurs in a single step directly between the donor and acceptor, tunneling through the intervening bases (bridge). Alternately, in the hopping and polaron mechanism HT occurs as the charge hops from one **G** to another **G** by tunneling through the intervening **A/T** base pairs. The length, composition and electronic coupling of the bridge between

the donor and acceptor plays a critical role in the rate of charge transfer. It has been found that HT can occur over both short distances (<10 Å) by the superexchange mechanism[34,35] and over long distances (>200 Å, 60 bases) by both the hopping and polaron mechanisms.[25,29,33,36-39]

To understand the distance dependence of each HT mechanism, it is necessary to understand the manner in which HT occurs in each mechanism. In the superexchange mechanism the energy levels of the bridge between the donor and acceptor have a higher energy than that of the excited donor. Thus the charge never rests on any single base in the bridge, but transfers in a single coherent step through the bridge to the donor. Charge transfer will be more efficient in systems with greater electronic coupling between the donor, bridge and acceptor and the shorter the bridges. Additionally, intercalation of the donor and/or acceptor into the DNA will increase the electronic coupling to the bridge, thus increasing the rate of charge transfer.[22] (**Figure 1.5**)

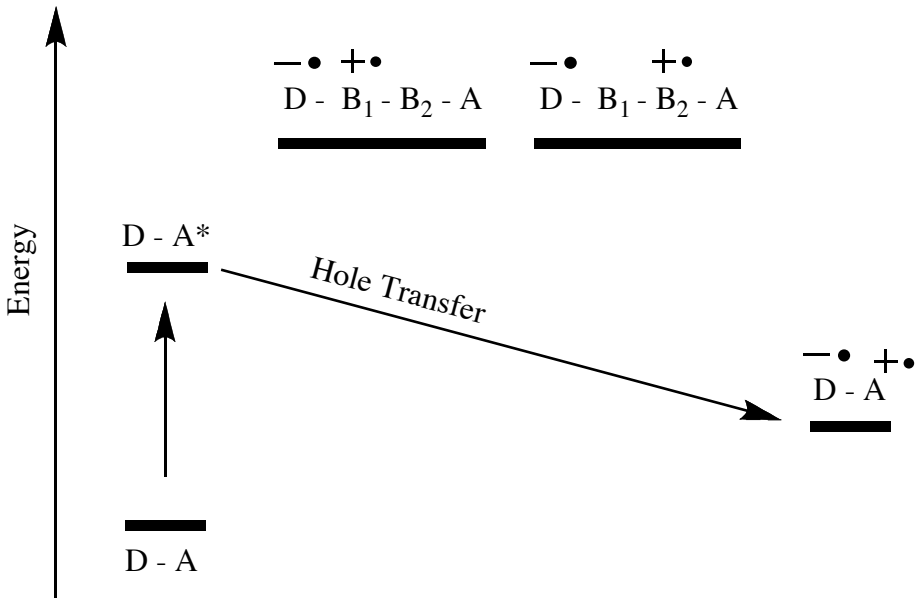

Figure 1.5: Superexchange mechanism of HT (D=Charge Donor, B=DNA Bridge, A= Charge Acceptor). Adapted from reference 20.

The two remaining mechanisms, hopping and polaron, require that the energy level of the bridge be lower that that of the donor. In the hopping mechanism, the charge transfers in a single coherent to the first charge carrier. The charge then resides on this charge carrier before undergoing a superexchange hop to the next charge carrier. The process continues until the acceptor traps the charge. (**Figure 1.6**)

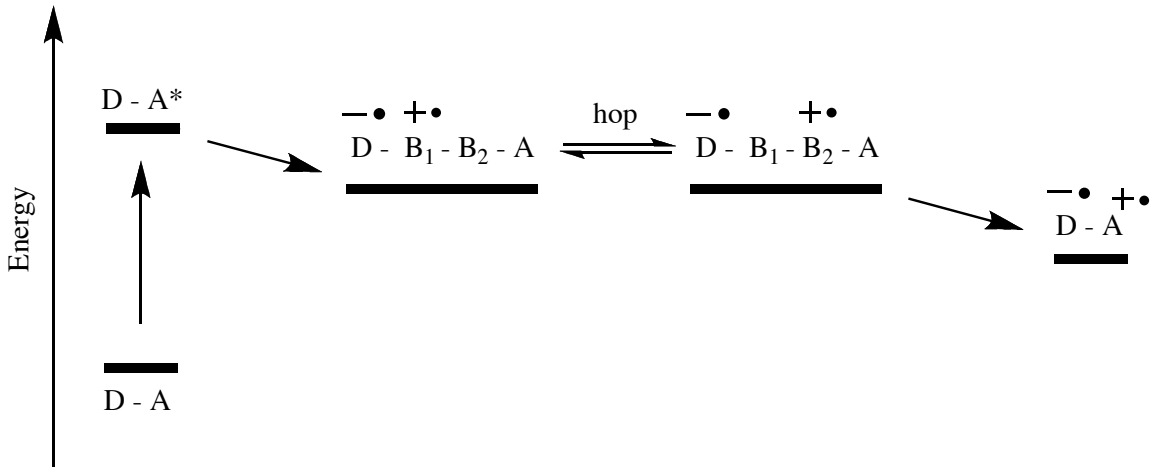

Figure 1.6: Hopping mechanism of HT (D=Charge donor, B=DNA Bridge, A=Acceptor). Adapted from reference 20

In the polaron mechanism, a physical distortion of the DNA (polaron) delocalizes the charge over several charge carriers in the bridge. This physical distortion increases the electronic overlap between the bridge and the donor/acceptor thus allowing efficient of HT. [31,40] The charge then undergoes a superexchange hop in the same manner as the hopping mechanism to the next region of DNA that supports the formation of a polaron. As with the other mechanisms, this process continues until the acceptor traps the charge.

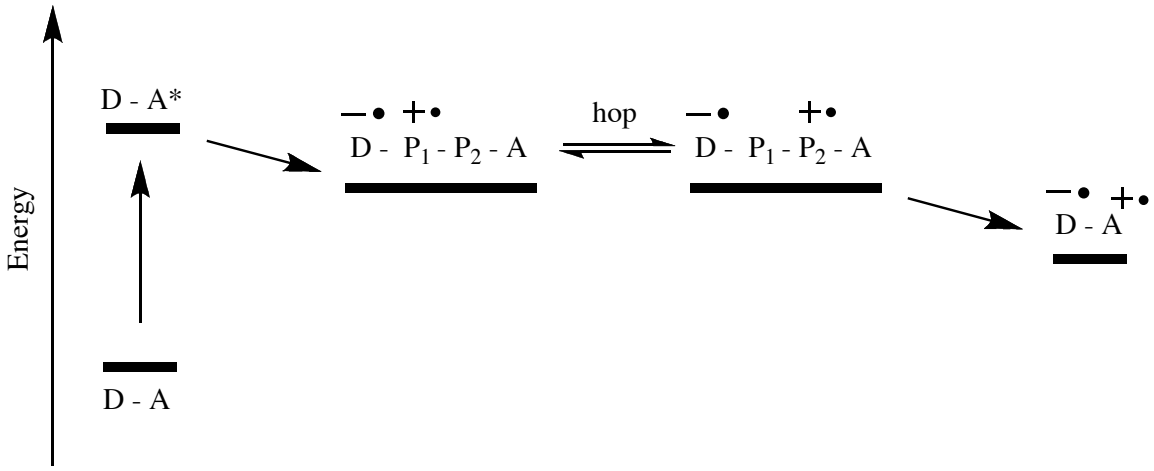

Figure 1.7: Polaron hopping mechanism of HT (D=Donor, P=polaron distorted DNA, A=Acceptor).

HT is initiated by direct excitation of the donor and the resulting hole travels through the DNA duplex by one of the above-mentioned mechanisms until it reaches the acceptor. Regardless of the HT mechanism used the nucleobase G is the charge carrier[40], as it is the most easily reduced of the four bases.[41] To evaluate the efficiency and rate of HT, the following must be considered: the mechanism of charge transport, the donor/acceptor system and the sequence between donor and acceptor.

1.2.2 Excess electron transport

Unlike HT, very little information is known about excess electron transport (EET) in DNA. EET is a LUMO-mediated process that involves the excitation of an electron to the LUMO of the donor, which then moves through the DNA stack to the electron acceptor via a hopping mechanism.[42,43]

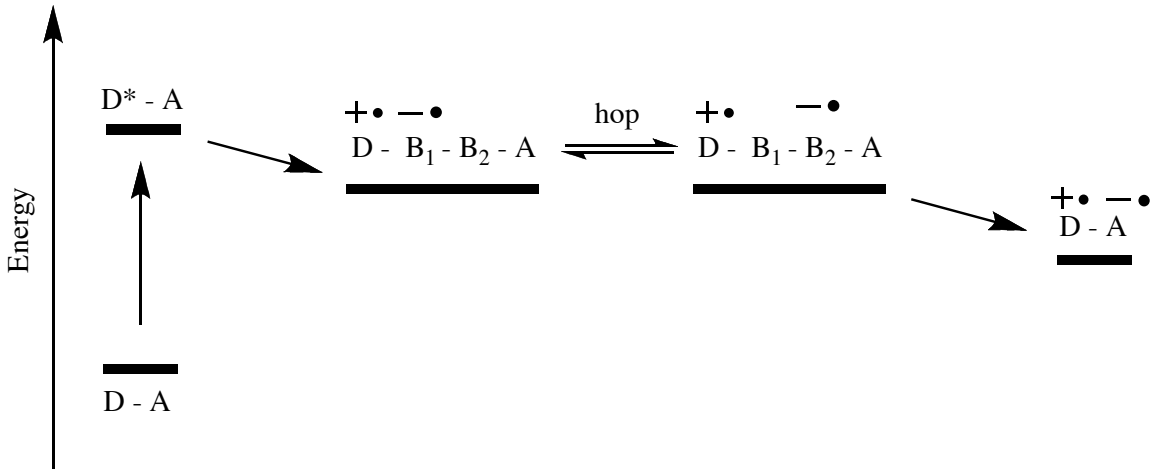

Figure 1.8: Hopping mechanism of EET (D=Electron Donor, B=DNA Bridge, A=Electron Acceptor).

Unlike the charge carrier in HT, the charge carrier in EET is proposed to be **T,** based on the relative reduction potentials of DNA bases.[40] Thus, if a hopping mechanism is used in EET, the charge is expected to hop from **T** to **T** by tunneling through intervening **C**/**G** sequences.[40,41] Electron donors for EET range from DNA capping compounds, such as a flavin analog used by the Carell group[44] (**Figure 1.9a**) and a stillbene diehter used by Lewis[45,46] (**Figure 1.9b**), to DNA base attachments, such as the pyrene-deoxyuridine used by Wagenknecht[42] (**Figure 1.9c**), and the tethered DNA intercalators, such as the naphthalene diamine, used by the Rokita group. (**Figure 1.9d**)[47,48]

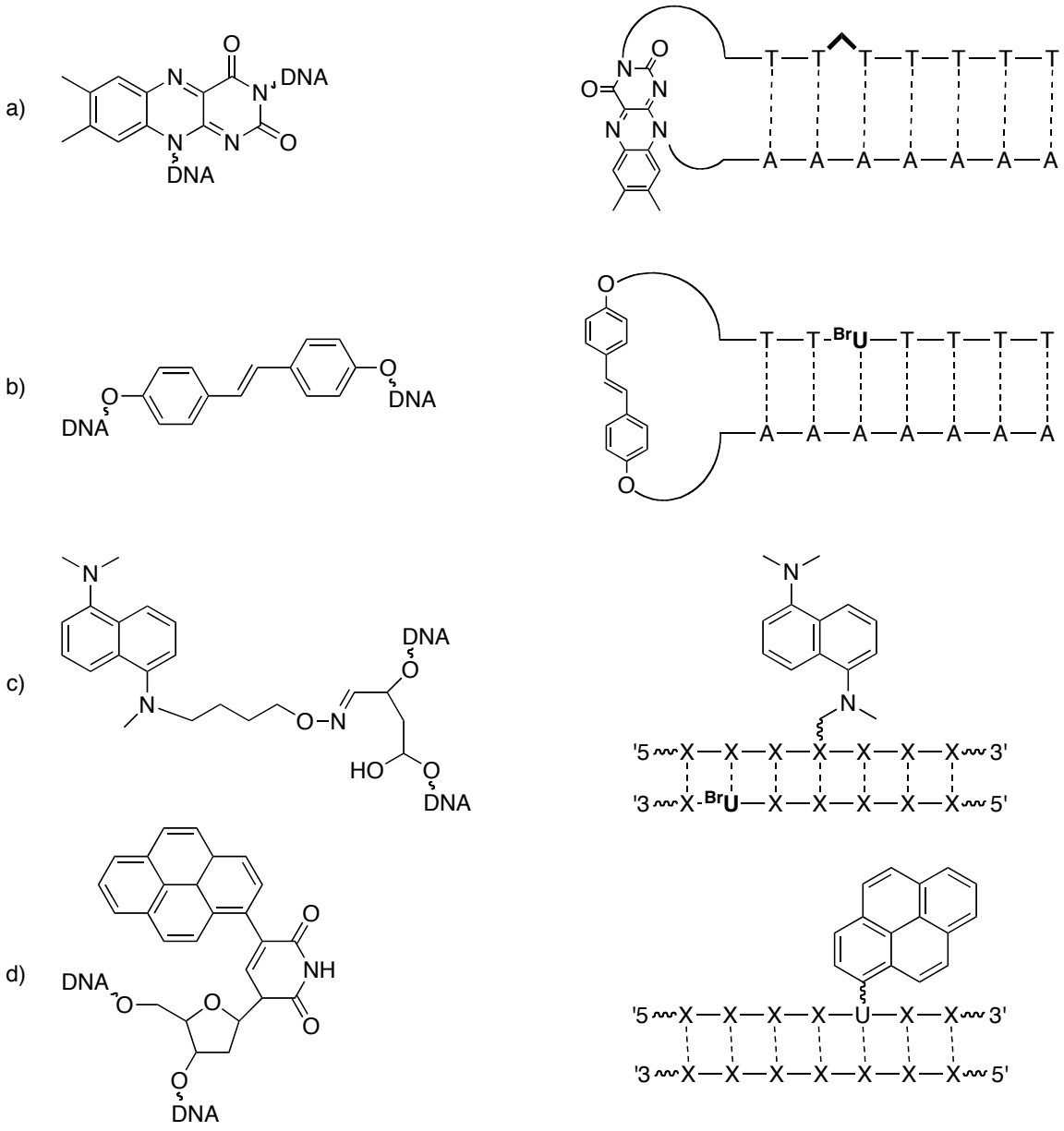

Figure 1.9: Examples of charge donor/acceptor and systems used in EET studies. (a) flavin used by Carell, (b) stillbene-4,4'-diether used by Lewis (figure adapted from Ref. 24), (c) diaminonapthalene used by Rokita, (d) pyrene-uracil used by Wagenknecht. (T^T=thymine dimmer missing phosphate backbone, X=any nucleobase) (figure adapted from Ref. 26).

The two main chemical electron acceptors used in EET are a thymine-thymine dimer (T^T) missing its phosphate backbone and 5-bromo-2'-deoxyuridine (^{Br}U). Both acceptors yield strand cleavage induced by EET through radical mediated processes.

(**Figure 1.10**) The major difference between these electron traps is that rate at which they undergo radical formation and, correspondingly, the rate of EET detection possible. In the case of the T^T, the rate of initial radical formation is 10^6 s^{-1},[22] while in the case of the ^{Br}U it is 10^{10} s^{-1}. The difference in rates has led to discrepancies in the measurement of the characteristics of EET as described below.

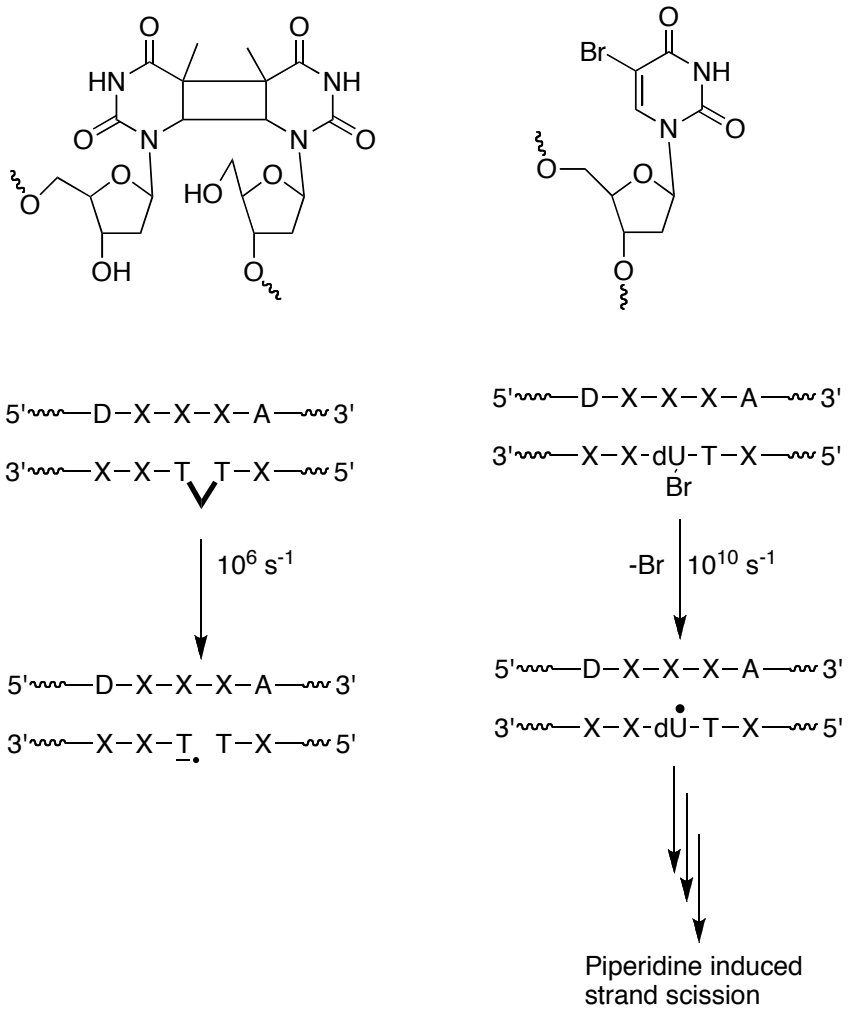

Figure 1.10: Comparison of electron acceptors used in EET (T^T=thymine dimmer missing phosphate backbone).

1.2.3 Investigations into general characteristics of EET

Investigations into the general characteristics and processes of EET have only recently been undertaken. To gain a clear understanding of how EET occurs in DNA,

four fundamental characteristics that need to be investigated are 1) distance dependence, 2) sequence dependence, 3) directional dependence, and 4) driving force dependence. Of the four characteristics, distance, sequence and directional dependence have received the most attention.

The distance dependence of EET has been studied the most. The distance dependence of charge transport is exponentially dependent upon two main factors β (the electronic coupling factor between the bridge and the donor and acceptor) an R (the distance between the donor and acceptor) according to **Equation 1.1**

$$k_{et} = k_0 \exp(-\beta R)$$

Equation 1.1: Distance dependence of electron transport in DNA**.**

Carell found that there is a weak distance dependence of 0.25 $Å^{-1}$ of EET when using the T^T electron acceptor.[49] The Rokita group also found a similarly weak distance dependence of 0.3 $Å^{-1}$ when the ^{Br}U electron trap.[47] These results indicate that the rate of superexchange electron transfer decreases only slightly the greater the distance between the donor and acceptor, indicating that EET has a weak distance dependence. Combined, these results support the hopping mechanism for EET transport in DNA.

The sequence dependence of EET has also been investigated. However, unlike the agreement on distance dependence of EET, conflicting results have been observed. Regardless of the sequence, the Carell group found a weak sequence dependence when using flavin capped DNA and the T^T acceptor in duplexes containing both A/T tracks and G/C tracks of duplex DNA. The Rokita and Wagenknecht groups contradicted this result.[48,50] In their studies, G/C bases between the donor and acceptor caused a reduction

in efficiency of EET. These results clearly indicate that research into the placement of the electron donor in the system needs to be undertaken.

The third fundamental area of EET that has been investigated is directional dependence of EET. As was seen with the studies on sequence dependence, conflicting results were obtained. The Carell group found no dependence on the rate of EET, regardless of the direction of transfer.[51] Conversely, the Rokita group determined that a distinct 3' to 5' directional dependence on EET existed.[43] It is important to note that the Carell group used PNA-DNA duplexes while the Rokita group used DNA-DNA duplexes. This difference makes direct comparison of the results difficult, as different platforms were used. More studies on this aspect of EET are also needed.

Efforts to understand the effect that the reduction potential, or driving force dependence, has on EET have been carried out by the Rokita lab. Using nonconjugated 1,5-diaminonapthalene (DAN) it was found that this compound was more efficient at promoting EET than its fully methylated analog, N1,N1,N5,N5-tetramethyl-1,5-diaminonapthalene (TMDN).[48] Based on the E_{ox}^{*} values of the compounds (DAN= -3.06 V vs. SCE, TMDN= -2.8 V vs. SCE) it was hypothesized that the difference in activity was related to their driving forces.[47,52]

The existence of a driving force dependence of EET is supported by Marcus theory. The Marcus theory of non-adiabatic electron transfer predicts the rate of electron transfer (k_{ET}) according to **Equation 1.2**. [53]

$$k_{ET} = \frac{4\pi^2 |V_{el}|^2}{h} \sqrt{\frac{1}{4\pi\lambda k_B T}} \exp\left(\frac{-(\Delta G_{ET} + \lambda)^2}{4\pi\lambda T}\right)$$

Equation 1.2: Marcus theory for the rate of nonadiabatic electron transfer (k_{et}). (V_{el}=electronic coupling of system, λ=reorganization energy, ΔG_{ET}=driving force of transfer process, k_B=Boltzmann's constant, h=Planck's constant)

This equation clearly shows that are three factors affecting the rate of electron transfer: (1) the electronic coupling between the initial and final states of the system (V_{el}), (2) the reorganization energy of the system (λ), and (3) the driving force of the transfer process (ΔG_{ET}). The driving force of the system can be further dissected to yield **Equation 1.3**.[17]

$$\Delta G_{ET} = 23.06(E_{ox} - E_{red}) - E_{00})$$

Equation 1.3: Determination of driving force of electron transport. (E_{ox}=oxidation potential of charge donor, E_{red}=reduction potential of electron acceptor, E_{00}=energy between 0 vibrational level of ground state and 0 vibrational level of excitied state of the electron donor)

When **Equation 1.2** and **Equation 1.3** are combined to give **Equation 1.4** it is clear that the oxidation potential of the electron donor (E_{ox}) plays a role in the rate of electron transport.

$$k_{ET} = \frac{4\pi^2 |V_{el}|^2}{h} \sqrt{\frac{1}{4\pi\lambda k_B T}} \exp\left(\frac{-\left((23.06(E_{ox} - E_{red}) - E_{00}) + \lambda\right)^2}{4\pi\lambda T}\right)$$

Equation 1.4: Combined equation for determination of rate of electron transport.

If it is assumed that the electronic coupling between the initial and final states of the system (V_{el}), the reorganization energy and the reduction potential of the electron acceptor ($E_{red.}$) of the systems are the same, then determination of the effect that the E_{ox} and E_{00} values have on electron transfer can be made.

1.3 Specific aims

The goal of my project was to determine if there is a driving force dependence of EET in DNA. To that end, I generated and characterized a series of 1,5-diaminonapthalene analogs with varying reduction potentials and used these compounds to investigate their relative efficiency of passing electrons to donors within duplex DNA.

Chapter 2

Synthesis and Characterization of 1,5-diaminonapthalene analogs for testing driving force dependence in excess electron transport in DNA

2.1 *Introduction*

The Rokita lab has developed an assay for screening aromatic amines for the ability to inject an excess electron using duplex DNA containing an abasic site, which is the site of electron injection, and a bromo-uridine (^{Br}U) electron acceptor.[47] (Figure 2.1)

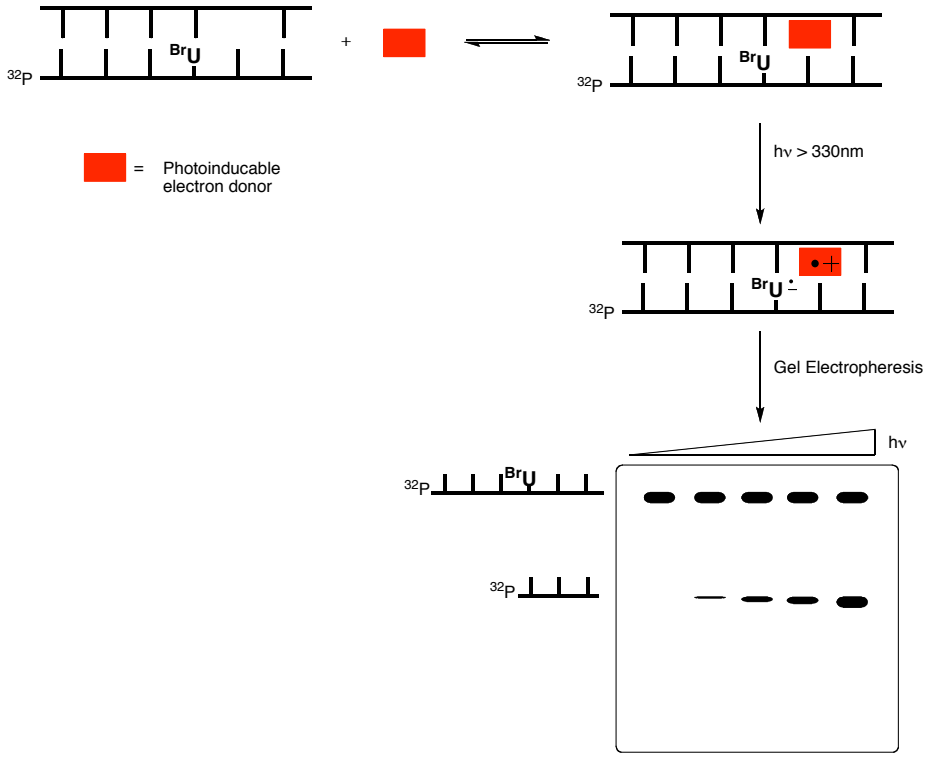

Figure 2.1: Cartoon of assay for EET using duplex DNA containing abasic site, ^{Br}U as electron acceptor and 5'-^{32}P label for detection using gel electrophoresis.

Using the assay defined in Figure 2.1, it is possible to screen a variety of electron donors through both non-covalent binding of the electron donor to the abasic site and covalent conjugation of the electron donor as previously examined.[47]

Both 1,5-diaminonapthalene (DAN, **1**) and N1,N1,N5,N5-tetramethyl-1,5-diaminonapthalene (TMDN, **2**) were able to promote strand scission induced by excess electron transport (EET) in the above mentioned assay. DAN (with a lower E_{ox} and E_{ox}^* values) was much more efficient at inducing strand scission than TMDN when the

compounds were screened.[48] DAN was able to inject an electron with greater reducing potential into the DNA duplex, which subsequently led to greater strand cleavage.

The question was posed as to what extent the E_{ox} and E_{ox}^{*} played in inducing strand cleavage, as DAN gave greater EET induced strand scission In general terms, E_{ox} and E_{ox}^{*} can be viewed as the driving force behind the excess electron that is injected into the DNA. Subsequently, a series of compounds was synthesized, characterized and used to determine what relative effect the driving force had on the rate of EET in DNA. (**Figure 2.2**)

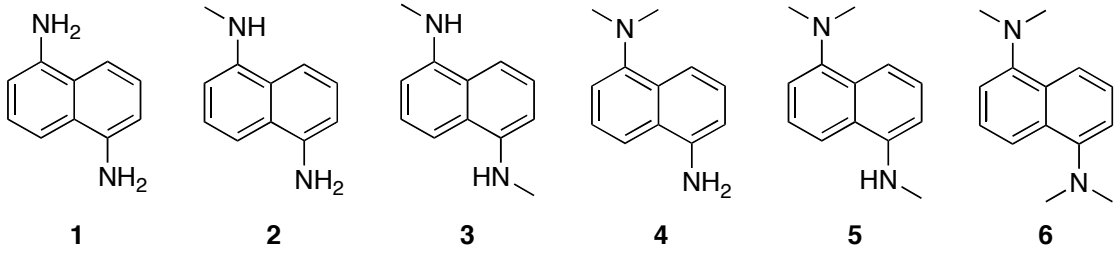

Figure 2.2: 1,5-Diaminonapthalene analogs needed to test the effect of driving force on the rate of EET in DNA.

TMDN was synthesized using a procedure that utilized exhaustive reductive amination. (**Figure 2.3)**

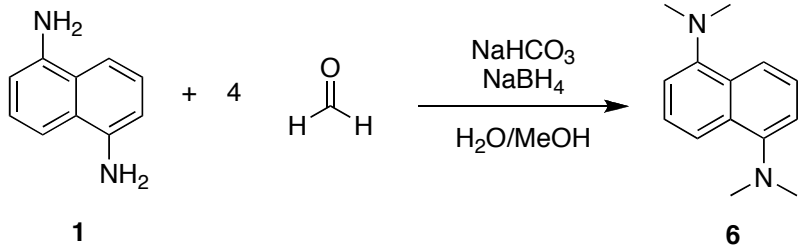

Figure 2.3: Exhaustive reductive amination of DAN to give TMDN.

Synthesis of **2**, **3**, **4**, and **5** using this method was not possible as there was no way to limit the reactivity of the amines sufficiently to prevent unwanted methylation. As this

method was not applicable for the synthesis of the remaining compounds, the synthesis of the desired compounds was undertaken with several goals in mind:

1) Use readily available reagents and materials to minimize synthetic steps;

2) Use well known synthetic procedures to produce the desired materials expeditiously and reliably;

3) Develop robust synthetic methodologies that could be used for the synthesis of multiple compounds.

With these criteria in mind, the Buchwald-Hartwig cross-coupling reaction was viewed as an excellent starting point for the synthesis of the desired materials. The Buchwald-Hartwig cross-coupling reaction allows direct generation of both primary and secondary amines, depending on the amine used.[54,55] (**Figure 2.4)**

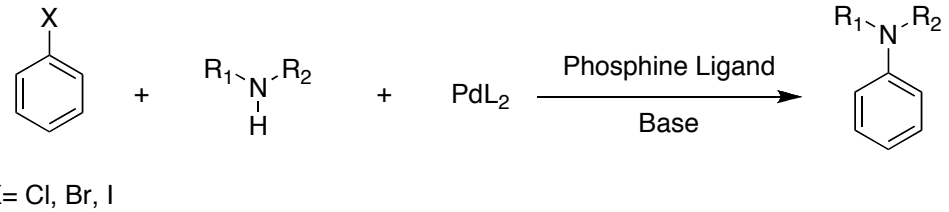

X= Cl, Br, I

Figure 2.4: General scheme for Buchwald-Hartwig cross-coupling reaction.

With the Buchwald-Hartwig cross coupling reaction as the basis of the chemistries for the generation of **2**, **3**, **4**, and **5,** an initial synthetic scheme was envisioned. (**Figure 2.5**)

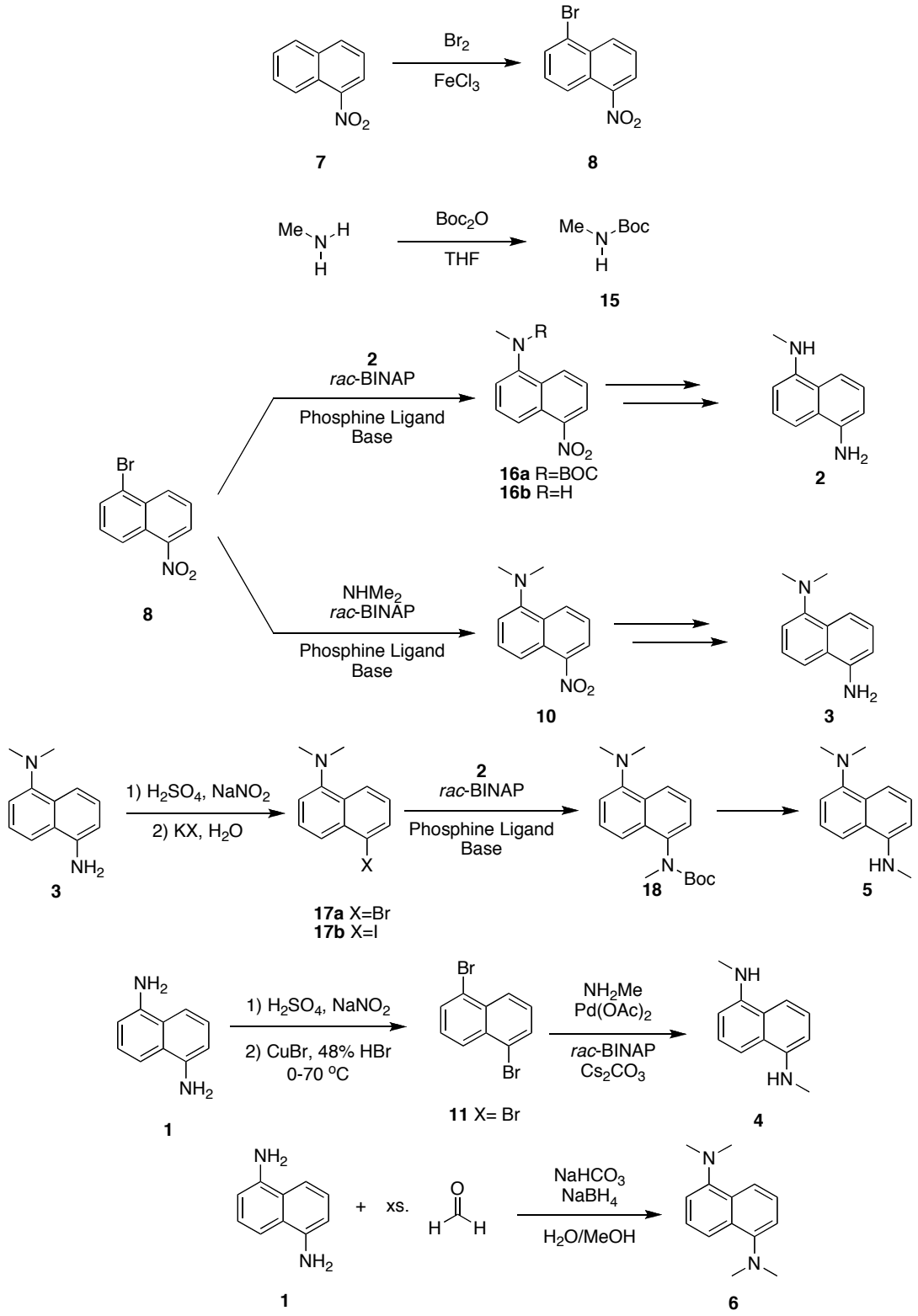

Figure 2.5: Initial synthetic schemes for generation of 1,5-diaminonapthalene analogs.

2.2 Preparation of N1-methyl-1,5-diaminonapthalene

Compound **8** was prepared using the literature procedure from the commercially available nitro naphthalene **7**.[56] (**Figure 2.6**)

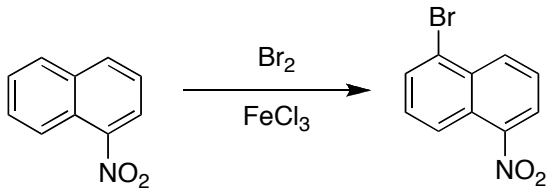

7 **8**

Figure 2.6: Preparation of 1-bromo-5-nitro-napthalene

Once the compound had been successfully prepared, efforts were directed toward the Buchwald-Hartwig cross-coupling reaction. **(Figure 2.7)**

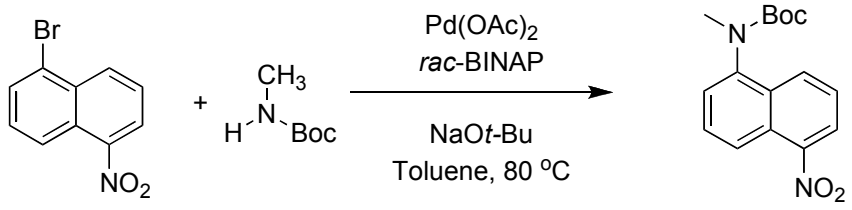

8 **9** **10**

Figure 2.7: Initial Buchwald-Hartwig cross-coupling attempt

Due to the low boiling point of methylamine, **9** was prepared using known chemistries.[57] This yielded a viscous oil at room temperature that was easier to handle. Initial reactions using conditions outlined in the literature did not yield the desired product. [58] All starting materials were consumed and none of the desired product was obtained when the mixture of products was purified. Use of sodium *tert*-butoxide in the presence of the nitro group appeared to cause decomposition to the starting material due to the strong basicity of the *tert*-butoxide.[59] Examination of the literature indicated that the use of cesium carbonate (Cs_2CO_3) instead of sodium *tert*-butoxide should allow the reaction to proceed without

decomposition.[59] To ensure that the nitro group in the reaction system was amenable to the use of Cs_2CO_3 a model reaction using benzylamine was examined. (**Figure 2.8**)

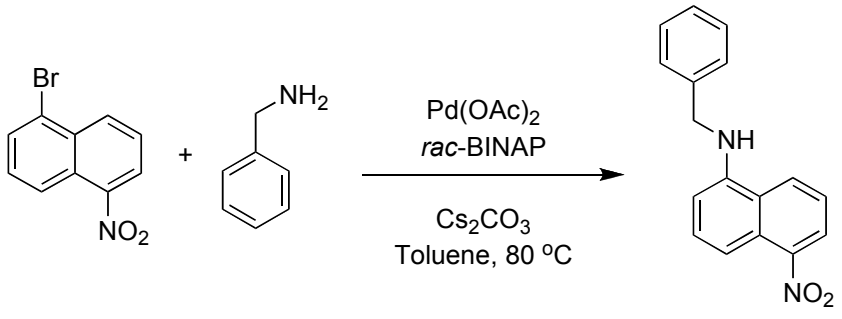

8 **11** **12**

Figure 2.8: Model reaction to determine the suitability of using Cs_2CO_3 in Buchwald-Hartwig reactions.

This reaction produced the desired product in 65% yield, thus validating the effectiveness of the Cs_2CO_3 at avoiding decomposition of **8**. The model reaction also proved the ability of **8** to effectively couple to primary amines.

Attention was then turned to the coupling of **8** with methyl amine. Since the model reaction showed that **8** could couple effectively with a primary amine, the use of methyl amine as the coupling partner was examined. The major hurdle was keeping the methyl amine in the reaction mixture as its boiling point of -6 ºC. This hurdle was overcome using a 2 M solution of methyl amine in THF and using a sealed reaction vessel, thus giving the desired material **13** in 65% yield. (**Figure 2.9**)

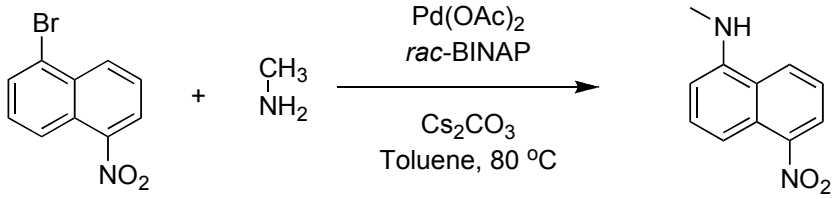

8 **13**

Figure 2.9: Synthesis of **13** from **8** and methyl amine.

With the successful generation of **13**, focus shifted to the reduction of the nitro group to the corresponding amine **2**. Initial attempts were made to reduce the nitro group using zinc dust, as described in a literature procedure.[60] **(Figure 2.10)**

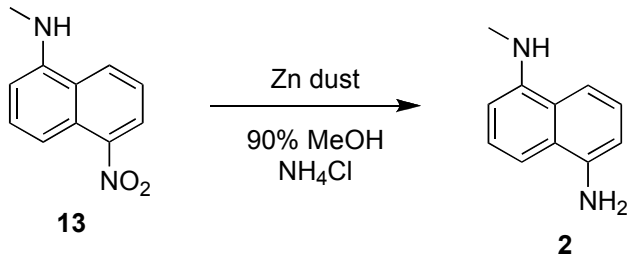

Figure 2.10: Initial attempt to reduce **13** using Zn dust to give **2**.

The reaction was attempted numerous times with varying reaction times, ranging from 10 minutes to overnight. However, none of these attempts yielded any of the desired material. The use of Zn dust to reduce the nitro group was abandoned and attention turned to hydrogenation.

Hydrogenation with a palladium catalyst will readily reduce an aryl nitro group to the desired amine.[61] Hydrogenation of **13** was undertaken under atmospheric pressure and room temperature using palladium-on-carbon (Pd/C), which yielded the desired product **2** in 54% yield. (**Figure 2.11**)

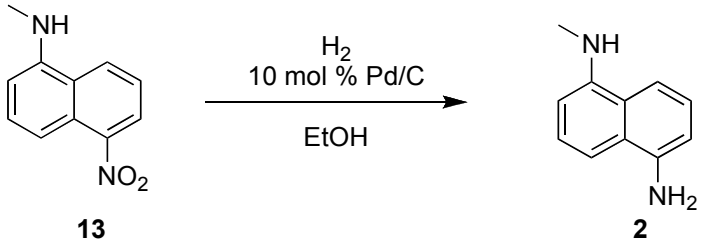

Figure 2.11: Catalytic hydrogenation of **13** to give **2**.

However, there were several drawbacks to catalytic hydrogenation:

(1) The low yield (54%) of the reaction;

(2) The use of hydrogen gas and the extended reaction time (18 hours).

The latter issue led to the investigation of a more viable route for the generation of **2**. A procedure based on Pd/C and formic acid[62] was used to reduce **13** to **2** with shorter reaction time (2 hr.) and higher yield (88%). (**Figure 2.12**)

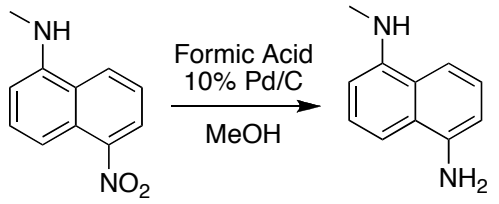

13 **2**

Figure 2.12: Reduction of nitro group using Pd/C and formic acid to yield **2**.

With the final step completed and one of the desired compounds in hand, attention turned to generation of the remaining compounds.

2.3 Synthesis of N1,N5-dimethyl-1,5-diaminonapthalene

Based on work by Cakmak[63], preparation of **15** was initially attempted using a photochemical bromination of **14** in chloroform. (**Figure 2.13**)

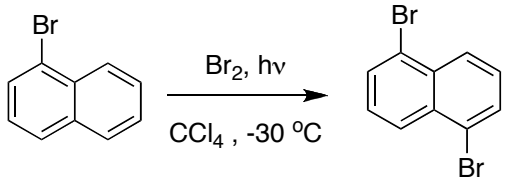

14 **15**

Figure 2.13: Attempted photochemical bromination of **14**.

The reaction yielded a complex mixture of species that were inseparable using silica gel chromatography. The photochemical bromination of **14** was abandoned and generation of **15** using Sandmeyer chemistry was attempted.[64] (**Figure 2.14**)

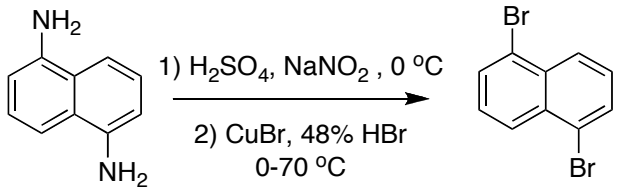

1 **15**

Figure 2.14: Preparation of **15** using Sandmeyer chemistry.

While successful in generating **15**, the Sandmeyer reaction had limited usefulness. The procedure for running and working up the reaction presented significant technical challenges including, but not limited to, significant foaming during generation of the desired material, excessive volumes of base to neutralize the acid used, and incomplete reaction. Based on literature precedence[58], an aryl iodide could be used in the Buchwald-Hartwig reaction, thus the generation of **16** was carried out, even though it suffered from some of the same issues experienced in the generation of **15**.[65] (**Figure 2.15**)

1 **16**

Figure 2.15: Preparation of 1,5-diiodonapthalene

Buchwald-Hartwig coupling using **16** and methyl amine was carried out as a direct route to **3**. (**Figure 2.16**)

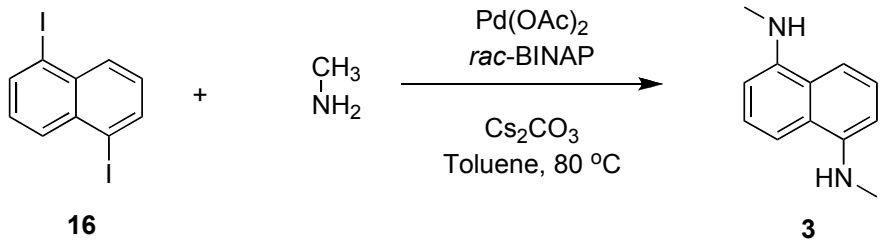

16 3

Figure 2.16: Generation of **3** using Buchwald-Hartwig coupling of **16** and methylamine.

The reaction was performed in a sealed tube in a similar fashion to that used in previous coupling reactions. The first attempt at obtaining **3** was met with an incomplete reaction. It was thought that there was insufficient catalyst loading. An increase from 1% palladium catalyst loading to 5% loading resulted in an increased yield from 50% to 92% of the desired product.

2.4 Preparation of N1,N1-dimethylnaphthalene-1,5-diamine

Based on literature precendence[54,58,59,66], it was evident dimethylamine would generate **17** in a Buchwald-Hartwig coupling reaction. Following the coupling, the nitro group could then be reduced to the amine using the same procedure as that used in the last step to generate **4**. (**Figure 2.17**)

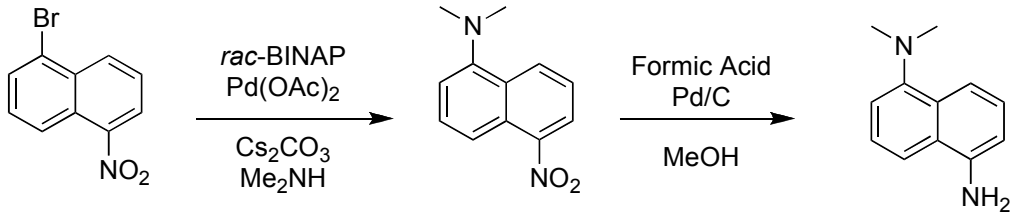

8 17 4

Figure 2.17: Generation of **4** using Buchwald-Hartwig coupling reaction and Pd/C with formic acid reduction.

This synthetic route proved to work very well and compound **4** was isolated in excellent yield (97%) as a dark red, viscous oil.

2.5 Preparation of N1,N1,N5-trimethylnaphthalene-1,5-diamine

Using chemistries already developed for the generation of the previous compounds, the synthesis of **5** was undertaken. (**Figure 2.18**) However the Sandmeyer reaction to produce **18** failed.

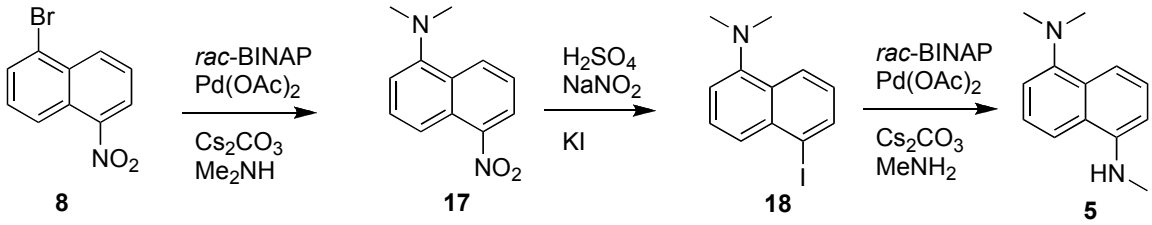

Figure 2.18: Proposed route for generation of **5** using chemical methodologies developed in this study.

A new route was envisioned using compound **13** as the starting material, protecting the amine, carrying out subsequent chemistry on the nitro group, and finally deprotection of the amine to yield **5**. (**Figure 2.19**)

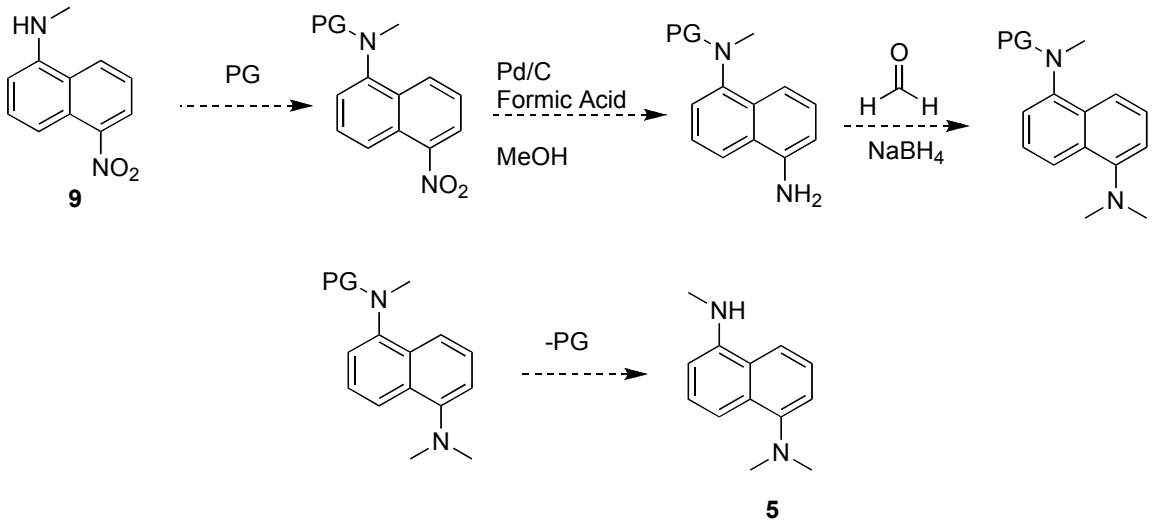

Figure 2.19: Proposed route for generation of **5** using protecting group (PG).

In this scheme, a protecting group would prevent additional alkylation of the secondary amine **9**. Due to the acidic conditions and reductive amination that the protecting group must endure, the 9-fluorenymethyl carbamate (Fmoc) protecting group

was chosen. After varying the reaction time from 3 to 48 hours and the reaction temperature from 0 °C to reflux, protection of **9** with Fmoc-OSu yielded starting material **9** but none of **19**. (**Figure 2.20)**.

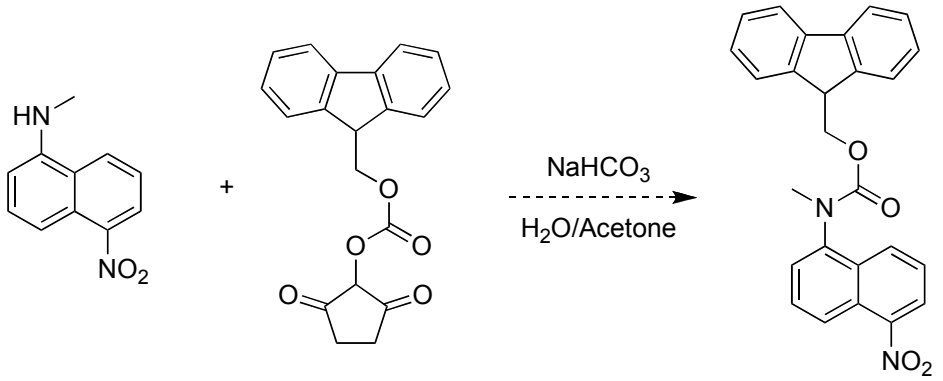

9 **19** **20**

Figure 2.20: Attempt at protecting **9** using Fmoc-Su.

Initial reactions using Fmoc-succinate (Fmoc-Su) (**19**) were carried out with no success. The more reactive Fmoc-Cl (**21**) was next examined as there are a variety of conditions that make it compatible with installation of the protecting group[67-71] (**Figure 2.21)**.

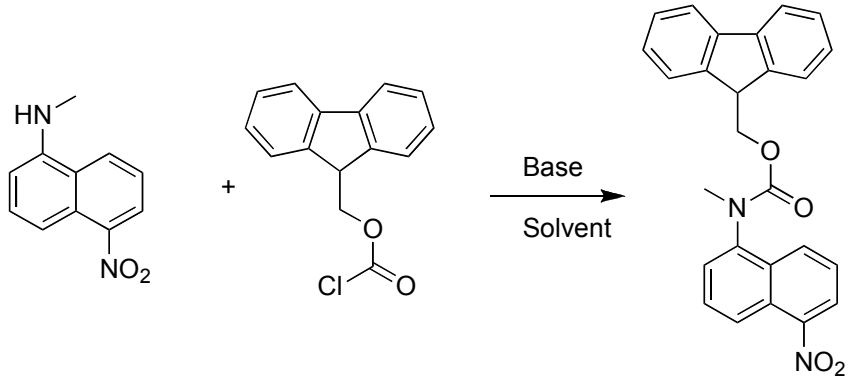

9 **21** **20**

Figure 2.21: Protection of amine group using Fmoc-Cl.

A variety of inorganic bases, $NaHCO_3$, Na_2CO_3, Cs_2CO_3, and CaH were examined in both CH_2Cl_2 and dioxane/water for their ability to successfully facilitate protection of **9**. Each reaction was carefully monitored by TLC (20 % ethyl acetate:hexanes) to gauge its

progress. Regardless of the base or solvent used, the starting material and the Fmoc-Cl were clearly visible with no new spots evident. It was determined that inorganic bases were not effective in this particular system. This was a surprising discovery since it had been reported that Na_2CO_3 has been used to attach the Fmoc protecting group to primary aromatic amines.[72]

The organic bases triethylamine, pyridine and DMAP were next examined in this protection reaction. All of these reactions were carried out in methylene chloride and were also monitored by TLC (20% ethyl acetate:hexanes) to determine progress of the reaction. None of the desired product was formed in any of the reactions; the starting material was recovered. Based on NMR of recovered materials after column chromatography it was determined that the Fmoc-Cl decomposed to 9-methylene-9H-fluorene (**22**) (**Figure 2.22)**.

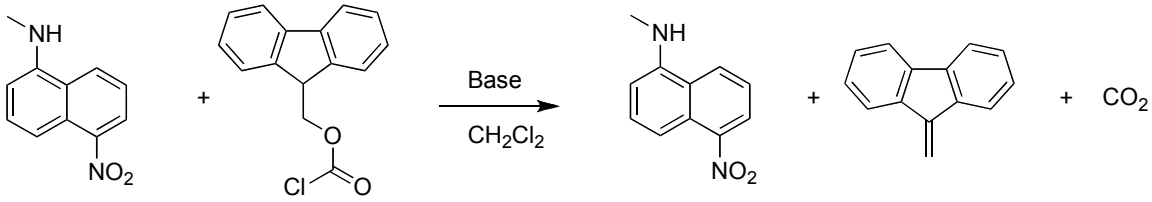

Figure 2.22: Proposed degradation products during Fmoc-Cl protection.

In an effort to simplify the protection scheme, compound **9** and Fmoc-Cl were stirred in a methylene chloride solution without base. A reaction appeared to occur, however, it was incomplete as indicated by the presence of starting materials by TLC. The reaction was allowed to proceed until no further change was observed. Attempts to isolate the new product that was formed were unsuccessful, therefore the crude product mixture was then subjected to reduction, which appeared to be successful as indicated by generation of a new spot when analyzed by TLC. A small quantity of **15** was isolated by

column chromatography, but it decomposed upon standing under nitrogen. Further attempts to produce **20** were abandoned due to susceptibility of the compound to decomposition.

Due to the difficulty in preparing **20**, an alternative protecting group was investigated. The idea to use an N-acyl group for protecting secondary amines came from the literature.[73,74] (**Figure 2.23)**.

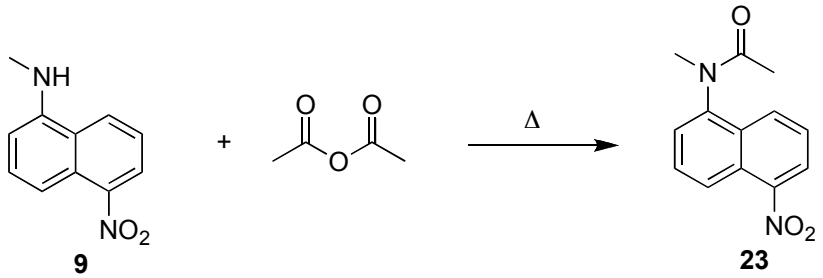

Figure 2.23: Acyl protection **9** for generation **5**.

The reaction went to completion and the desired product was isolated after column chromatography as an orange solid in 76% yield. The next obvious step was to convert the nitro group to the amine using previous conditions. Conversion of the nitro group into the primary amine was successfully completed using Pd/C and formic acid in methanol to give **24** in a good (84%) yield. (**Figure 2.24).**

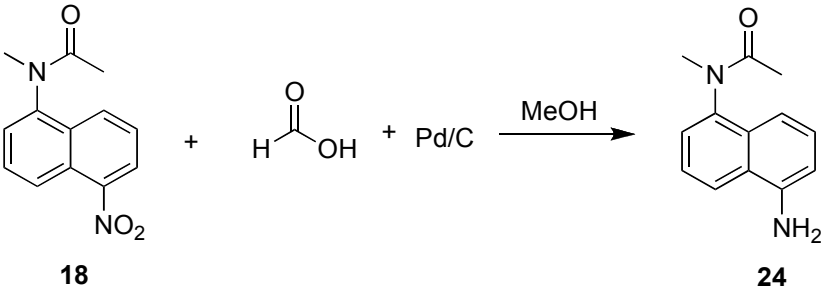

Figure 2.24: Reduction of **18** using Pd/C and formic acid to generate **24**.

Attempts to convert **24** to **25** under reductive amination conditions using formaldehyde and sodium borohydride under reported conditions[48] yielded a mixture of

compounds, none of which were the desired product. A new route using dimethyl sulfate and sodium carbonate in methanol was used to effectively prepare **25** in good (76%) yield.[75] (**Figure 2.25**).

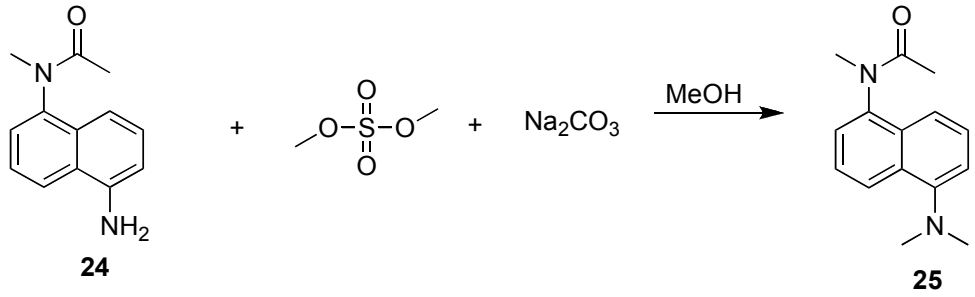

Figure 2.25: Methylation using dimethyl sulfate.

The final step undertaken was the deacylation of amide **25** to yield **5**. Initial attempts using hydrazine monohydrate failed to yield the desired product.[76] In a surprisingly simple procedure, 2 N HCl at reflux overnight was able to quantitatively convert **25** to **5**.[77] (Figure 2.26).

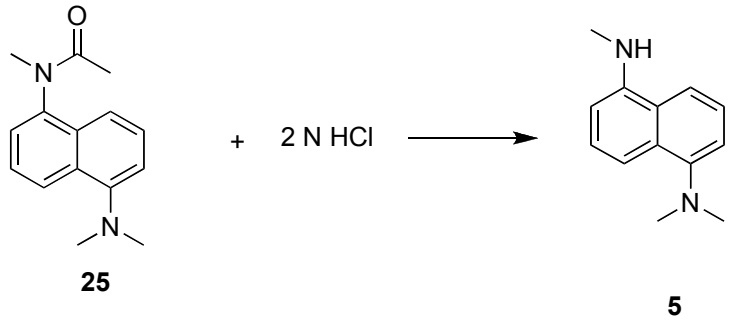

Figure 2.26: Deprotection of **25** to give **5**.

2.6 Preparation of N1,N1,N5,N5-tetramethyl-1,5-diaminonapthalene

Previously, the Rokita lab had identified the exhaustive reductive amination of **1** using formaldehyde and sodium borohydride ($NaBH_4$) as the route for preparation of TMDN. While this route is effective at generating the desired material, it suffers from the problem of competitive reaction of the sodium borohydride with either the imine that

is generated upon addition of the formaldehyde to **1** with the formaldehyde in the reaction mixture. As such, the chemistry used for the methylation of **25** was used to more efficiently generate **6**. (**Figure 2.27**)

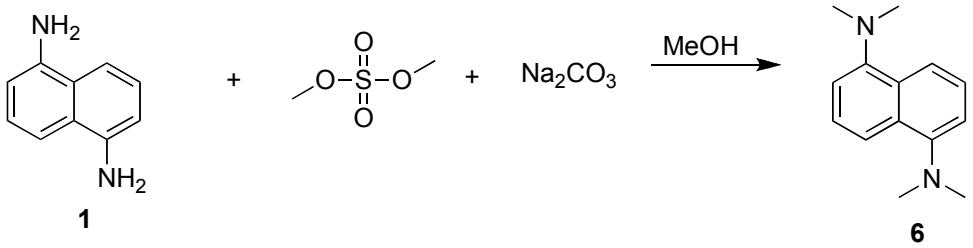

Figure 2.27: Generation of **6** using dimethyl sulfate and sodium carbonate.

The reaction proceeded efficiently (76% yield) in a shorter time frame (2 hr. vs. overnight) and is now considered the best way to produce **6** in the Rokita lab.

2.7 Characterization of 1,5-diaminonapthalene analogs

Characterization for the compounds focused on the determination of E_{ox}^* which is calculated from experimentally determined E_{ox}, and E_{00}. While the E_{ox} and E_{ox}^* values have been previously reported for **1** and **6**[47], all E_{00}, E_{ox} and E_{ox}^* were determined under the assay conditions mentioned above.

2.7.1 Determination E_{00} values for 1-6 using UV-Vis and fluorescence spectroscopy

Based on the mirror symmetry relationship between fluorescence and absorption spectra, the E_{00} values for each of the compounds can be determined from the intersection of the absorption and fluorescence spectra.[78] For the determination of the E_{00} values for **1-6** the λ_{max} and extinction coefficients (ε), and fluorescence spectra were needed. What

follows is a sample analysis for **2**. All other compounds were treated in the same manner and the data can be found in Appendix A.

The UV-vis analysis for **2** comprised of five sets of data acquired separately and averaged. In each experiment, serial additions of a stock solution of **2** were added to a UV-vis cuvette and the spectrum recorded. Consideration was taken in calculating the actual concentration of **2** as each addition changed the volume in the cuvette. The spectra were then overlaid as shown. (**Figure 2.28**)

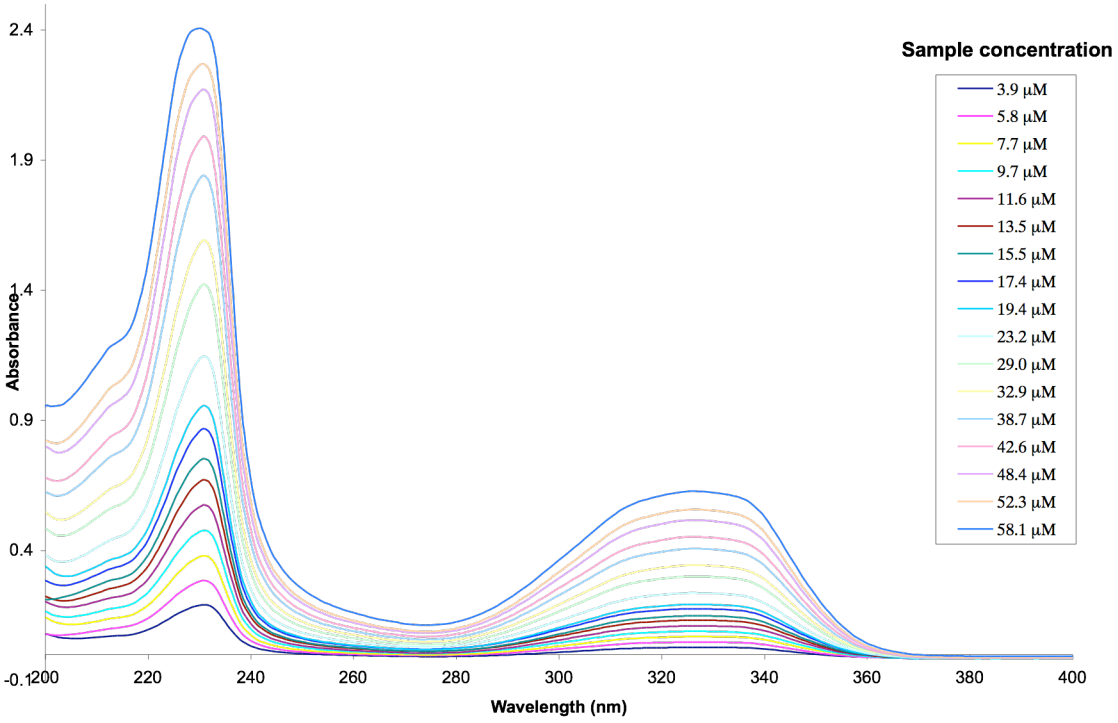

Figure 2.28: Overlayed UV-vis spectra of serial additions of **2** for determination of extinction coefficients of **2** in 100 mM NaCl, 10 mM sodium phosphate pH 7 buffer.

For each of the wavelengths, only the values corresponding to an optical density (OD) between 0.1 and 1 were used for determination of the extinction coefficient using linear fit. (**Figure 2.29**) The ε values reported for all compounds are a minimum of three separate experiments. (**Table 2.1**)

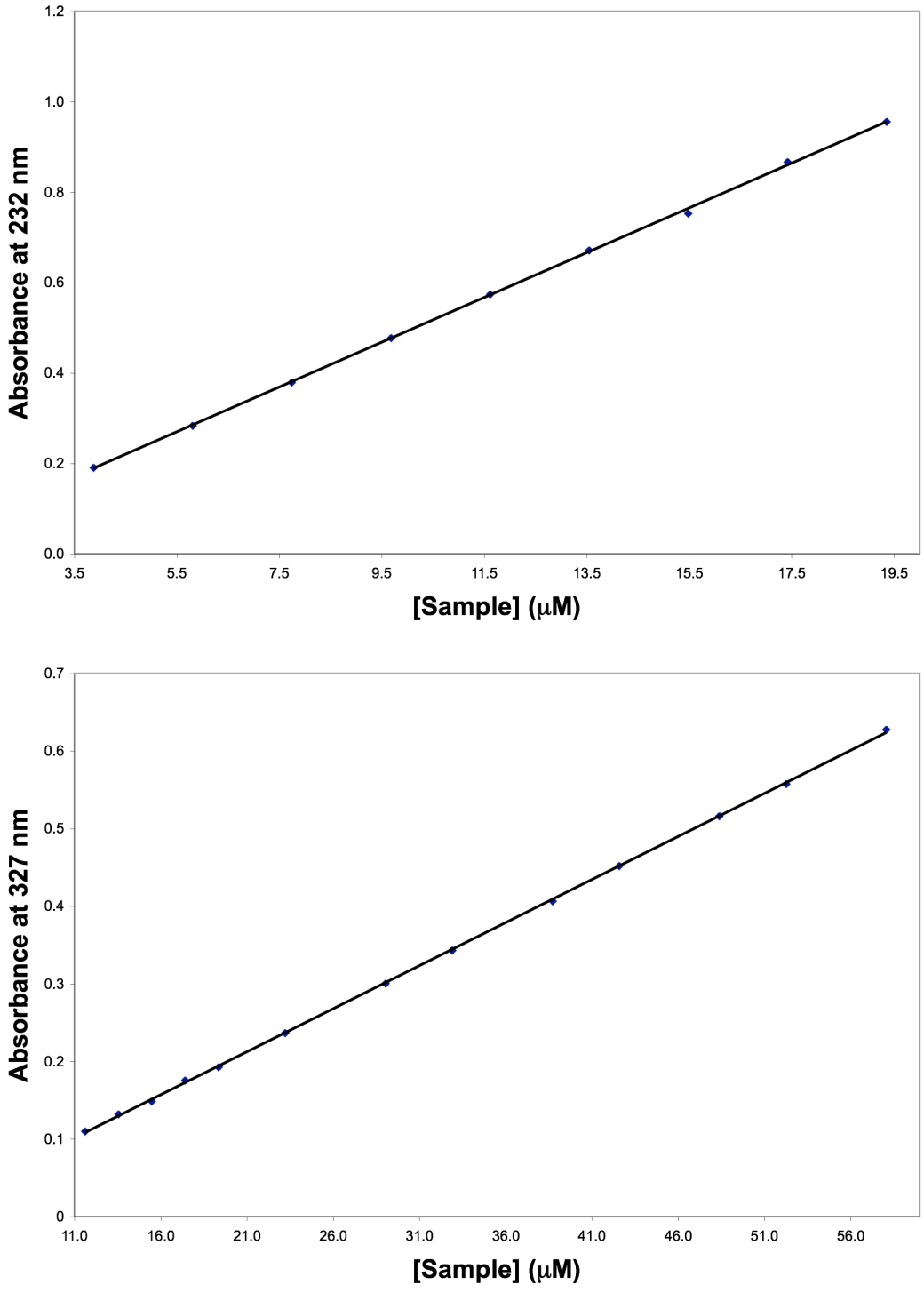

Figure 2.29: Linear fit of absoption maxima for **2** a) 232 nm, ε=49.9 $mM^{-1}cm^{-1}$, b) 327 nm ε=10.1 $mM^{-1}cm^{-1}$ for **2**. Black lines are linear fits using Origin 7.5.

With the successful determination of the absorption wavelengths and the corresponding extinction coefficients, attention was turned to the determination of the

fluorescence emission maxima for all of the compounds and the determination of the E_{00} values.

The fluorescence spectra for all compounds were carried out in 100mM NaCl, 10mM sodium phosphate pH 7 buffer. Attempts to obtain the fluorescence spectra under aerobic conditions were met with failure due to the lack of reproducibility, namely the maximum fluorescence intensity of the same sample measured multiple times gave erratic values. When attempts to limit the oxygen in the system were undertaken the maximum fluorescence intensity of the samples yielded reproducible values. All were bubbled with N_2 for 2 minutes and placed into the spectrophotometer. The analysis chamber was then purged with N_2 for a minimum of five minutes while the sample was stirred. Using the λ_{max} values determined in the UV-Vis studies, the fluorescence emission maxima were determined. (**Table 2.1**)

	λ_{max} (nm)	ε (mM^{-1} cm^{-1})	λ_{ex} (nm)	λ_{em} (nm)
1	231	50.0 ± 1.30	323	404
	324	8.86 ± 0.13		
2	231	50.5 ± 4.40	327	409
	326	10.7 ± 0.20		
3	232	42.4 ± 0.80	334	414
	332	10.8 ± 0.40		
4	231	33.9 ± 0.60	317	427
	318	7.28 ± 0.06		
5	232	28.9 ± 0.70	327	429
	327	7.88 ± 0.51		
6	231	22.0 ± 1.10	312	433
	312	5.93 ± 0.31		

Table 2.1: Tabulated results of Uv-Vis and fluorescence characterization of **1**-**6** for use in the determination of E_{00} values**.** (Error values represent standard deviation of a minimum of three separate determinations)

Normalizing the maximum intensity of absorption and emission spectra of each compound to the other allowed the determination of the E_{00} values through the use of the

mirror image rule for fluorescence. In fluorescence spectroscopy, a compound is excited from its ground state 0 vibrational energy level (S_0) to an excited singlet vibrational level (S_n^*). Once in the S_n^* vibrational energy, the electron undergoes rapid ($>10^{-12}$ sec) internal conversion to the S_0^* state. As the electron undergoes internal conversion it loses a small amount of energy. This loss of energy leads to emission relaxation of a less energetic electron, thus yielding shift in the emission spectrum called the Stokes shift. Based on the Franck-Condon factor, the electron will return to the ground state S_n and subsequently undergo internal conversion to return to the S_0, which leads to a mirror image of the excitation spectrum. As the excitation spectrum represents the $S_0 \rightarrow S_n^*$ and the emission spectrum represents the $S_0^* \rightarrow S_n$ transition, the point at which they cross represents the $S_0 \rightarrow S_0^*$ transition that cannot be experimentally measured. A sample E_{00} determination for **1** is shown. (**Figure 2.30**)

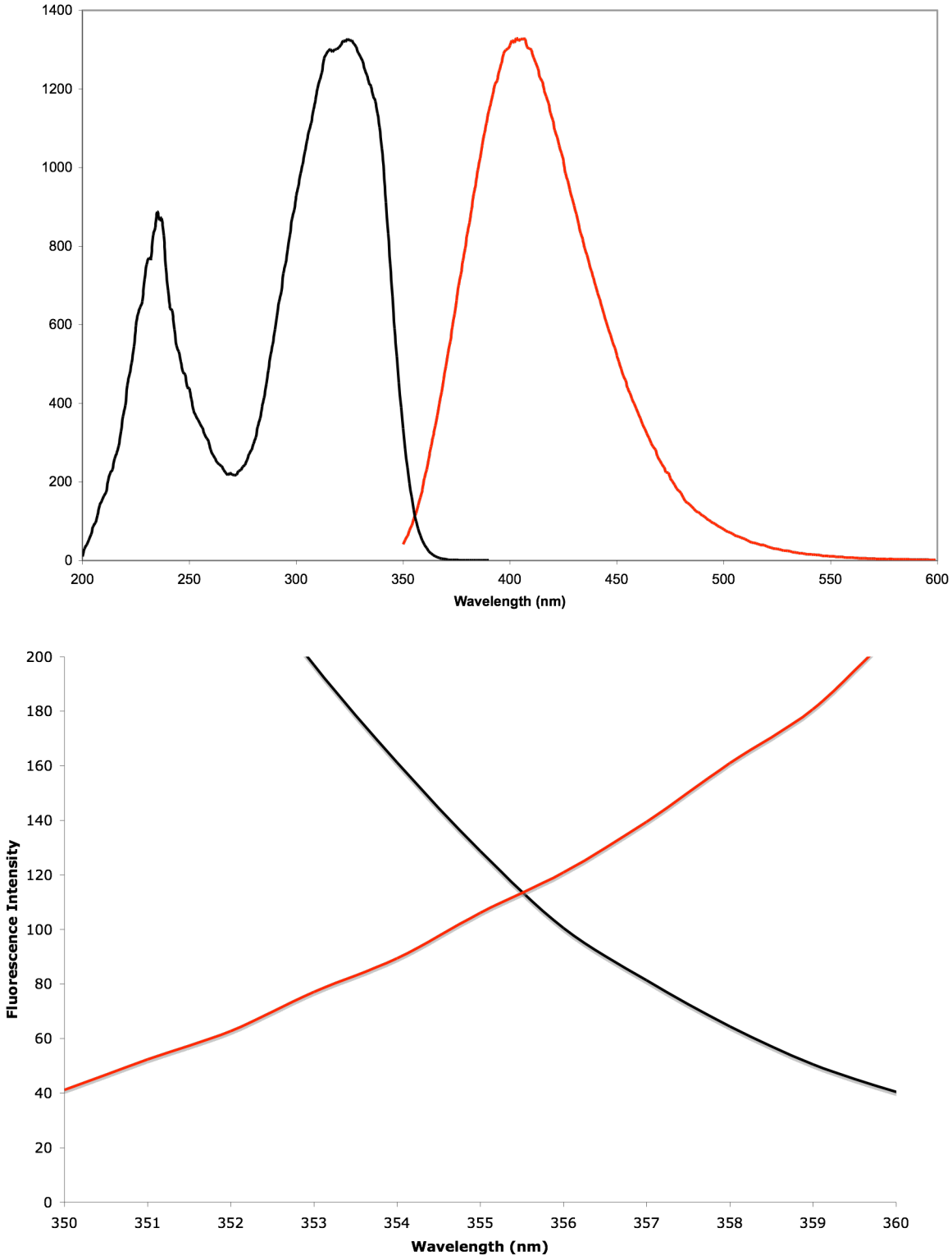

Figure 2.30: Determination of E_{00} value for **1** in 100 mM NaCl, 10 mM sodium phosphate pH 7 buffer.

Calculation of the E_{00} values was accomplished using the relationship between energy and wavelength. (**Equation 2.1**)

$$E = \frac{c \bullet h}{\lambda}$$

Equation 2.1: Conversion of wavelength to energy. c=speed of light ($3x10^8$ m/s), h=Planck's constant ($6.63x10^{-34}$ J s), λ=wavelength in nm**.**

While this equation does give the energy at the wavelength of interest, that energy is in units of Joules. Using conversions of 1 eV=$1.602x^{-19}$ J and 1eV=23.06 kcal/mol the E_{00} = energies for all the compounds can be readily calculated. (**Table 2.2**)

	1	**2**	**3**	**4**	**5**	**6**
λ_{00} (nm)	355	362	364	366	372	366
E_{00} (kcal/mol)	80.5	79.0	78.6	78.1	76.9	78.1

Table 2.2: Calculated E_{00} values for **1-6**. Estimated error ±0.2% based on ± 1 nm measurement of λ_{00}.

2.7.2 Determination of E_{ox}* values

E_{ox}^* values are calculated from the E_{oo} and E_{ox} values for all the compounds using **Equation 2.2**.[48]

$$E_{ox}^{*}(V) = E_{ox}(V) - \frac{E_{00}(kcal/mol)}{23.06}$$

Equation 2.2: Calculation for determining E_{ox}^*

With the E_{00} values determined above, the E_{ox} for each of the compounds was also necessary . Initial attempts to determine the E_{ox} value for DAN through cyclic voltammetry (CV) failed as DAN formed a polymer film on the platinum electrode.[79-81] Amy Finch, also from the Roktia lab, was able to measure the E_{ox} values by using alternating current voltammetry during an internship at the Army Research Labs in

Adelphi, MD.[82] Using the values of the E_{ox} determined by Amy Finch, the E_{ox}^* values were calculated. (**Table 2.3**)

	E_{ox} (V)	E_{ox}^* (V)
1	0.250 ± 0.020	-3.24± 0.02
2	0.220 ± 0.006	-3.24± 0.01
3	0.208 ± 0.000	-3.18± 0.00
4	0.380 ± 0.006	-3.01± 0.01
5	0.350 ± 0.002	-2.98± 0.00
6	0.400 ± 0.007	-2.99± 0.01

Table 2.3: E_{ox} and E_{ox}^* values for donors. E_{0x} values supplied by Amy Finch (Rokita lab member interning at Army research labs in Adelphi, MD).

The successful determination of the E_{ox}^* values begins to give insight into what to expect when the compounds are used in the Roktia lab assay. Initially, a continuum of E_{ox}^* values of **1**-**6** was envisioned, which would allow investigation of the driving force dependence of excess electron transport (EET) by allowing correlation of the rate of strand cleavage to the E_o^* values. However, the E_{ox}^* values show that it is more likely there will be two regimes of EET, those with a lower E_{ox}^* value (**1**, **2** and **3**) and those with a higher E_{ox}^* value (**4**, **5** and **6**). While this was unexpected, the two regimes should still allow the investigation of the driving force dependence of EET.

2.8 Summary

Through the use of Buchwald-Hartwig coupling reactions, compounds **2**-**5** were successfully prepared. While the initial synthetic route was a good starting point, multiple problems were encountered and overcome. The most serious problem that was encountered was the decomposition of **8** using the initial condition of sodium tert-

butoxide. This was overcome through the alternate use of Cs_2CO_3. The final synthetic scheme for the generation of **1**-**6** is summarized in **Figure 2.31**.

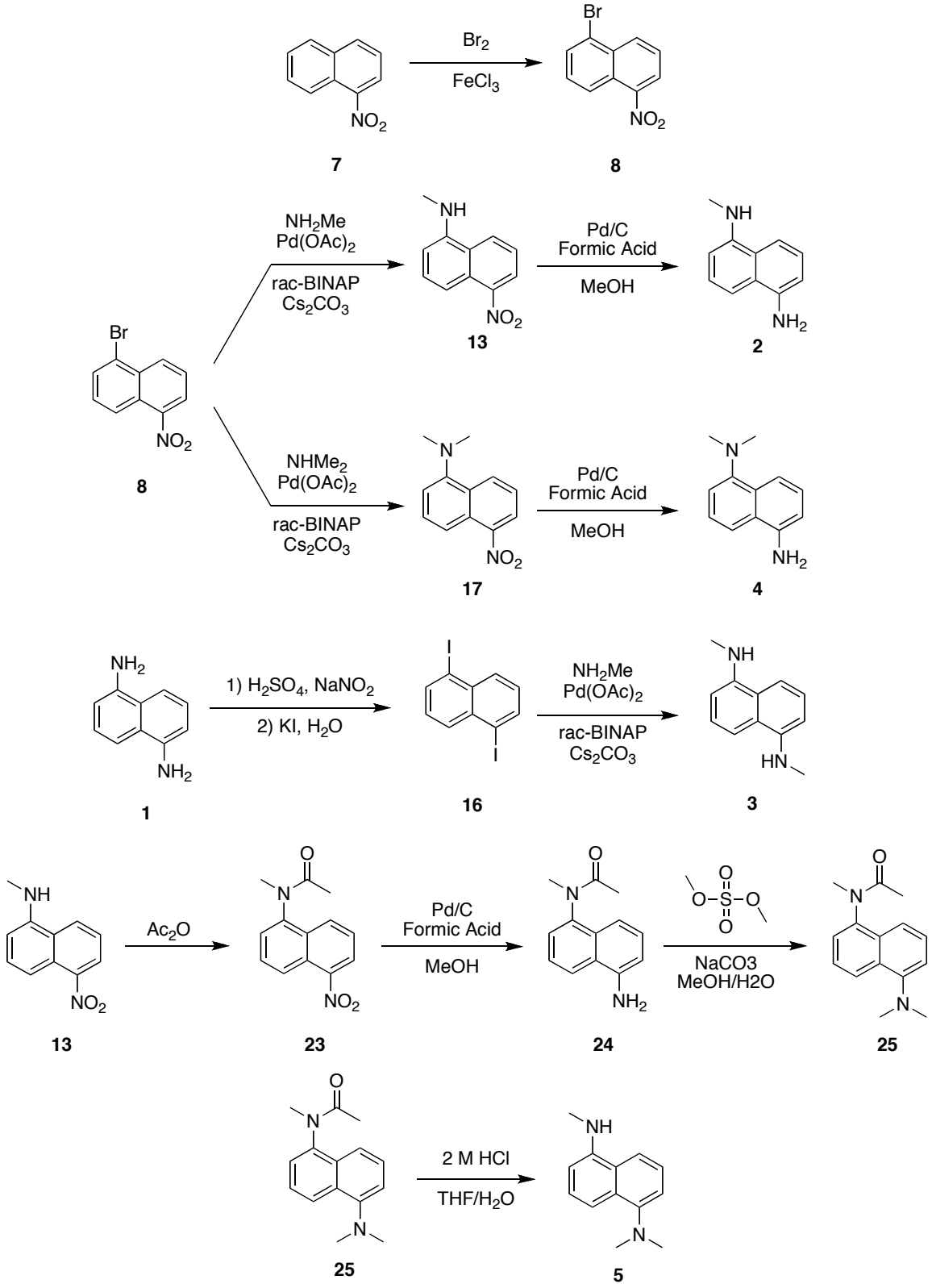

Figure 2.31: Final synthetic scheme for generation of compounds to be used in investigation of the driving force dependence of excess electron transport in DNA.

Once the compounds had been successfully synthesized the photophysical and electrochemical properties were determined. For all compounds the λ_{max}, ε, E_{00}, E_{ox} and E_{ox}^{*} were either physically measured (λ_{max}, ε and E_{ox}) or calculated from the measured values (E_{00} and E_{ox}^{*}). Based on the E_{ox} and E_{ox}^{*} values, two distinct regimes of initial rates of strand scisission induced by EET were expected when the compounds screened. From these two regimes the driving force dependence of EET should determinable.

2.9 Materials and methods

2.9.1 General

Solvents, starting materials, and reagents of the highest commercial grade were used without further purification. All aqueous solutions were prepared with water purified to a resistivity of 17.8-18.0 MΩ. All UV-vis measurements were made using a Hewlett Packard 8453 UV-vis spectrophotometer. Fluorescence spectra were obtained with a Hitachi F-4500 spetrophotometer. NMR spectra were recorded on a Bruker AM400 spectrometer (^{1}H, 400 MHz; ^{13}C, 100 MHz) and referenced to residual protons in the solvents. Chemical shifts (δ) are reported in parts per million (ppm), and coupling constants (J) are reported in hertz (Hz). Electrospray ionization mass spectrometry (ESI-MS) was carried out using a JEOL AccuTOF-CS spectrometer.

2.9.2 Preparation of N1-methylnaphthalene-1,5-diamine (2)

A solution of **6** (300 mg, 1.48 mmol) and methanol (20 mL) was added to an oven-dried round-bottomed flask with a magnetic stir bar. This mixture was stirred at room temperature until **6** was dissolved, at which time 10% palladium on carbon (200 mg, 0.13 mmol) and formic acid (2 mL) were added. The reaction was stirred under nitrogen atmosphere for two hours at room temperature. After two hours, the reaction

mixture was filtered through a plug of Celite 545®. The filtrate was diluted with CH_2Cl_2, and then washed with saturated $NaHCO_3$ solution, water and saturated NaCl solution. The organic layer was dried with anhydrous magnesium sulfate, filtered and concentrated to dryness. The crude material was purified by flash column chromatography on silica gel using 10% ethyl acetate:hexanes to give **2** as dark red solid (168 mg, 65%). ^{1}H NMR (400 MHz, $CDCl_3$, ppm 7.35 (t, *J* = 8.00, 1H), 7.23 (t, *J* = 2.71 Hz, 1H), 7.18 (d, *J* = 8.03 Hz, 1H), 6.77 (d, *J* = 2.57 Hz, 1H), 6.75 (d, *J* = 2.54 Hz, 1H), 6.62-6.56 (m, 1H), 4.41 (s, 1H), 4.11 (s, 2H), 2.99 (s, 3H). ^{13}C NMR ($CDCl_3$) δ 145.2, 143.1, 126.1, 125.5, 124.7, 124.5, 111.0, 110.3, 110.2, 104.3, 31.5.

2.9.3 Preparation of N1,N5-dimethylnaphthalene-1,5-diamine (3)

To an oven dried round bottom flask with a magnetic stir bar was added anhydrous toluene (2 mL) and ±-BINAP (65.6 mg, 0.105 mmol). The vial was sealed and heated to 80 ^{o}C until all ±-BINAP dissolved. The vial was cooled to approximately 30 ^{o}C and palladium acetate (47.5% palladium, 11.8 mg) was added. The resulting dark orange solution was cooled to room temperature and stirred for 5 minutes at which time **16** (125 mg, 0.329 mmol) was added. The reaction mixture was then stirred for 10 minutes before cesium carbonate (203 mg, 1.05 mmol) was then added. The mixture was stirred for an additional 20 minutes and then methyl amine (2 M solution in THF, 0.5 mL) was added. The vial was quickly sealed. The reaction was heated to 80 ^{o}C for 48 hours. The dark red reaction mixture was filtered through a plug of Celite 545®, and the plug was rinsed with several portions of CH_2Cl_2. The filtrate was concentrated to dryness. The resulting solid was purified by flash chromatography on silica gel using 5% ethyl acetate:hexane to 20% ethyl acetate:hexanes gradient to give the desired product as a dark red, viscous oil

(54.8 mg, 89% yield). 1H NMR (400 MHz, *CDCl₃*) δ ppm 7.33 (t, *J* = 7.96 Hz, 2H), 7.15 (d, *J* = 8.50 Hz, 2H), 6.60 (d, *J* = 7.56 Hz, 2H), 4.42 (s, 2H), 2.99 (s, 6H).

2.9.4 Preparation of N1,N1-dimethylnaphthalene-1,5-diamine (4)

Solution **6** (761 mg, 3.45 mmol) and methanol (100 mL) were added to an oven-dried, round-bottomed flask with a magnetic stir bar. The mixture was stirred until **17** was dissolved, at which time 10% palladium on carbon (370 mg, 0.350 mmol) and formic acid (2 mL) were added. The reaction was stirred under nitrogen atmosphere for two hours. After two hours, the reaction mixture was filtered through a plug of Celite 545®. The filtrate was diluted with CH_2Cl_2, washed with saturated $NaHCO_3$ solution, water and saturated NaCl solution. The organic layer was dried with anhydrous magnesium sulfate, filtered and concentrated to dryness to give the desired product (523 mg, 80%). 1H NMR (400 MHz, $CDCl_3$) δ ppm 7.69 (d, *J* = 8.52 Hz, 1H), 7.49 (d, *J* = 8.44 Hz, 1H), 7.36 (t, *J* = 7.94, 7.94 Hz, 1H), 7.27 (t, *J* = 7.94, 7.94 Hz, 1H), 7.06 (d, *J* = 7.37 Hz, 1H), 6.76 (d, *J* = 7.35 Hz, 1H), 4.09 (s, 2H), 2.87 (s, 6H).

2.9.5 Preparation of N1,N1,N5-trimethylnaphthalene-1,5-diamine (5)

To a round bottom flask was added **24** (100mg, 0.413 mmol), 25 mL THF and 5 mL 2 N HCl. The reaction mixture was heated to reflux and refluxed overnight. The reaction was then cooled to room temperature, and diluted with ethyl acetate. The resulting organic layer was then neutralized with saturated $NaHCO_3$, and washed with saturated NaCl. The organic layer was then dried over $MgSO_4$, filtered and concentrated to dryness to give the desired product (74.3 mg, 90%). 1H NMR (400 MHz, *CDCl₃* δ ppm 7.68 (d, *J* = 8.54 Hz, 1H), 7.51 (d, *J* = 8.48 Hz, 1H), 7.45 (m, 2H), 7.11 (d, *J* = 7.41 Hz, 1H), 6.64 (d, *J* = 7.51 Hz, 1H), 4.45 (s, 1H), 3.04 (s, 3H), 2.92 (s, 6H).

2.9.6 Preparation N1,N1,N5,N5-tetramethyl-1,5-diaminonapthalene (6)

A round bottom flask equipped with a magnetic stir bar and nitrogen inlet was charged with 6 mL methanol, 3 mL water and 3 mL THF. To this stirring solution **1** (100 mg, 0.632) and Na_2CO_3 (1.00 g, 9.44 mmol) were added in a single portion. Dimethyl sulfate (1 mL, 16.7 mmol) was then added to the solution and the solution was stirred overnight under N_2. The reaction was neutralized with 1 M NaOH to a pH >11, extracted with ethyl acetate. The organic layer was dried over $MgSO_4$, filtered and concentrated to dryness giving the desired material (109 mg, 80%). The NMR consistent with published values.

2.9.7 Preparation of 1-Bromo-5-nitronapthalene (8)

A mixture of 1-nitronapthalene (10.0g, 57.8 mmol) and $FeCl_3$ (0.064g, 0.40 mmol) was created in an oven-dried round-bottomed flask with attached condenser. The mixture was slowly heated to 90^{o}C in an oil bath until 1-nitronapthalene had melted. Br_2 (2.96 mL, 57.8 mmol) was added drop wise through the top of the condenser. The resulting mixture was heated for 2 hours at 90 ^{o}C. The resulting solid was recrystalized from ethanol to give a brown-yellow fluffy solid (6.28 g, 43%). 1H NMR (400 MHz, $CDCl_3$) δ ppm 8.53 (d, *J* = 8.57 Hz, 1H), 8.40 (d, *J* = 8.77 Hz, 1H), 8.18 (dd, *J* = 7.61, 1.04 Hz, 1H), 7.87 (dd, *J* = 7.48, 0.83 Hz, 1H), 7.48 (dd, *J* = 8.74, 7.53 Hz, 1H), 7.60 (dd, *J* = 8.50, 7.70 Hz, 1H). ^{13}C NMR (101 MHz, *$CDCl_3$*) δ ppm 147.3, 133.1, 132.6, 131.6, 129.3, 126.3, 125.5, 124.3, 123.5, 122.8. Melting Point: 119-120°C (lit. 119-120 °C)

2.9.8 Preparation of N-benzyl-5-nitronaphthalen-1-amine (13)

To an oven dried round bottom flask with a magnetic stir bar was added anhydrous toluene (2 mL) and ±-BINAP (25 mg, 0.040 mmol) was added to an oven dried round

bottom flask with a magnetic stir bar. The flask was sealed with a rubber septum and the mixture was heated to 80 ºC until all of the ±-BINAP dissolved. The resulting solution was cooled to approximately 30 ºC and palladium acetate (47.5% Palladium, 4.45 mg, 0.0198 mmol) was added. The mixture immediately turned orange and was stirred for 5 minutes. The resulting orange solution was cooled to room temperature. To this solution **8** (250 mg, 0.992 mmol) was added in a single portion, at which point the solution turned dark brown. The solution was stirred for 20 minutes at room temperature then cesium carbonate (450 mg, 1.40 mmol) was added. The mixture was stirred for 20 minutes then benzyl amine (127 mg, 1.19 mmol) was added. The flask was quickly sealed and heated to 80 ºC for 48 hours. By the end, the mixture was a dark red solution, which was cooled to room temperature and filtered through a plug of Celite 545®. The filter cake was rinsed with several portions of CH_2Cl_2 and the filtrate was concentrated to dryness. The crude material was purified by flash column chromatography on silica gel using 5% ethyl acetate:hexane to 10% ethyl acetate:hexanes gradient to give the desired product (179 mg, 65% yield). ^1H NMR (400 MHz, $CDCl_3$ δ ppm 8.30 (d, J = 8.53 Hz, 1H), 7.50 (m, 3H), 7.36 (d, J = 7.16 Hz, 1H), 7.16 (dd, J = 6.36 Hz, 1H), 3.37 (s, 3H), 2.94 (s, 6H), 1.80 (s, 3H).

2.9.9 Preparation of N-methyl-5-nitronaphthalen-1-amine (13)

Anhydrous toluene (100 mL) and ±-2,2'-bis(diphenylphosphine)-1,1'-binapthyl (±-BINAP, 247 mg, 0.397 mmol) was added to an oven dried round bottom flask with a magnetic stir bar. The flask was sealed with a rubber septum and the mixture was heated to 80 ºC until all of the ±-BINAP dissolved. The resulting solution was cooled to approximately 30 ºC and palladium acetate (47.5% Palladium, 71.3 mg, 0.317 mmol) was

added. The mixture immediately turned orange and was stirred for 5 minutes. The resulting orange solution was cooled to room temperature. To this solution **8** (1.00 g, 3.97 mmol) was added in a single portion, at which point the solution turned dark brown. The solution was stirred for 20 minutes at room temperature, and then cesium carbonate (1.29g, 3.97 mmol) was added. The mixture was stirred for an additional 20 minutes before methyl amine (2 M in THF, 2.40 mL) was added. The flask was quickly sealed and heated to 80 ºC for 48 hours. By the end, the mixture was a dark red solution, which was cooled to room temperature and filtered through a plug of Celite 545®. The filter cake was rinsed with several portions of CH_2Cl_2 and the filtrate was concentrated to dryness. The crude material was purified by flash column chromatography on silica gel using 5% ethyl acetate:hexane to 10% ethyl acetate:hexanes gradient to give the desired product (523 mg, 65% yield). 1H NMR (400 MHz, $CDCl_3$) δ ppm 8.05 (t, *J* = 8.50 Hz, 1H), 7.76 (d, *J* = 8.69 Hz, 1H), 7.53 (t, *J* =.22 Hz, 1H), 7.39 (t, *J* = 8.05 Hz, 1H), 6.67 (d, *J* = 7.72 Hz, 1H), 4.62 (s, 1H), 3.00 (s, 3H). ^{13}C NMR (101 MHz, *CDCL₃*) δ ppm 147.5, 144.8, 130.4, 126.0, 125.9, 124.6, 123.3, 122.5, 111.3, 105.5, 31.0. M.P.: 135-137 °C.

2.9.10 Preparation of 1,5-diiodonapthalene (16)[65]

To a solution of sodium nitrite (3.00 g, 44 mmol) and concentrated sulfuric acid (25 mL) at 0°C was added drop wise a solution of **1** (3.00 g, 19 mmol) in glacial acetic acid (25 mL). The mixture was stirred for 30 minutes at 0 ºC and then poured onto a mixture of ice (70 g) and urea (0.25 g). The resulting mixture was stirred for 20 minutes. A solution of potassium iodide (100g, 602 mmol) in water (100 mL) was slowly added. (Vigorous bubbling was noted.) The reaction mixture was stirred overnight under reduced pressure to remove gas that had evolved. The mixture was filtered and the

isolated solid was dissolved in methylene chloride 100 mL, and extracted 3x100 mL water, 2x100 mL saturated brine, dried of sodium sulfate. The mixture was then filtered. The filtrate was refluxed with activated carbon for 30 minutes. The mixture was filtered through Celite and concentrated to dryness to give a dark brown solid (4.5g, 63%). 1H NMR (400 MHz, *CD*Cl_3) δ ppm 8.13 (d, *J* = 3.53 Hz, 2H), 8.11 (d, *J* = 2.05 Hz, 2H), 7.24 (t, *J* = 7.84 Hz, 2H).

2.9.11 Preparation of N1,N1-dimethyl-5-nitronaphthalen-1-amine (17)

Anhydrous toluene (25 mL) and ±-2,2'-bis(diphenylphosphine)-1,1'-binapthyl (±-BINAP, 25 mg, 0.040 mmol) were added to an oven-dried round-bottomed flask with a magnetic stir bar. The flask was sealed with a rubber septum and the mixture was heated to 80^{o}C until all of the ±-BINAP dissolved. The resulting solution was cooled to approximately 30 ºC and palladium acetate (47.5% Palladium, 9.4 mg, 0.020 mmol) was added. The mixture immediately turned orange and was stirred for 5 minutes. The resulting orange solution was cooled to room temperature. **8** (100 mg, 0.40 mmol was added to the solution) in a single portion, at which point the solution turned dark brown. The solution was stirred for 20 minutes at room temperature then cesium carbonate (160 mg, 0.48 mmol) was added. The mixture was stirred for an additional 20 minutes before dimethyl amine (2 M in THF, 300 μL) was added. The flask was quickly sealed and heated to 80 ºC for 48 hours. The dark red solution was cooled to room temperature and filtered through a plug of Celite 545®. The filter cake was rinsed with several portions of CH_2Cl_2 and the filtrate was concentrated to dryness. The crude material was purified by flash column chromatography on silica gel using 5% ethyl to give the desired (64 mg, 75% yield) product as a dark red oil. ^{1}H NMR (400 MHz, $CDCl_3$) δ ppm 8.53 (d, *J* =

8.49 Hz, 1H), 8.13-8.07 (m, 2H), 7.54 (t, *J* = 8.14 Hz, 1H), 7.46 (t, *J* = 8.04 Hz, 1H), 7.14 (d, *J* = 7.48 Hz, 1H), 2.85 (s, 6H). ^{13}C NMR (101 MHz, $CDCl_3$) δ ppm 151.6, 147.3, 130.7, 130.1, 129.4, 126.5, 123.6, 123.1, 117.2, 115.5, 45.3.

2.9.12 Preparation of N-methyl-N-(5-nitronaphthalen-1-yl)-acetamide (23)

To a round bottom flask containing **13** (52.3 mg, 0.259 mmol) was added acetic anhydride (3 ml). The reaction mixture was refluxed overnight, yielding a yellow solution. The reaction mixture was then cooled to room temperature and diluted with 25 mL water. The resulting solution was adjusted to pH 7 using saturated sodium bicarbonate solution. The solution was extracted 3x50 ml methylene chloride. The organic layers were combined and washed with 100 mL water and 100 mL saturated NaCl solution, dried over magnesium sulfate, and concentrated to dryness to yield a yellow-orange solid. The resulting solid was purified by flash chromatography on silica gel using 5% ethyl acetate:hexane to 20% ethyl acetate:hexanes gradient to give the desired product (46.4 mg, 73% yield). 1H NMR (400 MHz, $CDCl_3$) δ ppm 8.30 (d, *J* = 8.53 Hz, 1H), 7.50 (m, 3H), 7.36 (d, *J* = 7.16 Hz, 1H), 7.16 (dd, *J* = 6.36 Hz, 1H), 3.37 (s, 3H), 2.94 (s, 6H), 1.80 (s, 3H).

2.9.13 Preparation of N-(5-aminonaphthalen-1-yl)-N-methyl-acetamide (24)

A solution of **23** (200 mg, 0.989 mmol) and methanol (20 mL) were added to an oven-dried, round-bottomed flask with a magnetic stir bar. The mixture was stirred until **23** was dissolved, at which time 10% palladium on carbon (105 mg, 0.0989 mmol) and formic acid (2 mL) were added. The reaction was then stirred under nitrogen atmosphere for two hours. After two hours, the reaction mixture was filtered through a plug of Celite 545®. The filtrate was diluted with CH_2Cl_2, washed with saturated $NaHCO_3$ solution,

water and saturated NaCl solution. The organic layer was dried with anhydrous magnesium sulfate, filtered and concentrated to dryness to give the desired product (175 mg, 81%). 1H NMR (400 MHz, *CDCl₃* δ ppm 7.88 (d, *J* = 8.53 Hz, 1H), 7.49-7.43 (m, 1H), 7.40-7.32 (m, 2H), 7.23 (d, *J* = 8.42 Hz, 1H), 6.85 (d, *J* = 7.38 Hz, 1H), 4.33 (s, 2H), 3.34 (s, 3H), 1.77 (s, 3H).

2.9.14 Preparation of N-(5-(dimethylamino)naphthalen-1-yl)-N-methylacetamide (25)

A round bottom flask equipped with a magnetic stir bar and nitrogen inlet was charged with 6 mL methanol, 3 mL water and 3 mL THF. To this stirring solution **24** (100 mg, 0.467) and Na_2CO_3 (198 mg, 1.87 mmol) were added in a single portion. Dimethyl sulfate (0.176 mL, 1.87 mmol) was then added to the solution and the solution was stirred overnight under N_2. The reaction was neutralized with 1 M NaOH to a pH >11, extracted with ethyl acetate. The organic layer was dried over $MgSO_4$, filtered and concentrated to dryness giving the desired material (93.6 mg, 80%). ^{1}H NMR (400 MHz, $CDCl_3$ δ ppm 8.30 (d, *J* = 8.53 Hz, 1H), 7.50 (m, 3H), 7.36 (d, *J* = 7.16 Hz, 1H), 7.16 (dd, *J* = 6.36 Hz, 1H), 3.37 (s, 3H), 2.94 (s, 6H), 1.80 (s, 3H). 13C NMR (101 mHz, $CDCl_3$) δ ppm 171.2, 152.3, 141.0, 132.3, 130.7, 127.1, 126.9, 125.3, 124.2, 117.1, 115.1, 45.9, 37.2, 22.2.

Chapter 3
Use of non-covalently bound 1,5-diaminonapthalene derivatives to investigate excess electron transport in DNA

3.1 Introduction

The Rokita lab has developed a photochemical assay using oligonucleotides containing an abasic site and a ^{Br}U that allows for screening of compounds to be used in the investigation of EET in DNA.[48] (**Figure 3.1**)

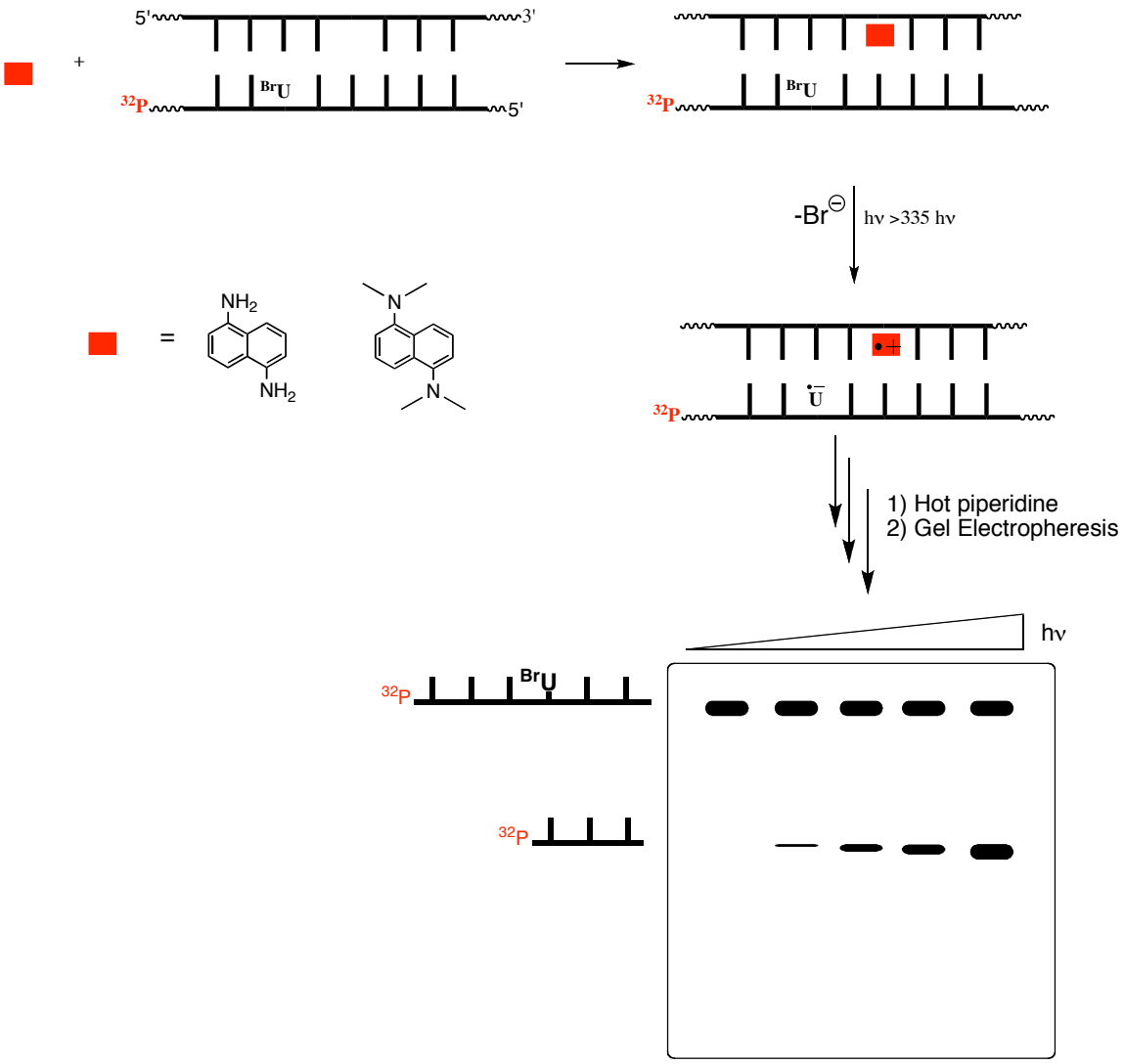

Figure 3.1: Non-covalent assay for screening compounds to be used investigation of EET in DNA.

The assay uses 1,5-diaminonapthyl amines as photoinducable electron donors due to their ready availability and their absorption maxima above 300 nm.[47] The use of the ^{Br}U as the electron acceptor was chosen for three reasons: 1) it is commercially available, 2) it

readily incorporates into oligonucleotides through standard phosphoramidite chemistry, and 3) it can be used to readily detect the effects of excess electron transport (EET) as formation of the uracil radical formation generates oxidized, base labile sites in the DNA.[83]

When in duplex DNA, the uracil radical can abstract either the C1' or the C2' hydrogen atom from the base adjacent to it.[84,85] Ultimately, the resulting radicals lead to either alkaline induced or direct strand scission. The relative percent of either form of strand scission has been proposed to depend on the conformation of the DNA.[84] However, the total amount of strand scission observed appears independent of both conformation of the DNA and presence of oxygen.[84]

While the ^{Br}U is an effective electron trap and subsequent indicator of strand scission induced by EET, it is not without its weaknesses. The major weakness encountered when using ^{Br}U in photochemical assays is that its absorption spectrum extends past 300 nm. This extended absorption band, coupled with the wavelengths used in the assay, lead to direct irradiation of the ^{Br}U, which then leads to a minor amount of background strand scission. This weakness does not affect the data obtained using the assay above as the 335 nm filter eliminates the possibility of direct irradiation of the ^{Br}U moiety.

In previous studies it was found that **1** showed greater efficiency at inducing strand cleavage due to EET than **6**.[48] When the efficiency of strand scission was compared to the E_{ox}^* values (-3.06 V and -2.8 V respectively), it was found that the compound with the larger negative oxidation potential had greater EET induced strand scission. Investigation of the correlation between the E_{ox}^* and the amount of EET

induced strand scission was carried out using the compounds prepared in Chapter 2 in the above assay (**Figure 3.1**) and oligonucleotides 1 and 2 (**ODN1** and **ODN2**) to determine the initial rate of strand scission induced by EET. (**Figure 3.2**) Correlation of the initial rates of strand scission and the E_{ox}^{*} values will allow the determination of the existence of a driving force dependence of EET.

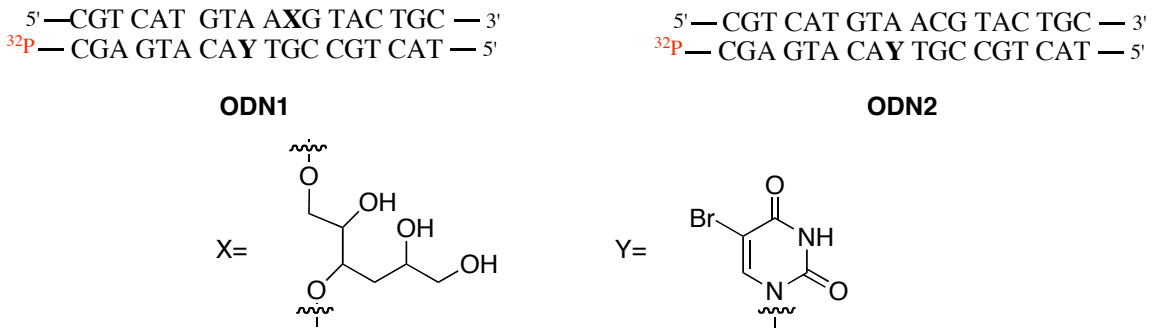

Figure 3.2: Oligonucleotides used to study driving force dependence of EET.

ODN1 and **ODN2** allowed for the determination of the extent to which several vital factors could affect driving force dependence of EET, namely:

1) The amount of direct strand scission versus scission at the 5'-thymine, allowing the determination of the amount of background scission
2) The amount of strand scission induced by the base lability of ^{Br}U
3) Qualitative verification that the compounds associated with the abasic site of the DNA, allowing the determination of the necessity of the abasic site for injection of excess electron into the duplex DNA

With these factors determined, correlation of the initial rates of strand scission and the E_{ox}^{*} values will give insight into the dependence of EET on driving force of the electron donor.

3.2 Results and Discussion

3.2.1 Screening of compounds 1-6 under aerobic conditions

Initial studies were carried out under aerobic conditions, as it had been shown previously, using a slightly DNA sequenced ,that the presence of ambient levels of molecular oxygen reduced the process of EET by less than 20% or led to degradation of the oligonucleotides.[48] The first study undertaken used all the compounds with **ODN1** at a fixed time point of photoirradiation. Additionally, a control containing only ODN1 was added to determine the effect of photolysis and piperidine treatment had on the duplex. (**Figure 3.3**). This study served two purposes: 1) Verify that all compounds would be active in the assay and 2) Determine the amount of scission induced by directed irradiation of the ^{Br}U.

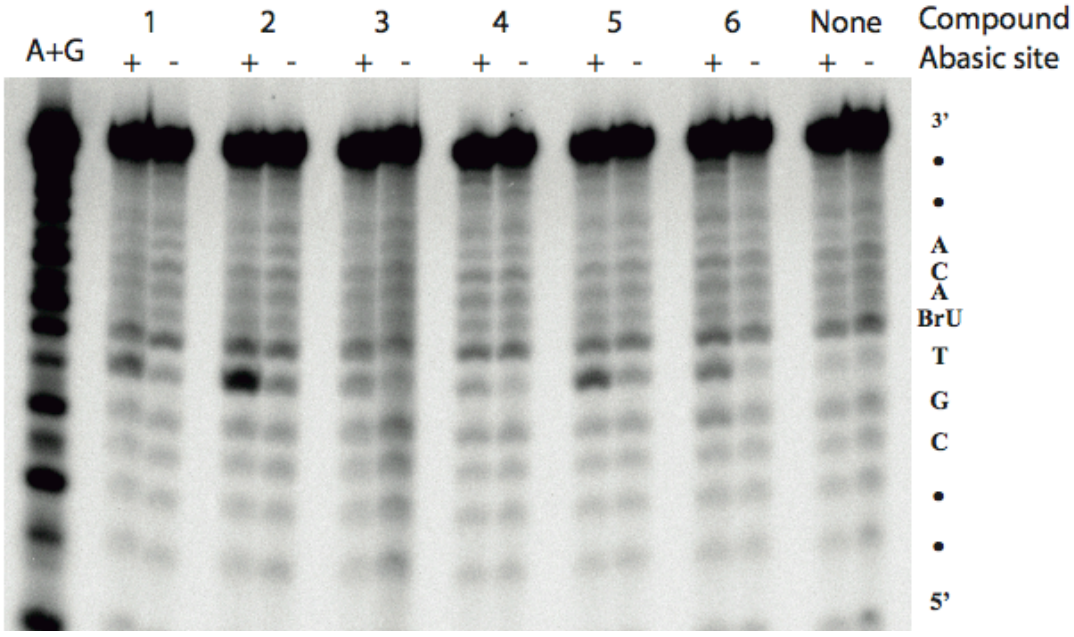

Figure 3.3: Phosphoimage of 20% denaturing polyacrylamide gel showing strand scission induced by EET for ^{32}**P-ODN**1(+) and ^{32}**P-ODN2**(-) using 1 uM electron donor (**1-6**) in 100 mM NaCl, 10 mM sodium phosphate pH 7 buffer. All samples were photoirradiated for 4 minutes under aerobic conditions and treated with piperidine.

When the amount of strand scission induced by EET was examined, (**Figure 3.4**), two important observations were made. There was a significant difference in the amount of scission induced at the 5'-thymine (5'-T) with the presence of the abasic site (**ODN1 5'-T**) versus without the abasic site (ODN2 5'-T), indicating that the all compounds are active in the assay and capable of inducing EET in the duplex DNA. Additionally, the amount of scission observed at the ^{Br}U with **ODN1** (ODN1 BrU) and **ODN2** (ODN2 BrU) indicated that the amount of background cleavage due to direct radiation is consistent regardless of the electron donor used.

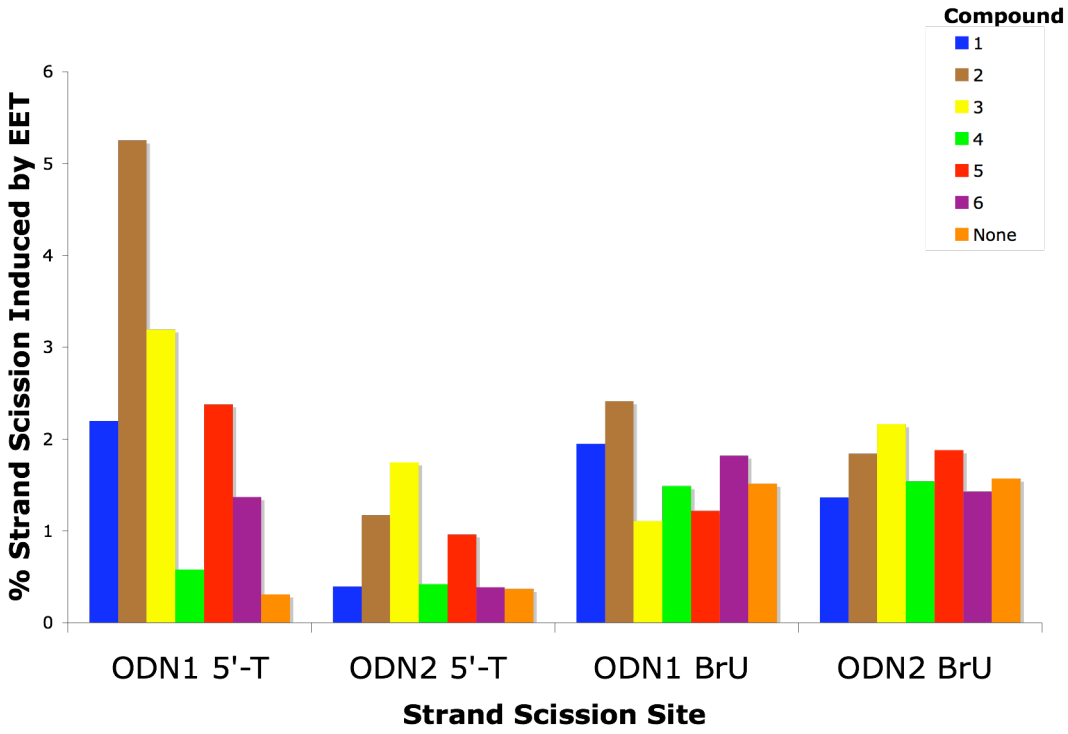

Figure 3.4: Analysis of a single detemination of stand scission induced by EET for **ODN1** and **ODN2** (**Figure 3.1**) under aerobic conditions using 4 minutes of photoirraditaion. Compounds used in assay are **1** (blue), **2** (brown), **3** (yellow), **4** (green), **5** (red), **6** (purple). Control sample with no electron donor (orange). Samples were prepared in 100 mM NaCl and 10 mM sodium phosphate pH 7 buffer. **ODN1** and **ODN2** concentrations were 1.5 μM and electron donor concentration was 1 mM.

Having successfully determined that the compounds were active in the assay, and having quantified the amount of background cleavage from direct irradiation of the ^{Br}U in the

assay conditions, attention turned to the determination of strand scission generated from the treatment of the samples with hot piperidine. ^{Br}U is known to induced strand cleavage when it is heated in hot alkaline conditions.[86] The overall amount of this cleavage occurring in this assay needed to be determined so that it could be accounted for in the analysis of subsequent data. All compounds were photoirradiated for four minutes in the presence of **ODN1**. After photoirradiation, one half of each sample was treated with hot piperidine while the second half was not. The samples were then analyzed. (**Figure 3.5**)

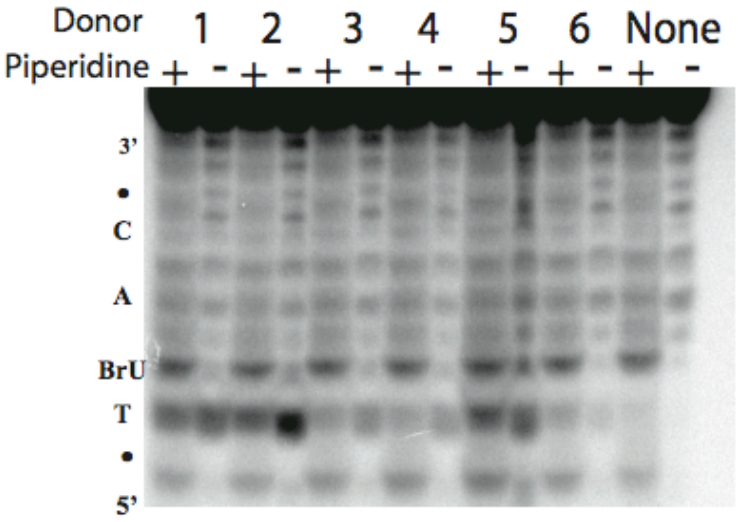

Figure 3.5: Phosphoimage of 20% denaturing polyacrylamide gel showing strand scission induced by EET for ODN1 with piperidine treatment (+) and without piperidine treatment (-) using 1 mM electron donor (**1-6**) in 100 mM NaCl, 10 mM sodium phosphate pH 7 buffer with 1.5 μM **ODN1**.

Analysis showed an increase in the strand scission at the ^{Br}U site of **ODN1** for samples that had been treated with piperidine. (**Figure 3.5**). This result was not unexpected due to the inherent base lability under hot basic conditions.[86] The most important result from this assay was that the overall amount of strand scission induced at the 5'T did not significantly increase for the electron donors. This result further indicated that the strand

scission that is induced at the 5'-T is due solely to the ability of **1-6** to induce strand scission due to EET in the duplex.

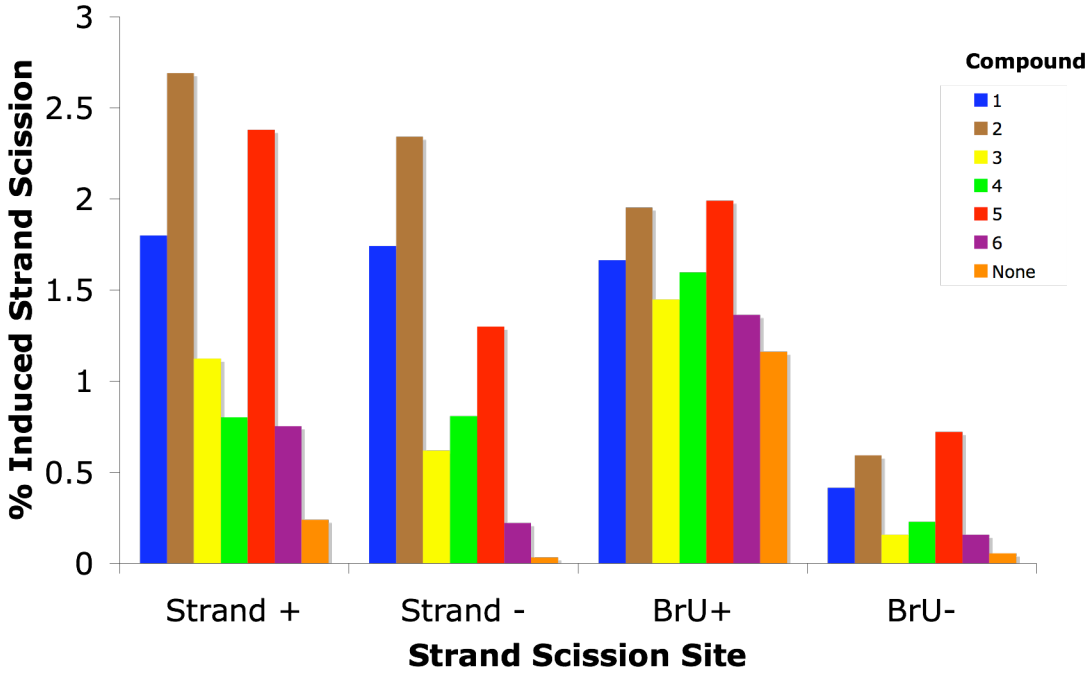

Figure 3.6: Analysis of a single determination of stand scission induced by EET for 1.5 mM **ODN1** (**Figure 3.5**) under aerobic conditions with (+) and without (-) treatment of hot piperidine using 4 minutes of photoirraditaion. Compounds (1 mM concentration in 100 mM NaCl, 10 mM sodium phosphate buffer) used in assay are **1** (blue), **2** (brown), **3** (yellow), **4** (green), **5** (red), **6** (purple). Control sample with no electron donor (orange).

From the studies above, factors that affected the interpretation of the amount of strand scission induced by EET were successfully analyzed. The presence of the abasic site and subsequent association of **1-6** were all critical for the detection of the amount of strand scission due to EET. Additionally, the consistent strand scission induced by the direct irradiation of the ^{Br}U indicated that the conformation of the DNA does not alter significantly enough to be detectable by this assay, therefore it is not an issue. Finally, the above studies indicated that the base lability of the ^{Br}U does not significantly increase the amount of 5'-T cleavage, thus allowing interpretation of the scission seen at 5'-T as solely due to the electron donor.

With the factors accounted for, determination of the initial rates of strand scission due to EET for **1-6** was undertaken to determine the driving force dependence of EET in duplex DNA.

3.2.2 Determination of initial rates for 1-6 under aerobic conditions

Determination of the initial rates for **1-6** was carried out by photoirradiating samples for increasing lengths of time under aerobic conditions. The time points 0, 0.5, 1, 2, 5, 10, 20, and 30 minutes were chosen as starting points to use for the determination of the initials rates as they had been used in previous studies.[43,47] Compound **1** was chosen for initial studies as it showed consistent results between the studies above. The samples were photoirradiated for the specified length of time and were treated with piperidine and analyzed by gel electrophoresis. (**Figure 3.7**)

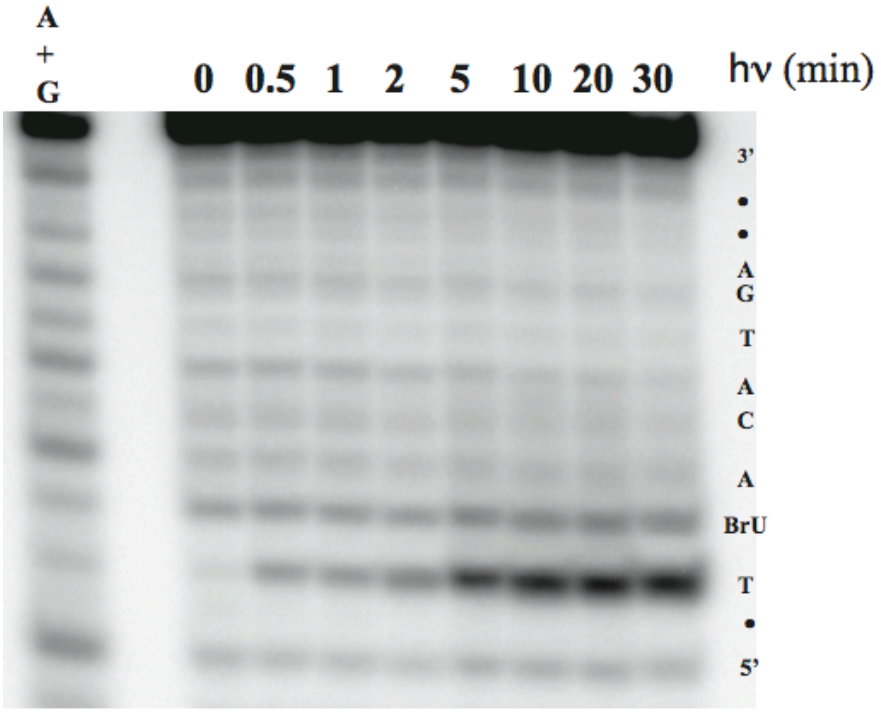

Figure 3.7: Phosphoimage of 20% denaturing polyacrylamide of initial rate of strand scission of **ODN1** (1.5 uM) due to EET for **1 (1** uM) under anaerobic conditions in 100 mM NaCl, 10 mM Sodium phosphate pH 7 buffer.

The amount of strand scission induced by EET was analyzed using ImageQuant 5.2 to determine the percent of the total area the 5'-T and ^{Br}U scission accounted for in each lane. Analysis and subsequent linear fitting of the data to an exponential growth curve using Origin 7.5 yielded several results. (**Figure 3.8**) A clear initial rate of 5'-T strand scission was observed when the 0, 0.5, 1, 2, and 4 minute time points were plotted, and was found to be 0.78%/minute. Additionally, it was noted that the amount of 5'-T strand scission reached a maximum value after being irradiated for 10 minutes. It was hypothesized that the maximal strand scission was due to the photodegradation of **1** upon extended exposure to light. Additionally, the amount of strand scission at ^{Br}U remained relatively constant, confirming that while some background cleavage did occur, it was not significant.

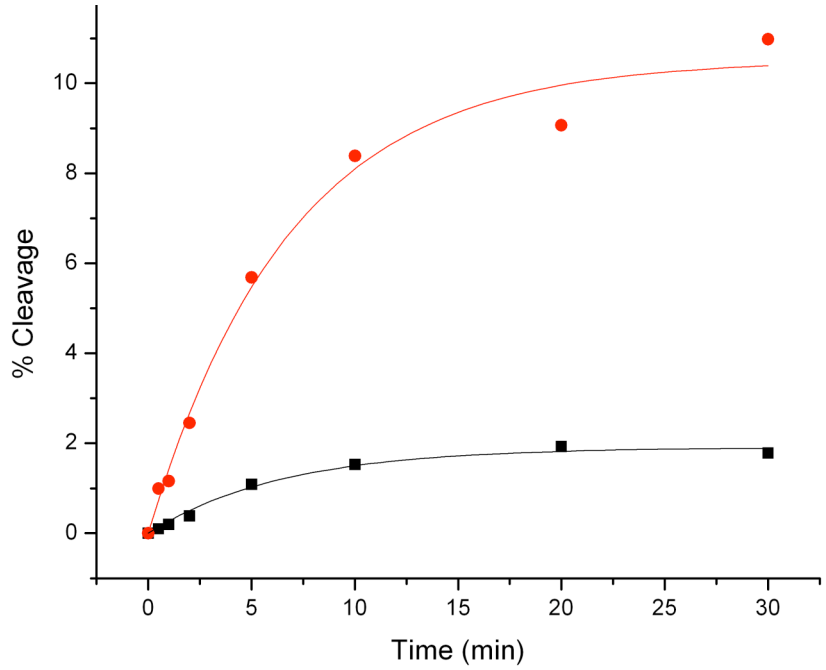

Figure 3.8: Analysis of a single detemination of stand scission induced by EET for **ODN1** (**Figure 3.7**) under aerobic conditions. Red=5'-thymine strand scission, black=scission at ^{Br}U. Lines represent fitting to exponential growth curve using Origin 7.5.

For **2**, **4**, and **6,** the time points (0, 0.5, 1, 2, 5, 10, 20 and 30 minutes) that had been used for the determination of the initial rate of **1** allowed for the determination (Table 3.1) and fitting (See Appendix 2 for fits) of the initial rates.

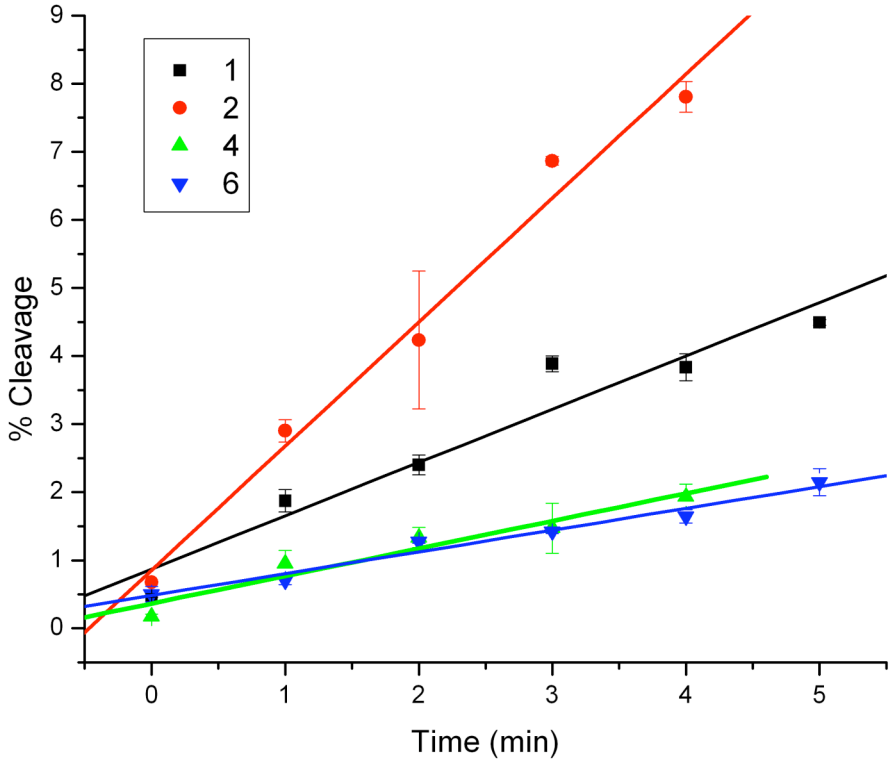

Figure 3.9: Initial rate determination of **1, 2, 4,** and **6** under aerobic conditions. Lines represent linear fit generated by Origin 7.5. All points are an average of two separate runs**.**

For **3** and **5,** maximal strand scission was observed within the first two minutes of irradiation indicating that both compounds rapidly decomposed and that a reduction in the time the samples were irradiated was needed to determine their initial rates. As such, time points of 0, 0.25, 0.5, 0.75, 1, 2, 3 and 4 minute were used. Using these time points, the initial rates were determined between 0 and 1 minute. (**Figure 3.9**)

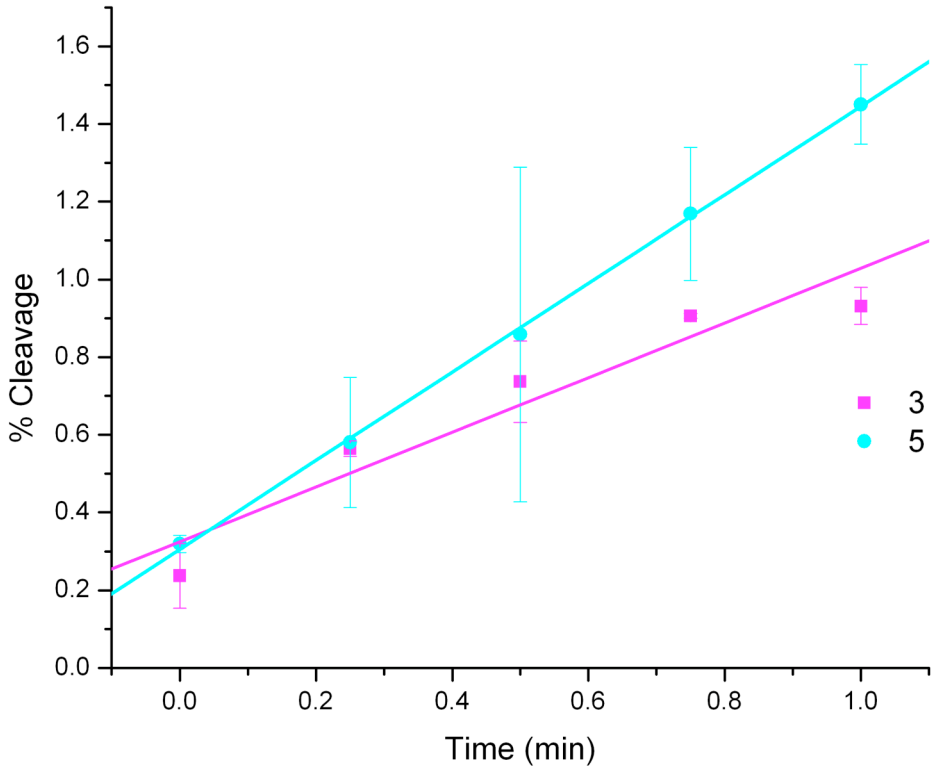

Figure 3.10: Initial rate plot for **3** and **5**. Lines represent linear fit generated by Origin 7.5. All points are an average of two separate runs**.**

When the initial rates were compiled and compared to the E_{ox}, E_{ox}^* (from Chapter 2), no obvious correlations were observed. (**Table 3.1**)

Compound	Initial Rate (% Cleavage/min)	E_{ox} (V)	E_{ox}^* (V)
1	0.78 ± 0.10	0.252	-3.24
2	1.82 ± 0.14	0.222	-3.24
3	0.70 ± 0.07	0.208	-3.18
4	0.41 ± 0.06	0.380	-3.01
5	1.14 ± 0.02	0.350	-2.98
6	0.33 ± 0.03	0.395	-2.99

Table 3.1: Comparison of initial rates of strand scission under aerobic conditions due to EET to E_{ox} and E_{ox}^* values for all compounds. Initial rate measurements are averages of two determinations, error is deviation from that average.

Based on the E_{ox} and E_{ox}^* values there should be two distinct groupings (**1**, **2**, and **3** vs. **4**, **5**, and **6)** of initial rates if a driving force dependence of EET exists. Analysis of the data

in **Table 3.1** showed no correlation to either E_{ox} or E_{ox}^{*}. It is important to note that these measurements were carried out under aerobic conditions as it had been previously shown that ambient oxygen conditions did not affect the amount of strand scission induced by EET.[48] To determine if this held true in my system, the same analyses were duplicated under anaerobic conditions.

3.2.3 Screening of compounds 1-6 under anaerobic conditions to determine O_2 dependence on EET

Previous studies had indicated that the presence of ambient concentrations of molecular oxygen reduced the amount of EET induced strand scission by no more than 20%.[48] The dependence of EET induced strand scission on the presence of O_2 was examined since no correlation of the initial rates of strand scission induced EET was observed in the aerobic studies above. All compounds were initially screened using **ODN1** and **ODN2,** as had been done in the aerobic studies. (Figure 3.11)

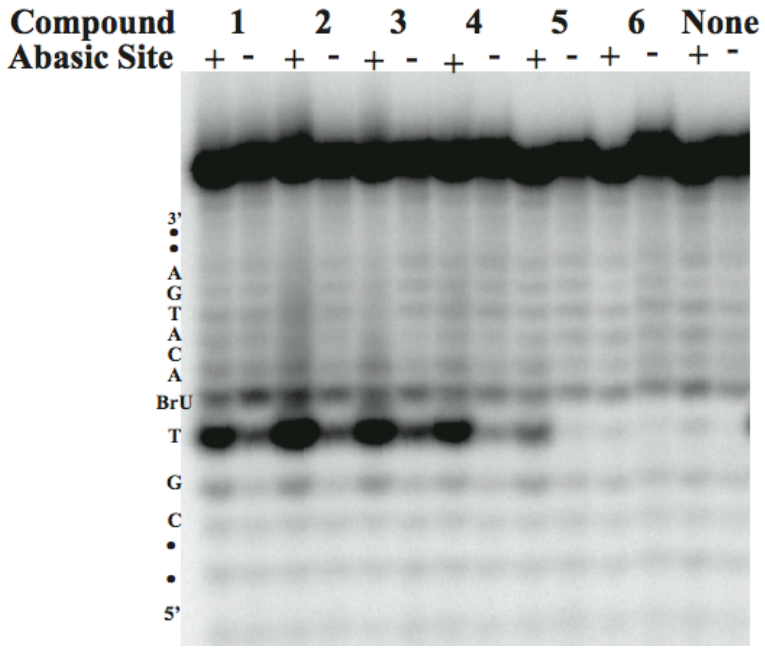

Figure 3.11: Phosphoimage of 20% denaturing polyacrylamide gel showing strand scission induced by EET for **1**-**6** using **ODN1**(+) and **ODN2**(-) under anaerobic conditions. All samples were photoirradiated for 4 minutes under anaerobic conditions and treated with piperidine. Samples were prepared with 1.5 μM of either **ODN1** or **ODN2** and 1 mM of **1**-**6** in 100 mM NaCl, 10 mM sodium phosphate pH 7 buffer.

When the amount of strand scission was analyzed, several significant observations could be drawn. (**Figure 3.12**) The most important conclusion was that under anaerobic conditions the amount of 5'-T cleavage was approximately 6-times greater than that observed in the aerobic system. Additionally, the amount of strand scission at ^{Br}U remained low and consistent regardless of donor used. Taken together, these observations indicated that the presence of O_2 decreased the efficiency of EET, as such subsequent studies were carried out under anaerobic conditions.

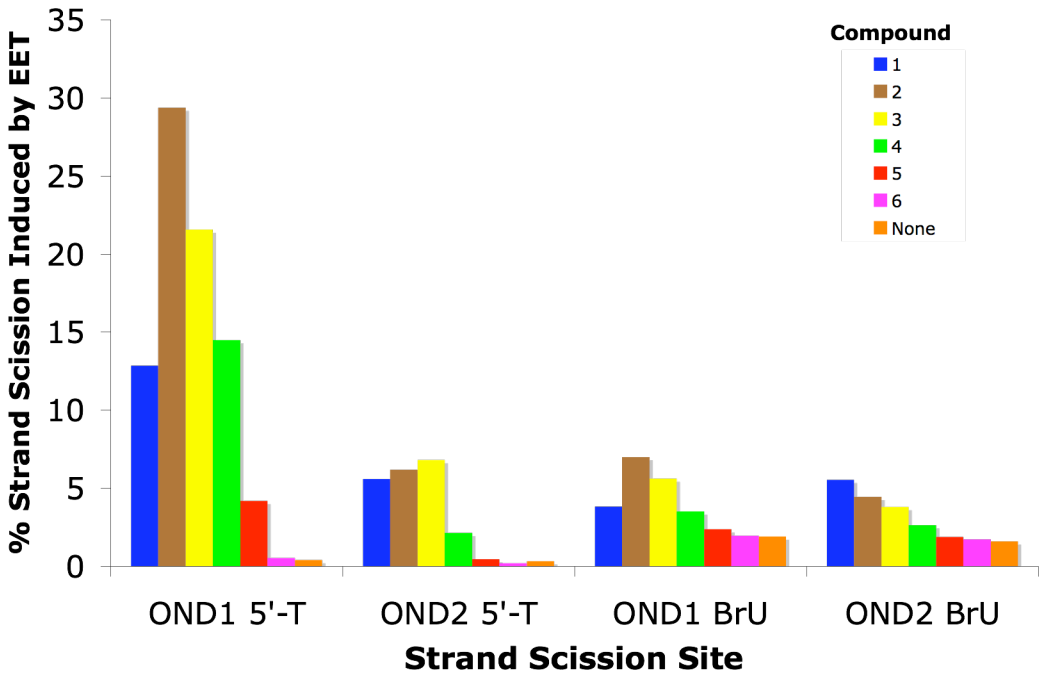

Figure 3.12: Analysis of a single determination of stand scission induced under anaerobic conditions by EET for **ODN1** (**Figure 3.11**) with (ODN1 5'-T and ODN1 BrU) and without abasic site (ODN25 5'-T and ODN2 BrU). Compounds used in assay are **1** (blue), **2** (brown), **3** (yellow), **4** (green), **5** (red), **6** (purple). Control sample with no electron donor (orange). All samples were photoirradiated for 4 minutes under anaerobic conditions and treated with piperidine. Samples were prepared with 1.5 μM **ODN1** and 1 mM of **1**-**6** in 100 mM NaCl, 10 mM sodium phosphate pH 7 buffer.

3.2.4 Determination of initial rates for 1-6 under anaerobic conditions

The initial rate of **1** was examined under anaerobic conditions using the same time points as in previous work (i.e. 0, 1, 2, 3, 4, 5, 10, 20 minutes), thus allowing direct comparison to the results obtained in the aerobic studies above. The samples were run under the same experimental conditions with the sole exception being the reduction of the amount of oxygen in the atmosphere in which the samples were assayed. When **1** was run under anaerobic conditions the resulting gel was significantly different to the one obtained under aerobic conditions. (**Figure 3.13**)

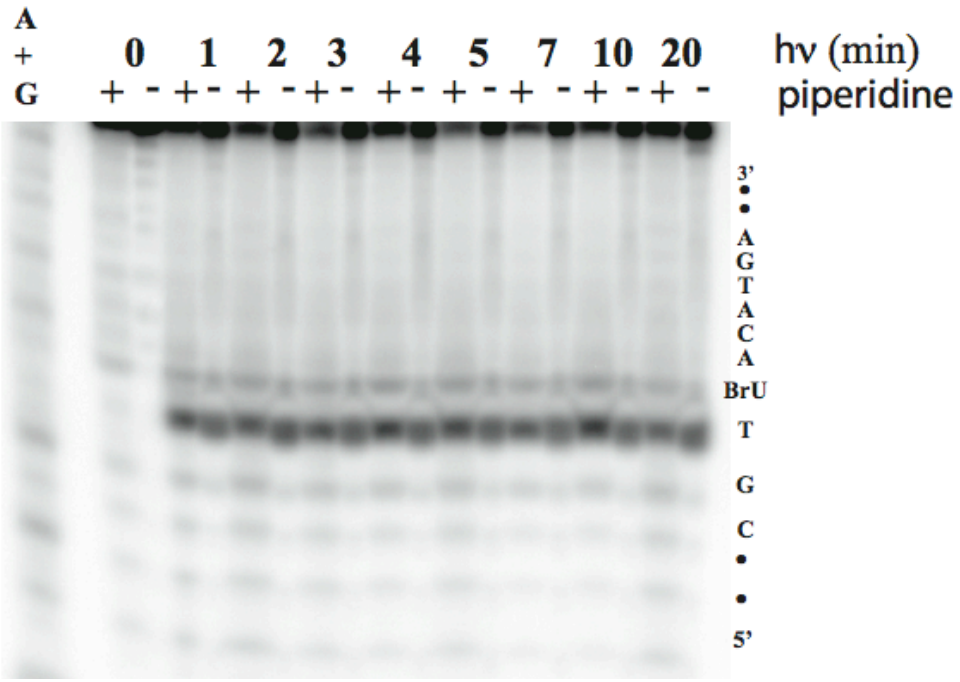

Figure 3.13: Phosphoimage of 20% denaturing polyacrylamide of initial rate of strand scission of **ODN1** (1.5 uM) due to EET for **1 (1** μM) under anaerobic conditions in 100 mM NaCl, 10 mM sodium phosphate pH 7 buffer.

When the amount of 5'-T strand scission induced by EET was analyzed it was clear that under anaerobic conditions **1** was achieving maximal strand scission within the first two minutes at a fast rate. This change in the time at which it achieved maximal strand scission and the increase in the rate were attributed to the lack of oxygen as it was the only variable change in the assay.

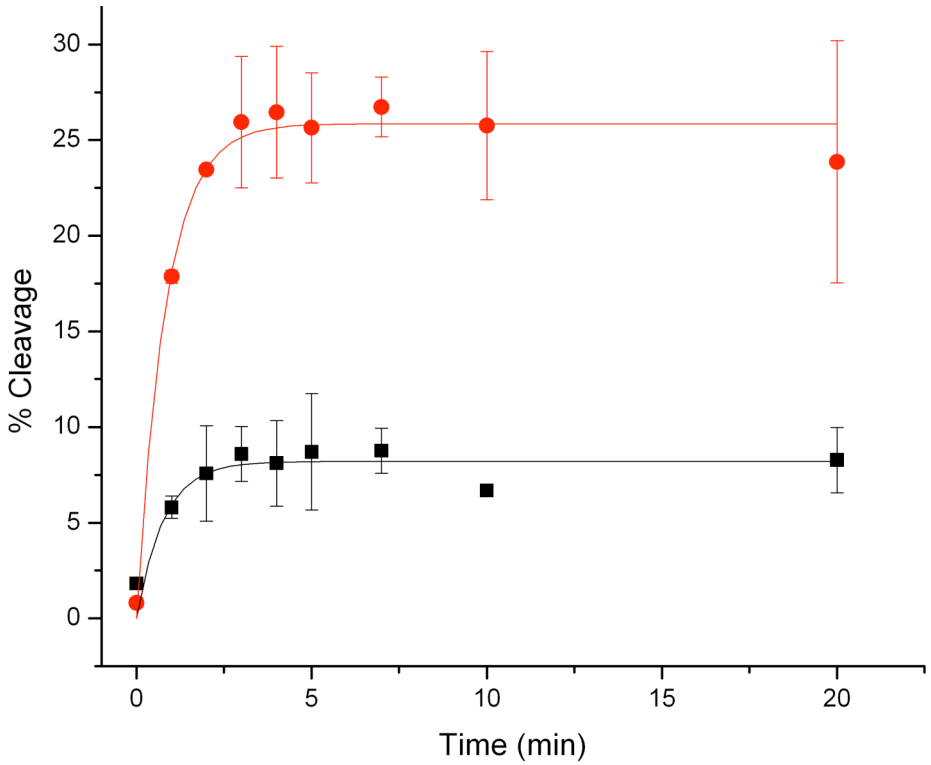

Figure 3.14: Analysis of stand scission induced by EET for **ODN1** (**Figure 3.7**) under anaerobic conditions. Red=5'-T strand scission, black=scission at ^{Br}U. Lines represent fitting to exponential growth curve using Origin 7.5**.**

As the initial rate could not be determined, two changes to the assay were envisioned:

1) Shortening the time the samples were exposed to light in an effort to gather more data points before equilibration of the system occurred.

2) Reducing the flux of the light that the samples were exposed to in an effort to slow the rate of decomposition of the sample.

Of the two options, only reduction of light flux was practical, as time points less than 1 minute were difficult to obtain under experimental conditions.

Reduction of the light flux was achieved by increasing the distance between the sample and the light source. With this increase in distance, a reduction in the light flux from 2mW/cm^2 to 0.8mW/cm^2 was obtained. With this reduction, the initial rate for **1** was again analyzed. Concurrently, the initial rate of **6** was also analyzed to ensure that

the strand scission induced by EET for these compounds could also be accurately measured. (**Figure 3.15**)

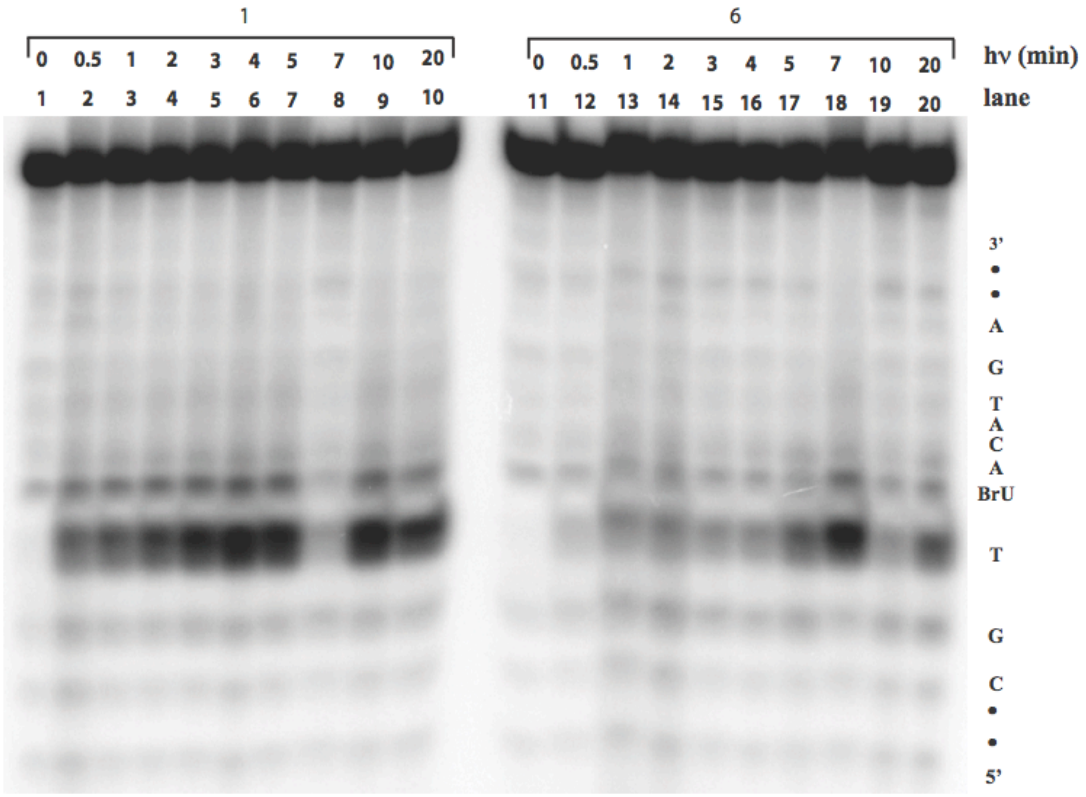

Figure 3.15: Phosphoimage of 20% denaturing polyacrlyamide gel of initial rate of strand scission of **ODN1** (1.5 μM) with **1** (1 mM, lanes 1-10) and **6** (1 mM, lanes 11-20) in 100 mM NaCl, 10 mM sodium phosphate pH 7 buffer under anaerobic conditions with a light flux of 0.8mW/cm^2.

Analysis of the data showed that, again, **1** achieved maximal amounts of strand scission within the first 2 minutes of irradiation, thus indicating that the flux of 0.8 mW/cm^2 was still too intense to allow accurate measurement of the initial rate. Compound **6** did not appear to achieve maximal strand scission, but since the initial rate of **1** was not able to be determined, **6** was of no consequence. Additional attempts to reduce the flux of light that the samples were exposed to by increasing the distance between the sample and the light source were not physically possible, thus an additional filter was used to further

reduce the light flux. The filter selected was a Pyrex® lid to a Petri dish. This filter was optimal because it was optically transparent at the desired wavelengths of irradiation (>330nm) and reduced light flux to 0.2 mW/cm^2. Both **1** and **6** were analyzed using this modified system and their initial rates of strand scission were determined. (**Figure 3.16**) For **6**, using the original time points (0, 0.5, 1, 2, 3, 4, 5, 10, and 20 minutes) and an additional time point at 40 minutes allowed for determination of the initial rate. For **1**, it was found that using 0-10 minute time points the initial rate could be determined.

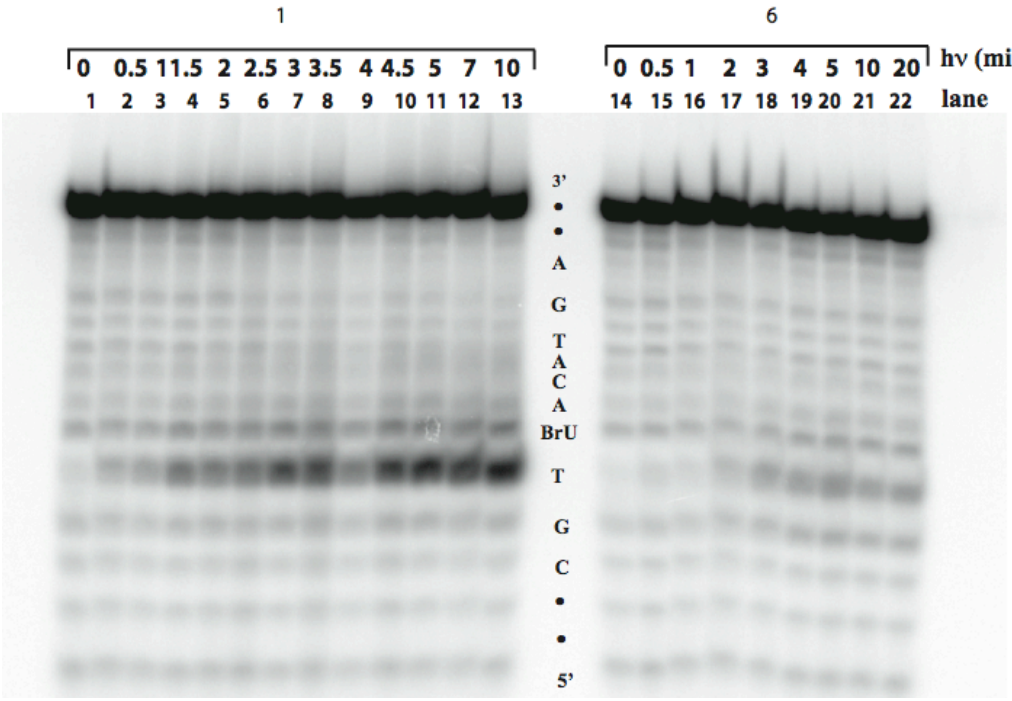

Figure 3.16: : Phosphoimage of 20% denaturing polyacrlyamide gel of initial rate of strand scission of **ODN1** (1.5 μM) with **1** (1 mM, lanes 1-10) and **6** (1 mM, lanes 11-20) in 100 mM NaCl, 10 mM sodium phosphate pH 7 buffer under anaerobic conditions with a light flux of 0.2mW/cm^2.

The initial rates of 5'-T strand scission induced by EET for **2** and **3** were determined using the same time points as **1**. Additionally, the initial rates of 5'-Ti for **4**, **5** and **6** all were determined using the time points developed for **6**. When all the initial rate data was acquired and summarized, (**Table 3.2**) two regimes, a fast and a slow, were found for the

rate of strand induced scission induced by EET. The fast regime was composed of the donors that had the strongest oxidation potentials (**1**, **2**, and **3**), which would be expected if there is a driving force dependence EET. However, the initial rate of **5** was also in the fast regime, which was unexpected as it should fit into the slow regime consisting of the donors with weaker oxidation potentials (**4** and **6**).

Cmpd	5'-Strand Cleavage Initial Rate ($\%\cdot min^{-1}$)	E_{ox}^* (V)
1	7.03 ± 1.05	-3.24
2	5.57 ± 0.57	-3.24
3	4.57 ± 0.38	-3.18
4	0.90 ± 0.10	-3.01
5	5.17 ± 0.44	-2.98
6	0.47 ± 0.07	-2.99

Table 3.2: Summary of initial rate of strand scission induced by EET for **1**-**6** compared to E_{ox} and E_{ox}^* values.

The samples were rerun. The initial results were indeed correct, and the initial rates were found to be 5.7%/min for **2** and 5.4%/min for **5**.(**Figure 3.17**) Based on the initial rate found for **5**, it clearly fits into the fast regime of strand scission. However, based on the E_{ox} and E_{ox}^* values, it should fit into the slow regime of strand scission.

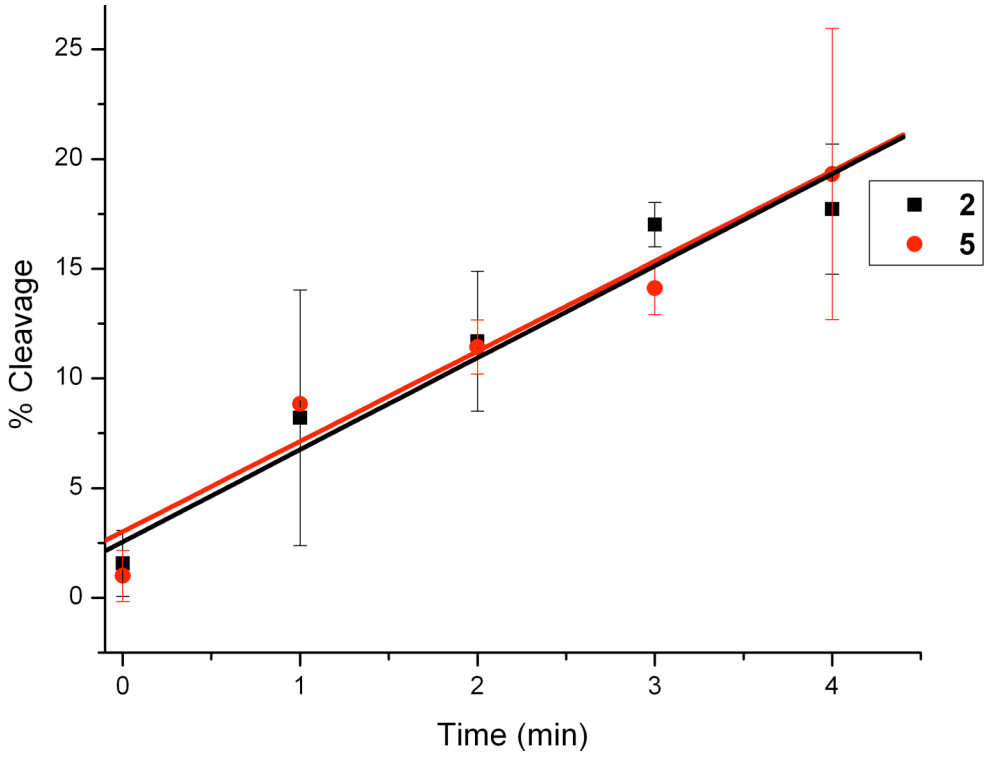

Figure 3.17: Initial rates of stand scission induced by EET for **ODN1** (**Figure 3.16**) under anaerobic conditions. Red=5'-T strand scission, black=scission at ^{Br}U. Lines represent linear fitting using Origin 7.5**.** Points represent average of two runs, error bars represent range of measurements.

If there is a driving force dependence on EET in DNA the initial rate does not fit predictions that compounds with stronger reducing potential (**1**, **2**, **3**) should induced greater strand scission in **ODN1**. There are many possible explanations for this discrepancy, including differences in binding affinities of the compounds to the abasic site, different levels of photostability, and different possible orientations upon binding to the abasic site. The first possible explanation, different binding affinities, was examined first as there is precedence for measuring the binding affinity of small molecules to DNA.[87]

3.2.5 Binding studies of 1 to duplex DNA

Initial binding studies to determine the binding constant of **1** to **ODN1** were attempted using competitive dialysis. In competitive dialysis, **ODN1** is placed in a

dialysis unit and dialyzed in a solution containing a known concentration of **1**. At equilibrium, the concentration of **1** on the exterior of the dialysis unit equals that inside the dialysis unit. If an excess of the **1** is found inside the dialysis unit, then that change can be attributed to binding of the **1** to **ODN1**. Several technical issues were immediately encountered when this procedure was attempted. The major issue was detection of **1** in the dialysis buffer recovered from the dialysis unit. As a control, a 1 mM concentration of **1** were placed in the dialysis buffer and dialyzed versus five empty dialysis units for 24 hours. Removal and analysis of the samples by UV-Vis showed that there was no **1** in the solution recovered from the dialysis unit. The dialysis buffer was analyzed and found to have the correct concentration of **1**. One possible reason that **1** was not observed in the solution recovered from the dialysis unit may be due to the possibility the compound could be sticking to the dialysis membrane. To test this hypothesis, the experiment above was repeated and the dialysis solution was recovered from the unit. At this point, the dialysis unit was washed multiple times with diethyl ether in an attempt to dissolve any material stuck to the walls and membrane of the unit. The ether washes were combined and concentrated to dryness and 500 μL of ddH_2O was added to the flask. The UV-Vis was measured. As with previous results, no sample was observed in either the dialysis buffer or the ether extracted sample. These same experiments were attempted with a 100μM solution of **1** as it was hypothesized that the concentration was too low. The studies also failed. As such, the method was abandoned in favor of an alternate method for determining binding constants, namely fluorescence anisotropy.

The use of fluorescence anisotropy (FA) to measure the binding of proteins to DNA is well understood and commonly used in general.[88-91] It is less common to use

fluorescence anisotropy to measure the binding of small molecules to DNA and proteins. However, precedence exists as to the validity of the using this method to determine the binding constants of **1-6** to duplex DNA.[92-95] Initial work was carried out on **1** as a test to ensure the method would work for the determination of the binding constants.

The first challenge that had to be overcome was optimization of the parameters to ensure that the measurement could be accurately carried out. The first parameter that needed to be optimized was the excitation and emission wavelengths. As reported above, the fluorescence excitation and emission wavelengths were previously determined to be 323 nm and 404 nm respectively. When the emission and excitation wavelengths were measured on the FA instrument, they were found to be 312 nm and 406 nm. While this change in wavelengths would appear to be significant, when the excitation spectrum was analyzed, there was less than a 10% difference in the intensity between 312 nm and 324nm. Thus, the difference was deemed negligible.

The second parameter that needed to be optimized was the concentration of the sample to be used. Ideally the concentration of the sample needs to be sufficient enough that when scanned it gives a total intensity of not less than 10,000 units. The concentration of **1** also needed to be low enough that large quantities of duplex DNA solution wouldn't be consumed. Concentrations ranging from 10nM to 100nM were sampled, with 20 nM being chosen as optimal.

Studies were subsequently undertaken and immediately presented unexpected results. Attempts to obtain a stable baseline of **1** without the addition of duplex DNA were met with failure. Instead of observing a stable baseline for total intensity, a

decreasing baseline was observed. Additional measurements indicated that the total intensity had stabilized around ~7,500 units.(**Figure 3.18**)

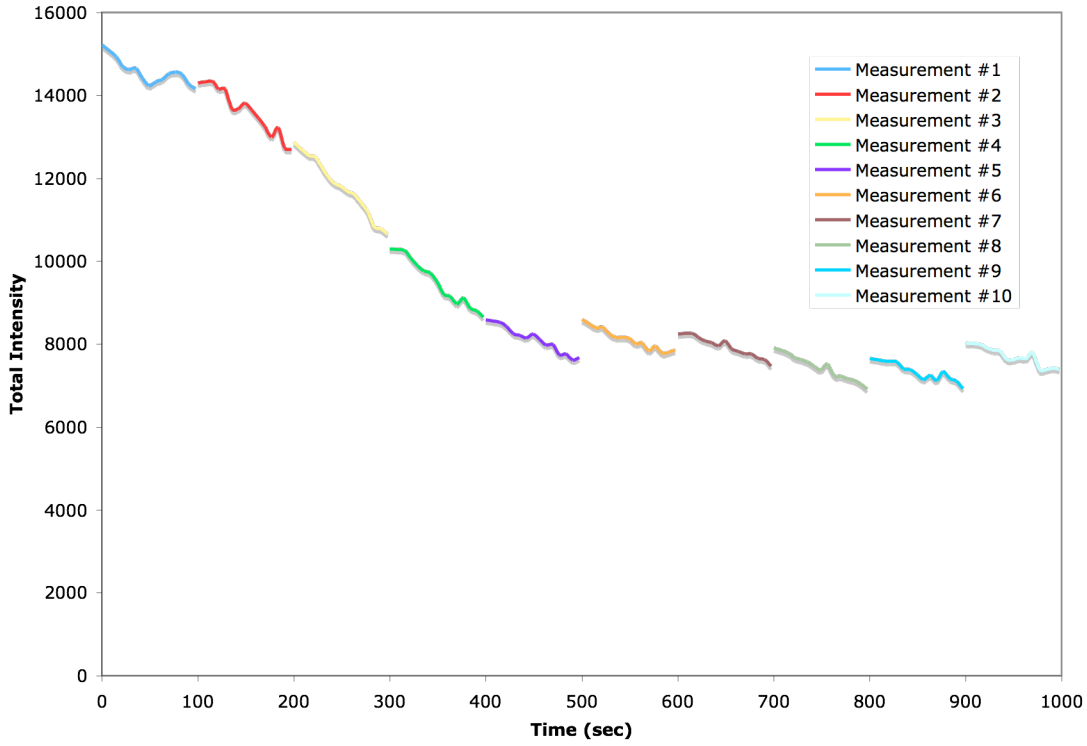

Figure 3.18: Fluorescence intensity measurements acquired during fluorescence anisotropy measurements. Sample scanned was a 20 nM solution of **1** in 100 mM NaCl and 100 μM sodium phosphate buffer .

The drop and then leveling off of the total intensity indicated that there was possible degradation of the compound under the experimental conditions used. To investigate this possibility, all compounds were examined for decomposition. Initial experiments were carried out on **1** as the FA experiment indicated that decomposition occurred. A. Each scan was a continuous lamp measurement of the emission intensity taken at 1 minute 10 second increments. As expected, the sample showed significant degradation upon scanning. (**Figure 3.19**)

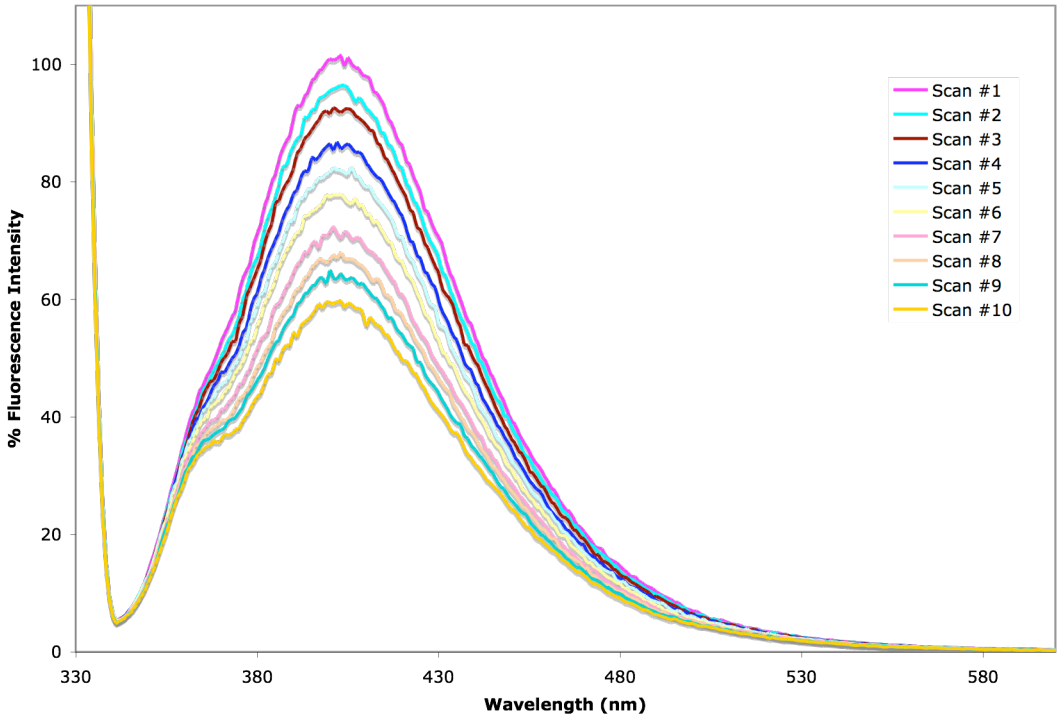

Figure 3.19: Flurescence emssion spectra for **1**. Emission scan of 100 nM solution of **1** in 100 mM NaCl, 10 mM sodium phosphate pH 7. Sample was measured at 312 nm excitation and 406 nm emission wavelengths, and scanned ten times from 320 nm to 600 nm at a rate of 240 nm/min.

Analysis of the scans showed that over the course of 10 scans (11.2 minutes total time) the total intensity of the sample decreased by 41% at a rate of 3.7%/minute.

All remaining compounds were then subjected to the same procedure to determine the rate at which each decomposed. The overall amount and rate of decomposition varied, but all compounds decomposed significantly. (**Table 3.3**)

Compound	% Decrease in Fluorescence Intensity	Rate of Decrease in fluorescence intensity (%/min)	E_{ox} (V)	E_{ox}^* (V)
1	41	3.7	0.250	-3.24
2	67	6.0	0.220	-3.24
3	58	5.2	0.208	-3.18
4	30	2.7	0.380	-3.01
5	34	3.0	0.350	-2.98
6	38	3.4	0.400	-2.99

Table 3.3: Total amount of fluorescence intensity and rate of decomposition of **1-6** compared to the E_{0x} and E_{ox}^* values for the compounds.

Based on the rates of decomposition for all the compounds, the initial rates determined above were no longer valid as it is impossible to determine whether the initial rate observed comes from the compound studied or from its decomposition product.

3.3 Summary

Attempts to determine the driving force dependence of excess electron transport in DNA were carried out under both aerobic and anaerobic conditions. As investigations were undertaken, it was found that **5** did not fit into the predicted model. As a result, it was hypothesized that differences in the binding of the compounds to the **ODN1** could account for the differences observed in the initial rates. Subsequent investigation of the binding constants led to the discovery that compounds **1**-**6** decompose upon exposure to the intense light used in the analysis. The discovery that **1**-**6** decompose rapidly indicates that the compounds might not be able to be used to determine the driving force dependence of EET in duplex DNA. To test this hypothesis, attention was turned to determination using a system employing covalent attachment of the donor to the DNA.

3.4 Materials and Methods

3.4.1 General

All other chemicals were purchased from Fisher Scientific or Aldrich at enzymatic grade or better and used without further purification, unless otherwise specified. All aqueous solutions were prepared with distilled deionized (dd) water (Barnstead NANOpure II purifier, ≥17.8 MΩ·cm). Oligonucleotides were purchased either from IDT DNA (Coralville, IA) or from TriLink Biotechnologies (San Diego, CA) with standard desalting purity. Light flux was measured using a Model UVX digital radiometer (UVP, San Gabriel, CA).

3.4.2 Radiolabeling oligonucleotide with 5'-^{32}P-ATP[48]

A 25 μL solution was prepared containing 1.2 μL of ^{Br}U containing oligonucleotide (^{Br}U-ODN), 4 μL γ-^{32}P-ATP (Perkin Elmer Life Sciences, 5 mC_i/mL), 2.5 μL of T4 polynucleotide kinase buffer (70 mM Tris-HCl, 10 mM $MgCl_2$, 5 mM dithiothreitol), 1.3 μL T4 polynucleotide kinase (New England Biolabs), and 16 μL water.

This solution was incubated for 60 minutes at 37 °C, according to the supplier's standard protocol. After incubation, 5 μL ddH2O were added to make a total volume of 30 μL. During incubation, a P6 Micro Bio-Spin column (Biorad, Hercules, CA) was drained and spun down for 2 minutes at 1000 times gravity to remove any remaining buffer. The buffer was exchanged, according to the manufacturer procedure which entailed washing the column with 300 μL water and spinning down for 2 minutes at 1000 times gravity three times. Excess salt and ATP were removed from the radiolabled sample by passing it through a prewashed P6 column for four minutes at 1000 rcf. The amount of radioactivity in the resulting solution (^{Br}U-ODN*) was measured by adding 1 μL of sample to approximately 1 mL of scintillation fluid (Fisher Scintific-Safe Plus 50 %). The decays per minute (dpm) were then measured with a Packard 1600TR Liquid Scintillation Analyzer.

3.4.3 Preparation of double-stranded DNA for irradiation

A solution of 1.5 μM ^{Br}U-ODN, 2 μM of abasic solution containing oligonucleotides, sufficient amounts of ^{Br}U-ODN* to give 200kdpm/sample, 100 mM NaCl, 10 mM sodium phosphate (pH 7.0) was prepared. The resulting solution was

heated in 90 ºC for 30 minutes, and then allowed to cool to room temperature over not less then three hours to ensure proper annealing. The samples were then split into 25 μL aliquots for use in the photochemical assay.

3.4.4 General photochemistry setup

The apparatus for photochemistry consists of a 1000 W xenon arc lamp, a 330 nm UV cutoff filter, an aluminum cooling block in which the samples rest so that their temperature remains at ~10 ºC and a glove bag (for anaerobic work only). (**Figure 3.20**)

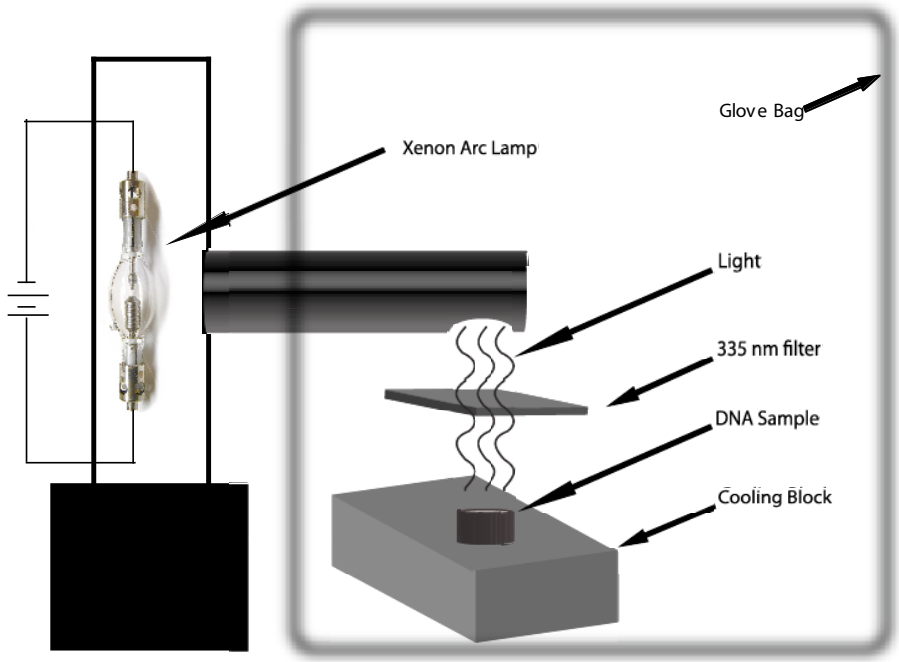

Figure 3.20: Apparatus used to irradiate electron donors for investigating excess electron transport in DNA.

3.4.5 Piperidine treatment of samples[48]

Samples designated for piperidine treatment were suspended in 30 μL of 10% v/v piperidine and incubated at 90ºC for 30 minutes. After incubation, the samples were

dried in the Speed-Vac for 60 minutes. The dried samples were then treated with 30 μL of water and dried in the Speed-Vac three times to remove any residual piperidine.

3.4.6 Maxam A+G Lane sequencing reaction (A+G Lane)[96]

ODN2* (10 μL) and 2 μL calf thymus DNA (1 mg/ml) were combined with 3 μL of 10% v/v formic acid and incubated at 60 ºC for 30 minutes. The sample was then dried in the Speed-Vac and treated with piperidine as described above.

3.4.7 Denaturing polyacrylamide gel electrophoresis (PAGE) analysis

The radioactive, dried samples were dissolved in 5 μL loading buffer (8M urea, 40% sucrose, 0.05% bromophenol blue, 0.05% xylene cyanol in 1x Tri-borate-EDTA (TBE) buffer). The samples were loaded onto a 20% PAGE gel, which had been prerun for 30 minutes, and the gel was then run at 65 W for 1 hr and 30 minutes. The gel was exposed to a phosphorimaging plate overnight, and then scanned using a Molecular Dynamics Storm Phosphorimager (Sunnyvale, CA). Analysis was carried out using ImageQuant 5.2.

Chapter 4
Analysis of covalently bound electron donors on driving force dependence of excess electron transport

4.1 Introduction

The use of covalent attachment of the electron donor to the DNA imparts significant advantages over the use of a non-covalent system. The first major advantage is that in the covalent system there is a 1:1 ratio of electron donor:acceptor, while in the non-covalent system there is an almost 1000 fold excess of donor:acceptor. This reduces the possibility of multiple injections of electrons from multiple donors. Secondly, covalent attachment ensures a fixed distance between the donor and acceptor, as the exact site of attachment is known. A third advantage is that the covalent system limits the number of orientations that the donor can adopt with respect to the acceptor, thus enhancing the efficiency of EET.

The system to be used to investigate the driving force dependence of EET utilizes covalent attachment of the electron donor to the DNA duplex and incorporation of the modified nucleobase ^{Br}U as a the electron acceptor (**Figure 4.1).** Previously, this system had been used to determine the distance dependence and sequence dependence of EET with an analog of **6**.[47,48] As this system had proven to be effective at measuring EET efficiency, it was used with **26** and **27** to investigate the driving force dependence of EET. Compounds **26** and **27** were chosen as the electron donors in the system since their non-covanlent analogs **1** and **6** showed significant differences in EET in the non-covalent system.[47,48]

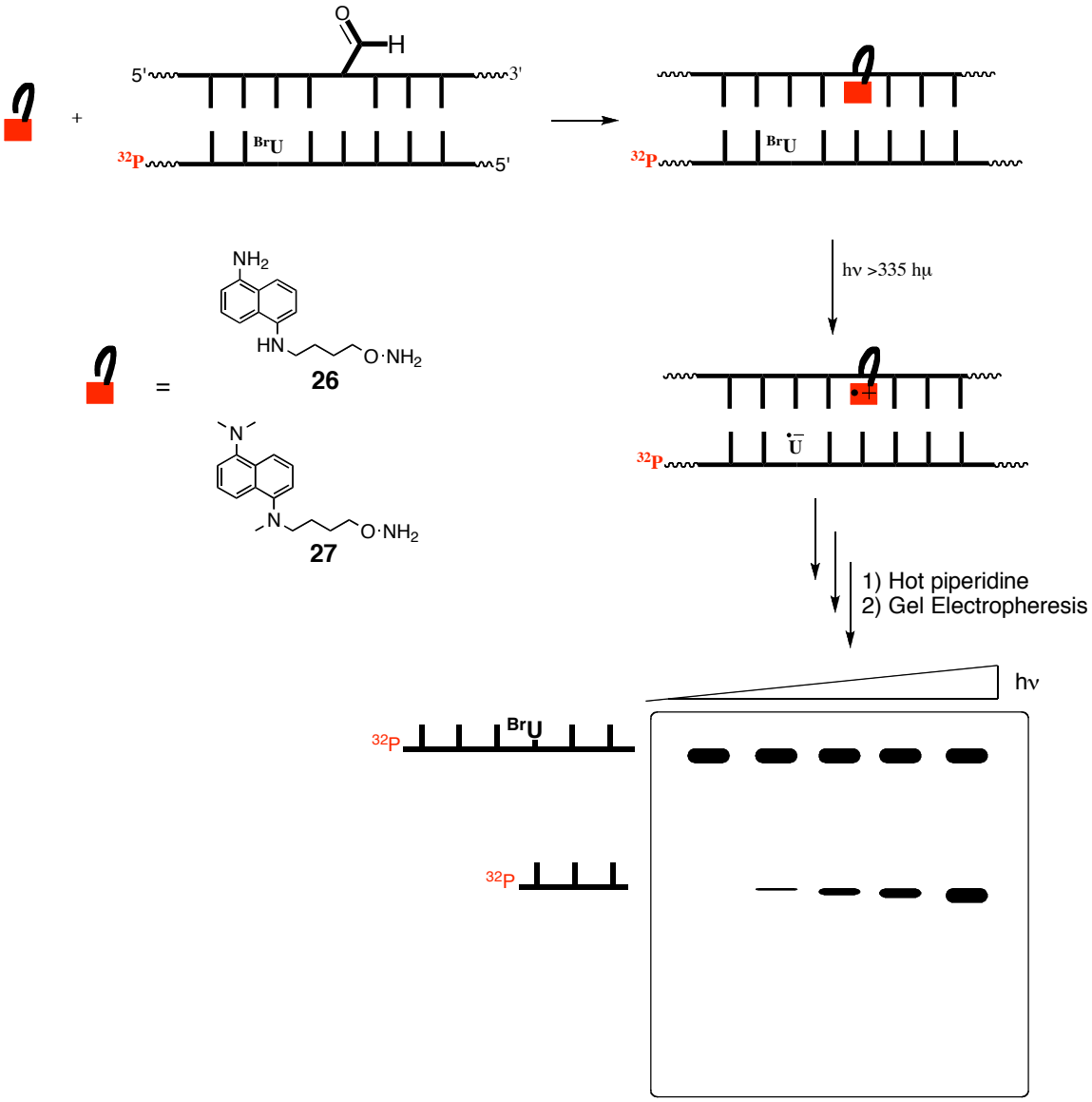

Figure 4.1: Covalent assay for determination of driving force dependence of EET in DNA.

4.2 Results and Discussion

4.2.1 Preparation of and conjugation of 26 and 27 to abasic DNA

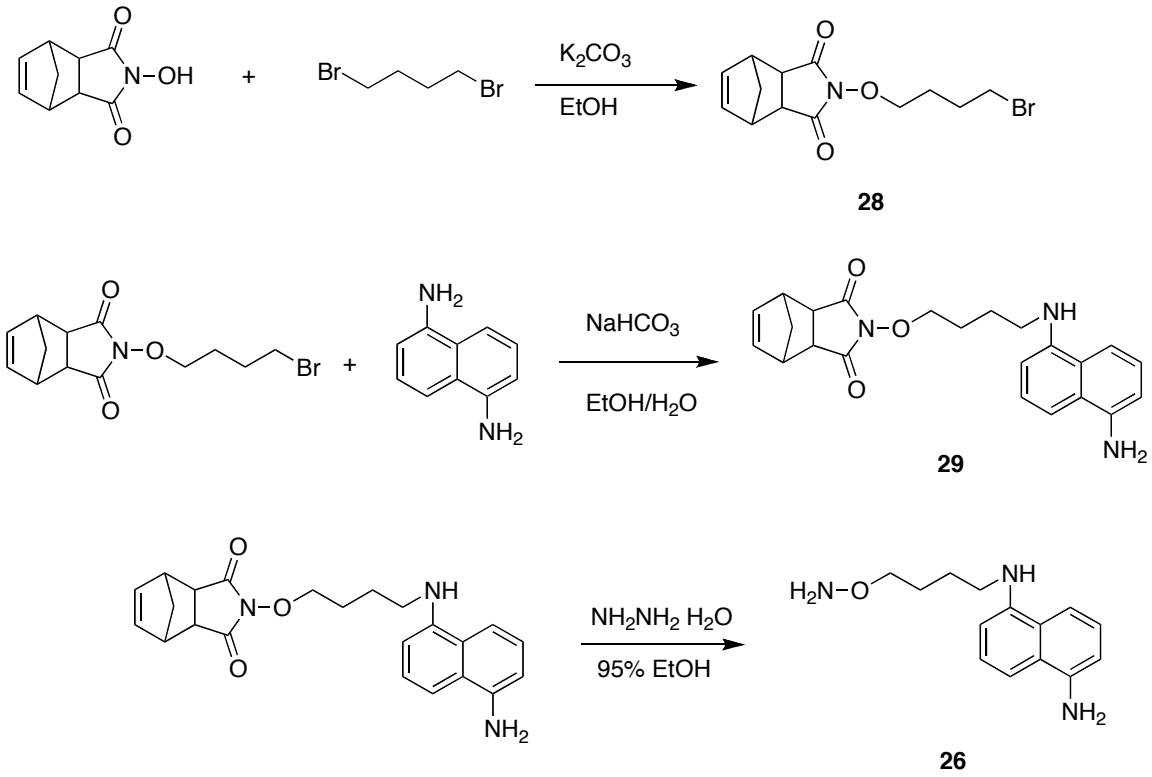

Figure 4.2: Synthetic route for generation of **26**.

The synthetic route for generation of **26** has been reported previously and is summarized in **Figure 4.2**. [48,82] Synthesis of **26** for this work followed the same procedure without incident. The possibility that **26** could be conjugated to the DNA in two possible conformations was studied. (**Figure 4.3**). While there was a low probability that the aromatic amine would couple to the oxidized abasic, the possibility needed to be eliminated.

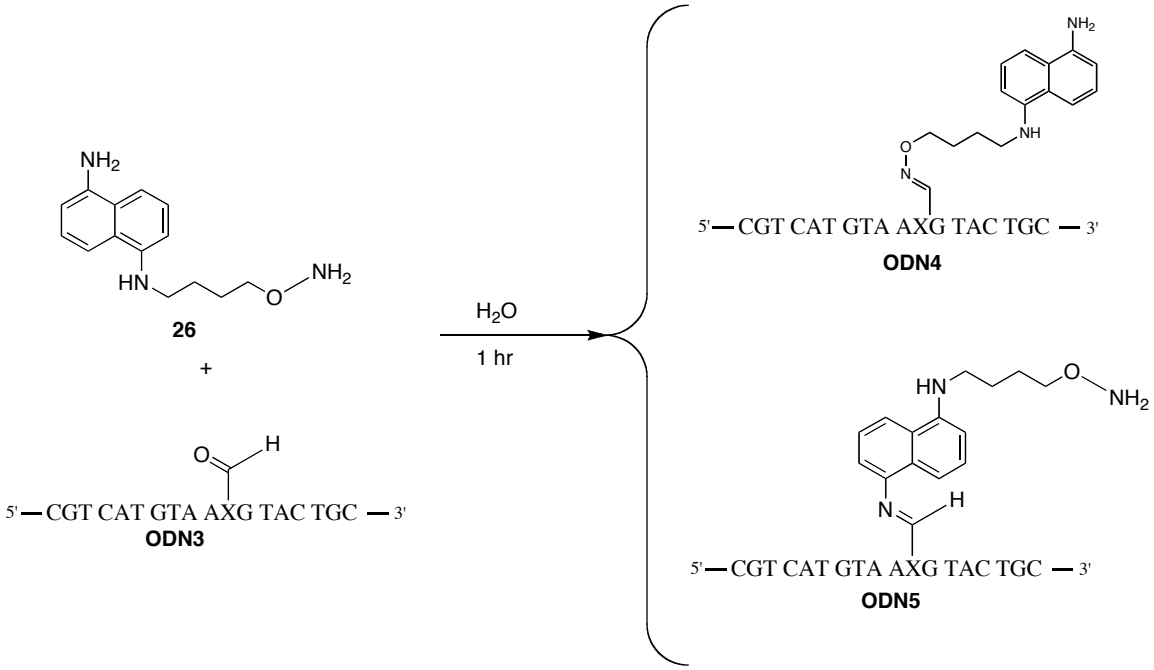

Figure 4.3: Possible conjugation of **26** to oxidized abasic site.

To investigate these possibilities, a model reaction was carried out using **26** and benzaldehyde as a surrogate for the oxidized abasic site. There are three possible products that could be formed in this reaction, **30**, **31** and **32**. (**Figure 4.4**) Based on predicted NMR shift, these alternatives can be accurately identified. The benzylic hydrogen in **30** is predicted to have a shift of 8.4 ppm when the benzaldehyde reacts with the hydroxylamine. When the benzaldehyde reacts with the aromatic amine as in **31**, the benzylic proton is predicted to have a shift of 8.1 ppm. If the benzaldehyde reacts with both amines as in the case of **31**, the corresponding peaks mentioned above are both expected to be seen.

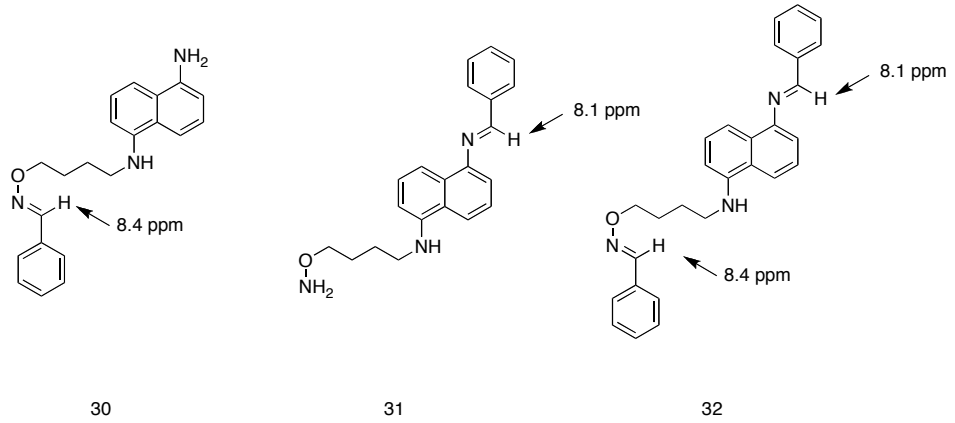

30 31 32

Figure 4.4: Model reaction of **2** with benzaldehyde to determine site of reaction with aldehyde functionality. ^{1}H chemical shifts were predicted using ChemDraw 8.0.

In the presence of sub-stoichiometric amounts of benzaldehyde relative to **26**, **30** was formed as indicated by the benzylic proton at 8.42 ppm. No **31** or **32** were visible by NMR analysis. When the reaction was carried out with an excess of benzaldehyde **32** was the only product identified with benzylic peaks observed at 8.04 ppm and 8.42 ppm. The results obtained from the sub-stoichiometric reaction were not surprising as hydroxylamines are expected to be more reactive than aromatic amines as the neighboring group effect due to the electron donating ability of the oxygen adjacent to the nitrogen. Possible steric interactions between the benzylic hydrogen and the γ-proton on the naphthalene ring is an additional factor that would inhibit the formation of **31**. Only one mode of conjugation is then expected when **26** is conjugated to the abasic DNA is the one where the hydroxylamine

Preparation of **27** had been previously reported by treating **26** with formaldehyde and $NaBH_4$.[48] As was described in Chapter 2, the use of dimethyl sulfate and $NaHCO_3$ as conditions for methylating the amines gave the desired product in a more efficient manner. These conditions were applied to **26** and the desired material (**33**) was generated

with comparable yield to literature 3 hours.[48] Subsequent deprotection of **33** using the optimized procedures from above yielded **27** in a 76% yield. (**Figure 4.5**)

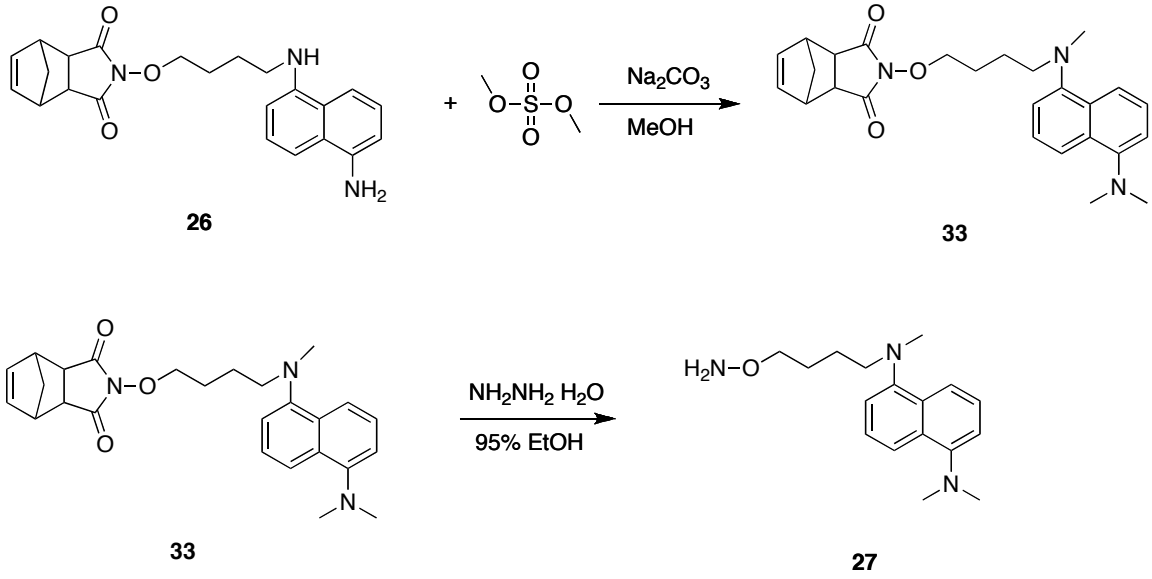

Figure 4.5: Preparation of **27**.

Conjugation of **26** and **27** to **ODN3** followed by HPLC purification was carried out using literature procedures to yield **ODN4** and **ODN6**. [48] (**Figure 4.6**) The conjugated oligonucleotides were then annealed with **ODN7** to give the duplexes for use in the assay above.

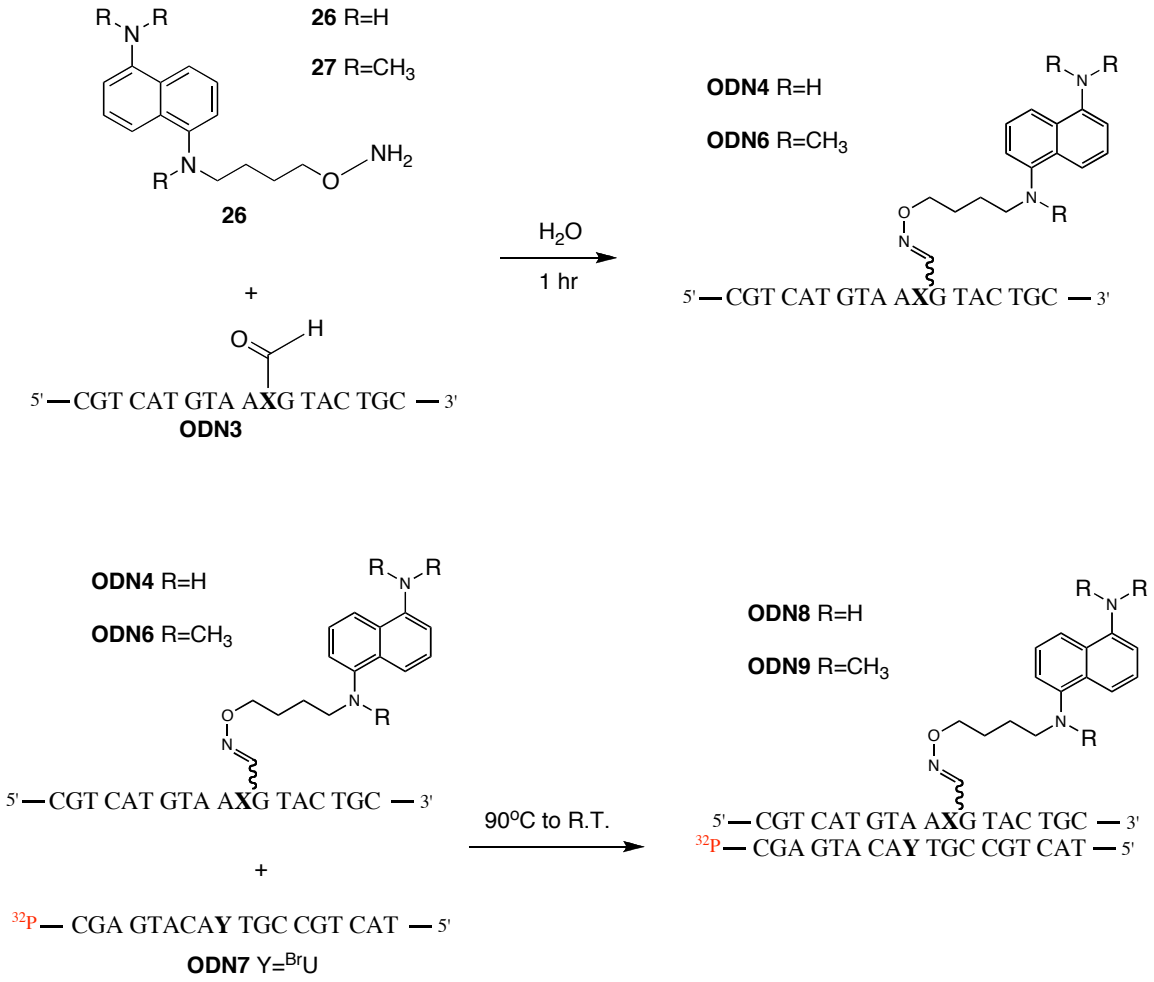

Figure 4.6: Preparation of **ODN8** and **ODN9**.

4.3 Determination of driving force dependence in DNA dependent EET

Based on the E_{ox}^{*} values for **1** and **6** in Chapter 2 and observations using the non-covalent anaerobic system in Chapter 3, **ODN8** should have a greater initial rate of strand scission induced by EET than **ODN9** as **1** had a greater E_{ox}^{*} than **6**. Using **ODN8** and **ODN9** whether there is a force dependence of EET in DNA.

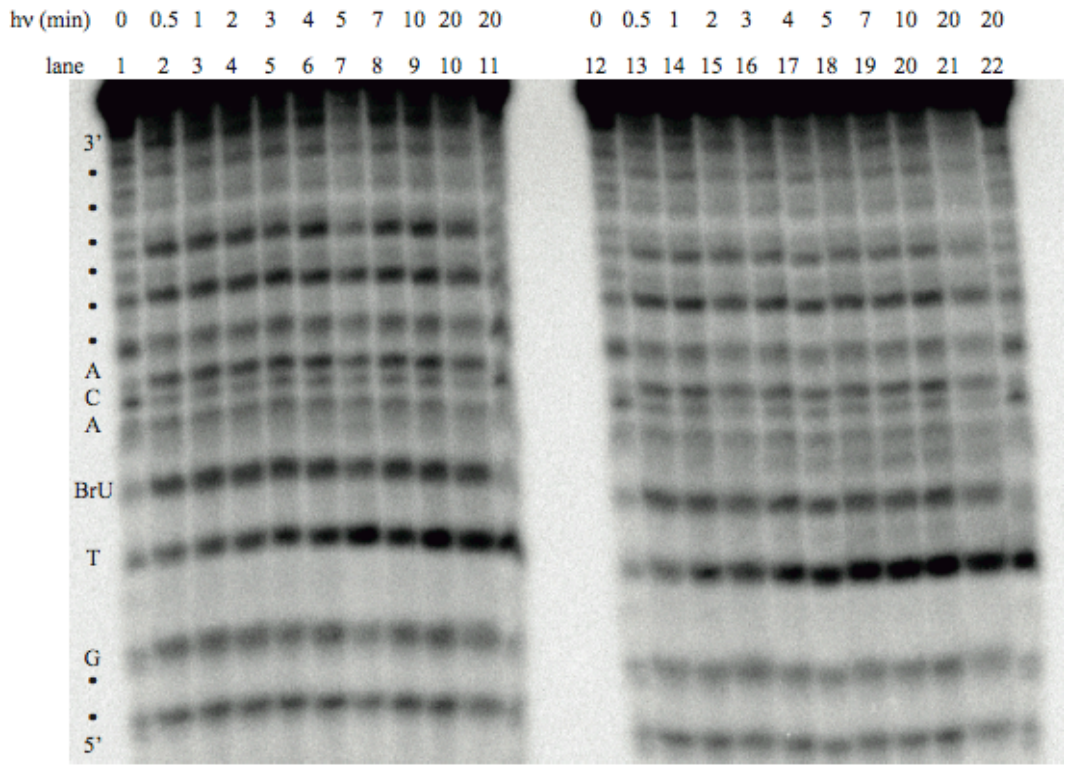

Figure 4.7: Phosphoimage of 20% denaturing polyacrylamide gel showing strand scission induced by EET for **ODN8** (lanes 1-11) and **ODN9** (lanes 12-22). All samples were photoirradiated for the indicated times and analyzed after treatment with piperidine at 90 ºC (lanes 2-10, 12-21) or directly without treatment with piperidine (lanes 1, 11, 12 and 22**).** Samples comprises of 1.5μM **ODN8** or **ODN9** in 100 mM NaCl∫ and 10 mM sodium phosphate pH 7 buffer.

Analysis of the data yielded the initial rates of strand scission as 2.0%/min for **ODN8** and 1.3%/min for **ODN9**.) While there appears to be no significant difference in the initial rates of **ODN8** and **ODN9,** closer inspection of the initial rate graph appears to indicate that the initial rate of **ODN8** might occur within the first three data points (0, 0.5 and 1 minute). When these three data points were analyzed as the potential "maximal" initial rate, a 4-fold difference in initial rates between **ODN8** and **ODN9** was observed**.** While this might seem to be a significant difference in the initial rates, when this difference is compared to the 14-fold difference seen in the non-covalent system (Table 3.2), it is insignificant.

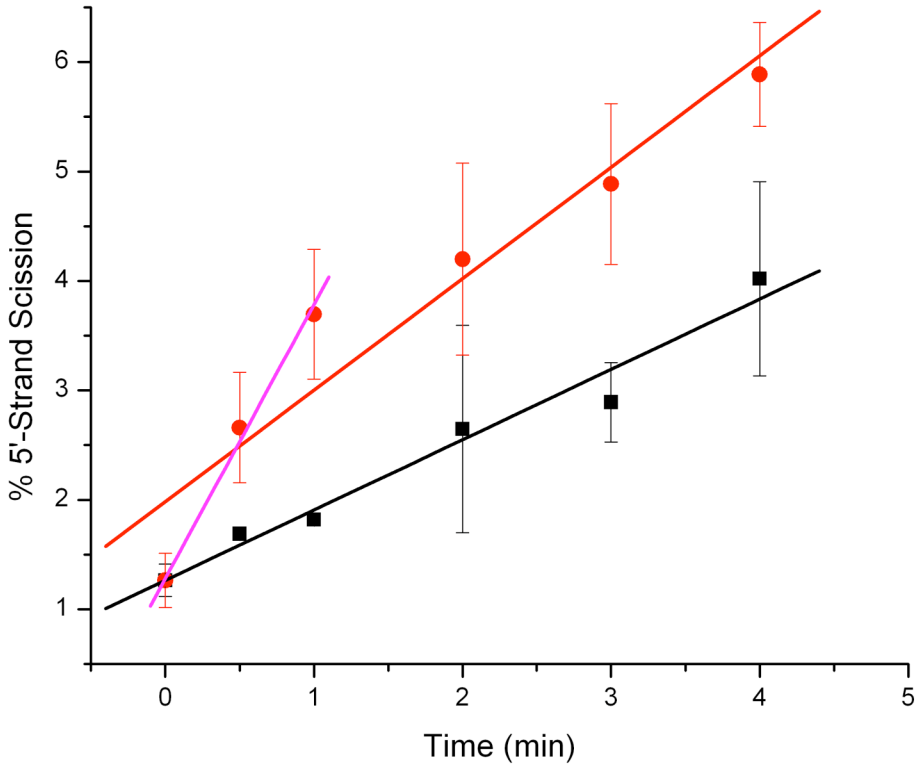

Figure 4.8: Analysis of strand scission for ODN8 and **ODN9**. Red and black lines represent linear fit of initial rates of strand scission as generated by Origin 7.5. Red and magenta line represents "optimal" initial rate for **ODN9**. Error bars indicate averages of independent two runs

Verification that the results obtained were not due to decomposition or hydrolysis of **ODN4** and **ODN6** during the annealing process was carried out. To investigate this possibility, samples were heated to 90 ^{0}C and then cooled to room temperature. Analysis by HPLC and MALDI-TOF of the heated and the non-heated samples showed the same mass for **ODN4** and **ODN6** (5606 and 5652, respectively) within experimental error (± 5 mass units) of the instrument, thus ruling out decomposition or hydrolysis of the oligonucleotides as a factor affecting the initial rate of strand cleavage induced by EET. (**Figure** 4.9)

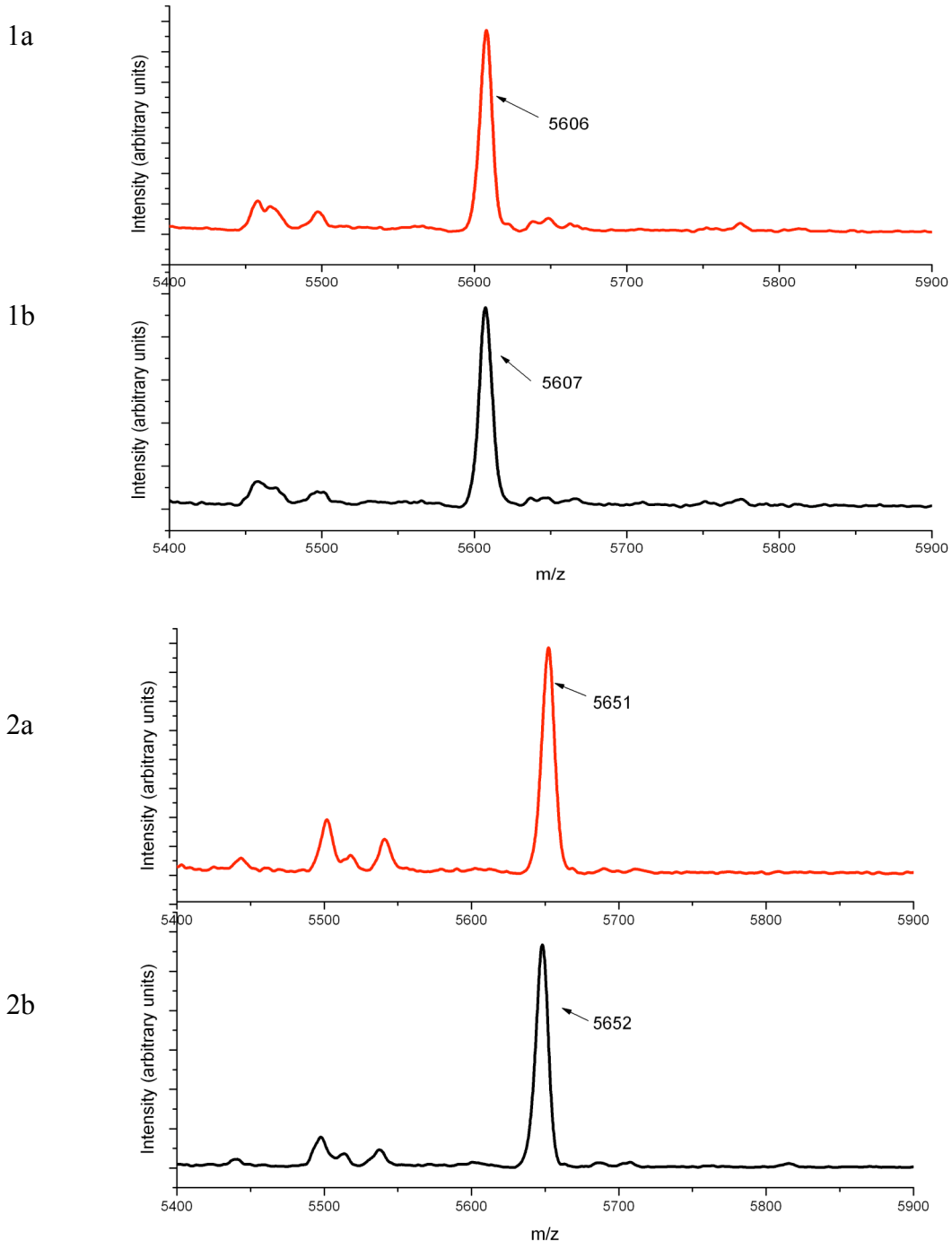

Figure 4.9: MALDI-TOF traces for **ODN4** (1a and 1b) and **ODN6** (2a and 2b) samples (Red= non-heated samples, Black=heated samples). Theoretical mass: **ODN4** = 5605, **ODN6**=5648.

4.4 Summary

Based on the initial rate studies illustrated in **Figure 4.8**, there appears to be no driving force dependence on EET using **ODN8** and **ODN9** under these experimental conditions. A closer examination of the data indicates that there could only be as much as a 4-fold difference in the initial rates, but when compared to the non-covalently bound system, this difference is negligible.

Investigation into the stability of the oligonucleotides to the annealing conditions was undertaken in an effort to determine if decomposition of the conjugates affected the initial rates found. However based on HPLC and MALDI-TOF data decomposition does not appear to be an issue. In conclusion, using the 1,5-diaminonapthalene analogs in the covalently bound assay indicated that there is no driving force dependence on excess electron transport in DNA using **1**-**6** and the DNA sequences.

4.5 Materials and Methods

4.5.1 General

Solvents, starting materials, and reagents of the highest commercial grade were used without further purification. All aqueous solutions were prepared with water purified to a resistivity of 17.8-18.0 MΩ. DNA concentration was determined using a Hewlett Packard 8453 UV-vis spectrophotometer and extinction coefficients at 260 nm provided by the vendor. NMR spectra were recorded on a Bruker AM400 spectrometer (^{1}H, 400 MHz; ^{13}C, 100 MHz) and referenced to residual protons in the deuterated solvents. Chemical shifts (δ) are reported in parts per million (ppm), and coupling constants (J) are reported in hertz (Hz). Electrospray Ionization mass spectrometry (ESI-MS) was carried out using a JEOL AccuTOF-CS spectrometer while matrix assisted laser

desportion/ionization time of flight mass spectrometry was performed using a Shimadzu Axima-CFR MALDI-TOF.

4.5.2 N-(4'-Bromobutyloxy)-5-norbornene-2,3-dicarboximide (28)

A round bottom flask equipped with a magnetic stir bar, reflux condenser and nitrogen inlet was charged with 1,4-dibromobutane (Aldrich) (3.02 g, 14.0 mmol), K_2CO_3 (1.64 g, 11.9 mmol) and 20 mL of acetone. A solution of *N*-hydroxy-5-norbornene-2,3-dicarboximide (717 mg, 4.00 mmol) in 20 mL of acetone was slowly added to the reaction mixture over 30 minutes. The reaction mixture was then refluxed overnight and cooled to room temperature. The resulting solid was removed by filtration. The filtrate was then concentrated to dryness and purified by silica gel flash chromatography (hexanes:ethylacetate 1:0 to 1:1), yielding 988 mg (79%) of the desired product as a clear viscous oil. NMR analysis agreed with previously published values.[48]

4.5.3 1,5-Diaminonaphthalene derivative (29)

A round bottom flask equipped with a magnetic stir bar, reflux condenser and nitrogen inlet was charged with 1,5-diaminonaphthalene (1.24 g, 7.67 mmol), $NaHCO_3$ (792 mg, 9.44 mmol) and 24 mL ethanol–H2O (2:1). To this solution, **29** (988 mg, 2.00 mmol) in ethanol 32 mL was added over 30 minutes. The reaction was stirred at 70 ºC under N_2. The reaction mixture was concentrated to dryness and the residue was dissolved in 50 mL CH_2Cl_2 and and washed with 100 mL H_2O and 100 mL saturated NaCl solution. The organic layer was dried over $MgSO_4$, filtered and concentrated to dryness. Purification by silica gel chromatography using a Chromatotron (Analtech, Newark, DE) with (hexanes-ethyl acetate 4:1 to 1:1) yielded 591 mg (48%) of the desired material as a purple solid. NMR analysis consistent with published values.[48]

4.5.4 N,N,N'-Trimethyl-1,5-diaminonaphthalene derivative (33).

A round bottom flask equipped with a magnetic stir bar and nitrogen inlet was charged with **29 (**430 mg, 1.10 mmol), Na_2CO_3 (369 mg, 4.40 mmol), 12 mL methanol, 6 mL water and 6 mL THF. Dimethyl sulfate (417 μL, 4.40 mmol) was then added to the solution and the solution was stirred at room temperature overnight under N_2. The reaction was neutralized with 1 M NaOH to a pH >11, extracted with ethyl acetate. The organic layer was dried over $MgSO_4$, filtered and concentrated to dryness, yielding the desired material (381 mg, 80%) as a light purple solid.. NMR analysis was consistent with previously published values.[48]

4.5.5 N-(4-Aminooxybutyl)-N,N',N'-trimethyl-1,5-diaminonaphthalene (27).

A round bottom flask equipped with a magnetic stir bar, reflux condenser and nitrogen inlet was charged with **33** (25 mg, 0.06 mmol) and 5 mL 95% ethanol. Hydrazine monohydrate (Fisher, 1 mL) was added to reaction mixture. The reaction was refluxed under N_2 and monitored by TLC (1:1 hexanes:ethyl acetate) and ESI-MS for consumption of starting material (30 minutes). The reaction was removed from the heat and concentrated to dryness. The residue was purified by silica gel flash chromatography (hexanes-ethyl acetate 1:0 to 1:1). The desired product **27** was obtained as a colorless syrup in 68% yield (11 mg). NMR and ESI-MS agree with published values.[48]

4.5.6 N-(4-Aminooxybutyl)- 1,5-diaminonaphthalene (26).

A round bottom flask equipped with a magnetic stir bar, reflux condenser and nitrogen inlet was charged with **30** (20 mg, 0.06 mmol) and 5 mL 95% ethanol. Hydrazine monohydrate (Fisher, 1 mL) was added to reaction mixture. The reaction was refluxed under N_2 and monitored by TLC (1:1 hexanes:ethyl acetate) and ESI-MS for

consumption of starting material (3 hours). The reaction was removed from the heat and concentrated to dryness. The residue was purified by silica gel flash chromatography (hexanes-ethyl acetate 1:0 to 1:1) to yield 11 mg (80%) of desired product as a colorless syrup in 80% yield. ESI-MS agrees with literature data.[82]

4.5.7 Conjugation of 26 and 27 to abasic DNA. [48]

Abasic site containing **ODN3** (120 μM) and 2 mM sodium periodate in 100 mM sodium acetate (pH 5.0, 40 μL) were combined and incubated at 4 °C in the dark for 60 minutes. After incubation, salts were removed using a prewashed (3 times with 400 μL ddH_20 and spin down for 2 minutes at 1000 rcf) P6 Micro Bio-Spin column (Biorad) for four minutes at 1000 rcf. The solution was then incubated with a 25 mM either **26** or **27** in HPLC grade acetonitrile (50 μL) at 37 °C for 1 hour.

The excess **26** or **27** were removed by passage through a prewashed (3 times with 400 μL ddH_2O and spin down for 2 minutes at 1000 rcf) Biorad Micro Biospin P6 Column for four minutes at 1000 rcf.

4.5.8 Oligonucleotide Conjugate Purification.[48]

ODN4 and **ODN6** were purified by reverse phase HPLC (C-18) using a gradient of 10 % acetonitrile in 50 mM triethylamine acetate buffer (pH 5.0) to 30 % acetonitrile in 35 mM triethylamine acetate over 15 min (1 mL/min). Material corresponding with **ODN4** or **ODN6** (as determined by absorbance at 260 nm and 330 nm) was collected and dried in a Speedvac (Savant) overnight. Dried samples were redissolved in ddH_2O and the concentration was determined by UV-Vis spectrometry based on the molar extinction coefficients provided for the oligonucleotides by the manufacturer (Trilink Biotechnologies).

4.5.9 Labeling Oligonucleotide with a 5′ - [^{32}P].

A 25 μL solution containing 1.2 μL **ODN7** (5 mM stock solution), 4 μL γ - [^{32}P] – ATP (Perkin Elmer Life Sciences, 250 $mC_i/\mu L$), 10 units T4 polynucleotide kinase (New England Biolabs), 2.5 μL of T4 polynucleotide kinase buffer (70 mM Tris-HCL, 10 mM $MgCl_2$, 5 mM dithiothreitol) and 16.3 μL ddH_2O was incubated for 60 minutes at 37 °C according to suppliers standard protocol. After incubation, 5 μL ddH_2O was added to make a total volume of 30 μL. Excess salt and ATP were removed by passage through a prewashed (3 times with 400 μL ddH_20 and spin down for 2 minutes at 1000 rcf) P6 Micro Bio-Spin column (Biorad, Hercules, CA) for four minutes at 1000 rcf. Radioactivity of the resulting oligonucleotide (**ODN7***) was measured by adding 1 μL of sample to approximately 1 mL of scintillation fluid (Fisher ScintiSafe Plus 50 %) and measured dpm with a Packard 1600TR Liquid Scintillation Analyzer.

4.5.10 Preparation of Double Stranded DNA.

ODN7 (1.5 μM) was incubated with 2.0 μM **ODN4** or **ODN6** and sufficient **ODN7*** to give 100 kdpm/sample in a solution of 10 mM sodium phosphate buffer (pH 7.0) and 100 mM NaCl. The mixture was placed in a 90 °C bath and cooled slowly to room temperature over no less then three hours to allow for proper annealing.

Chapter 5
Conclusion and Final Discussion

The purpose of this dissertation was to look at the driving force dependence of excess electron transport in DNA.

Based on Marcus theory, it is predicted that the oxidation potential of the electron donor would affect the rate of electron transport. To that end a series of 1,5-diaminonapthalene analogs with varying reduction potentials was synthesized. The compounds were screened in an assay where the electron donor was non-covalently attached to the duplex DNA. In this system, it initially appeared that a driving force dependence of EET was indeed observed. However one compound **5** did not agree with predicted results. Attempts were made to determine whether the binding affinity of the compounds to the duplex DNA explained the anomalous result. The attempts were unsuccessful as it was found that the compounds decomposed under the conditions used to measure the binding constants.

Compounds **1** and **6** were used in an assay where the electron donor was covalently attached to the duplex DNA. Using this assay, no driving force dependence of EET was observed using either **1** or **6**. This result must not be considered the final answer as to whether a driving force dependence of excess electron transport exists. Based on Marcus theory, there are two regions that exist for the driving force dependence of EET in DNA:

1) The normal region where an increase in the driving force leads to an increased rate of charge transfer.
2) The inverted region where an increase in driving force leads to a drecrease in the rate of charge transfer.

It is not known which region of the Marcus curve the compounds tested fall into, so making the broad generalization that a driving force dependence of EET does not exist with these compounds is premature.

Future work on this project should attempt to determine where these compounds lie on a Marcus curve. To do this, compounds with lower reducing potentials such as 1-aminoanthracene and 2-aminoanthracene should be used in the assay. Additionally the positioning of the electron donors with respect to the acceptor should be examined. A reduction in the number of alternate routes that the excess electron can sample by positioning the electron donor at the end of the duplex will simplify the determination of a driving force dependence of EET. Previous results have shown that there is a distance dependence on EET[47], this dependence coupled with a different electron donor should allow the determination of the driving force dependence of excess electron transport.

Appendix A
E_{00} Determinations for compounds 2-6

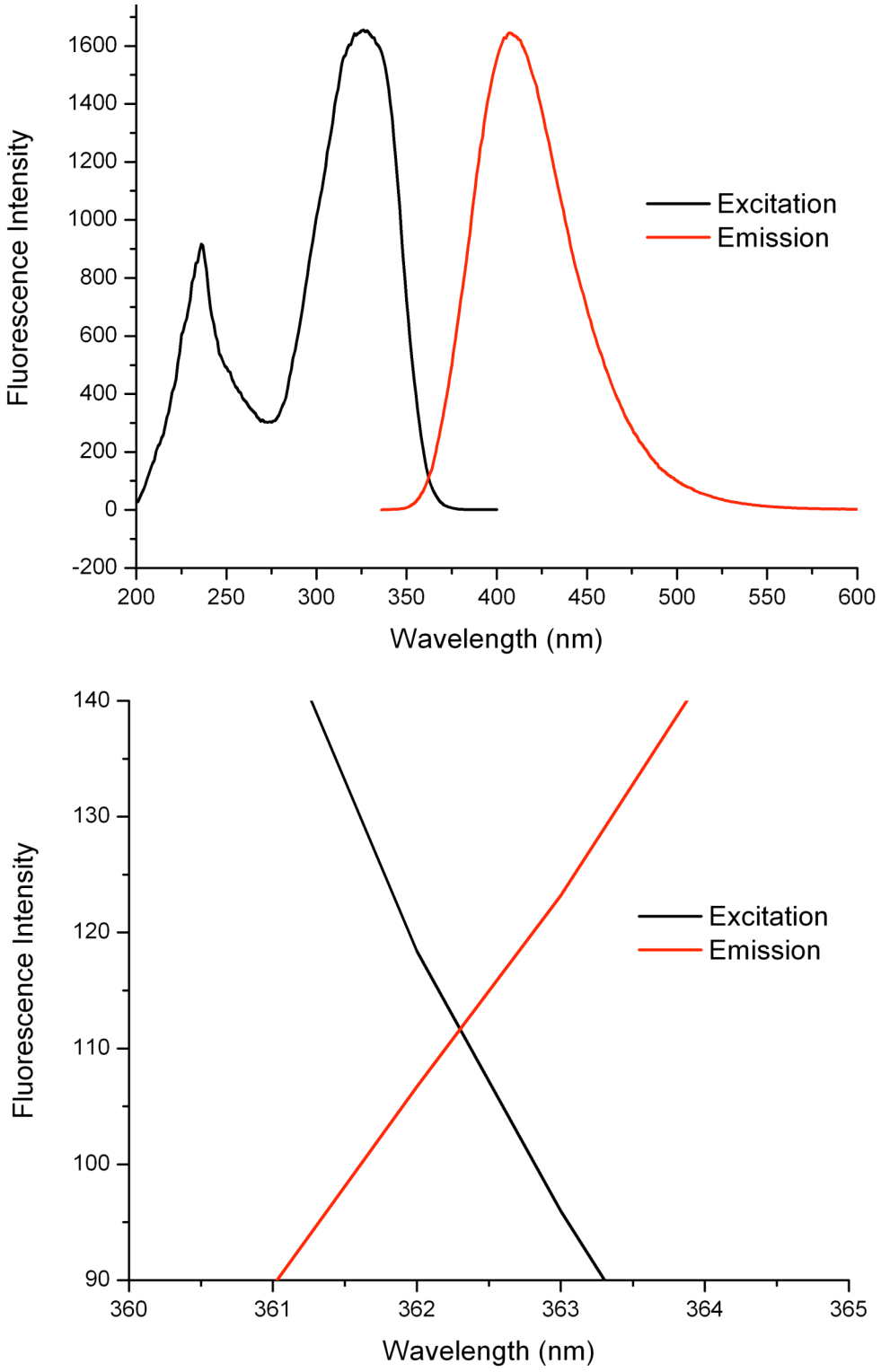

Figure A.1: Determination of E_{00} value for **2** in 100 mM NaCl, 10 mM sodium phosphate pH 7 buffer.

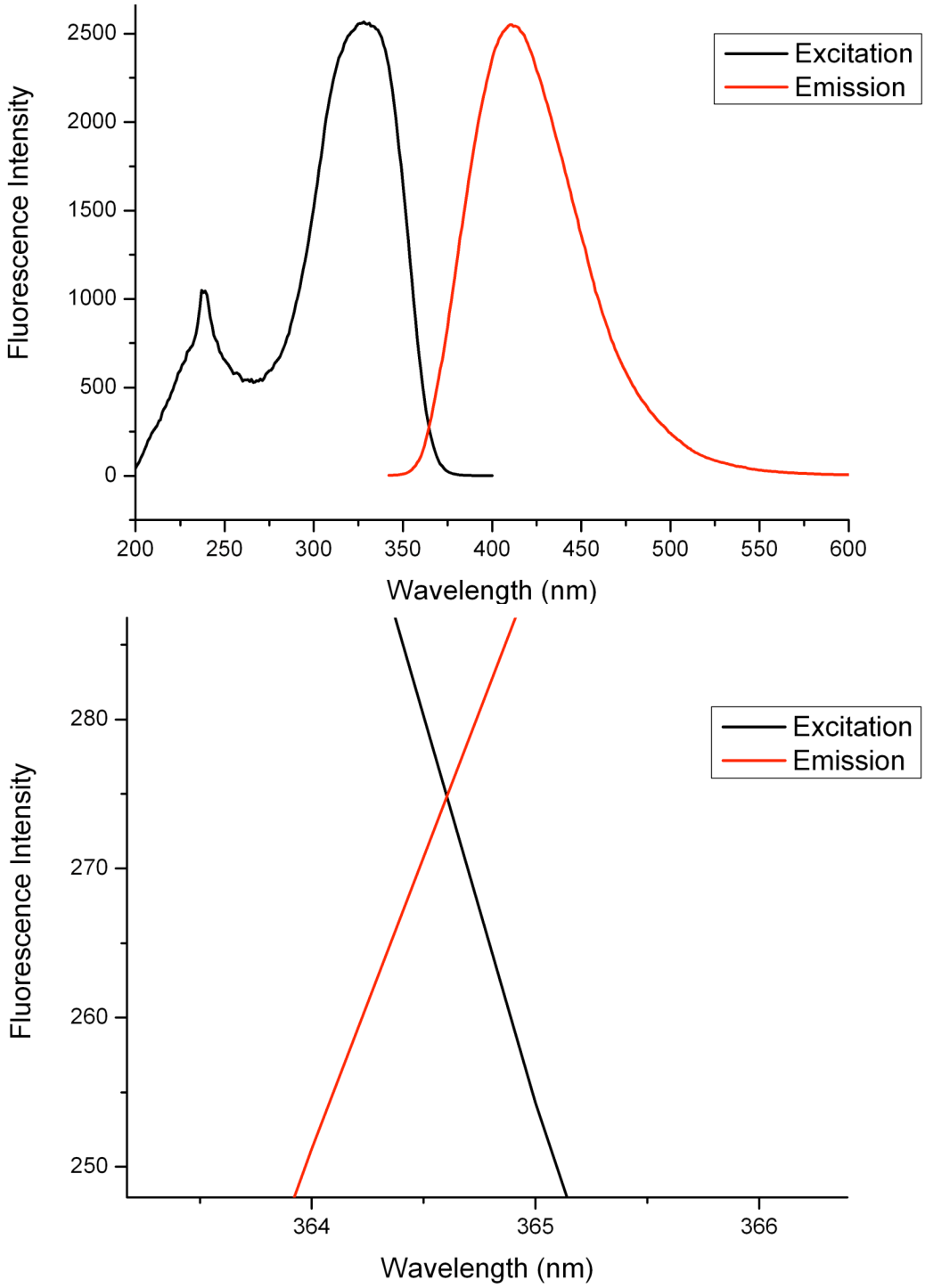

Figure A.2: Determination of E_{00} value for **3** in 100 mM NaCl, 10 mM sodium phosphate pH 7 buffer.

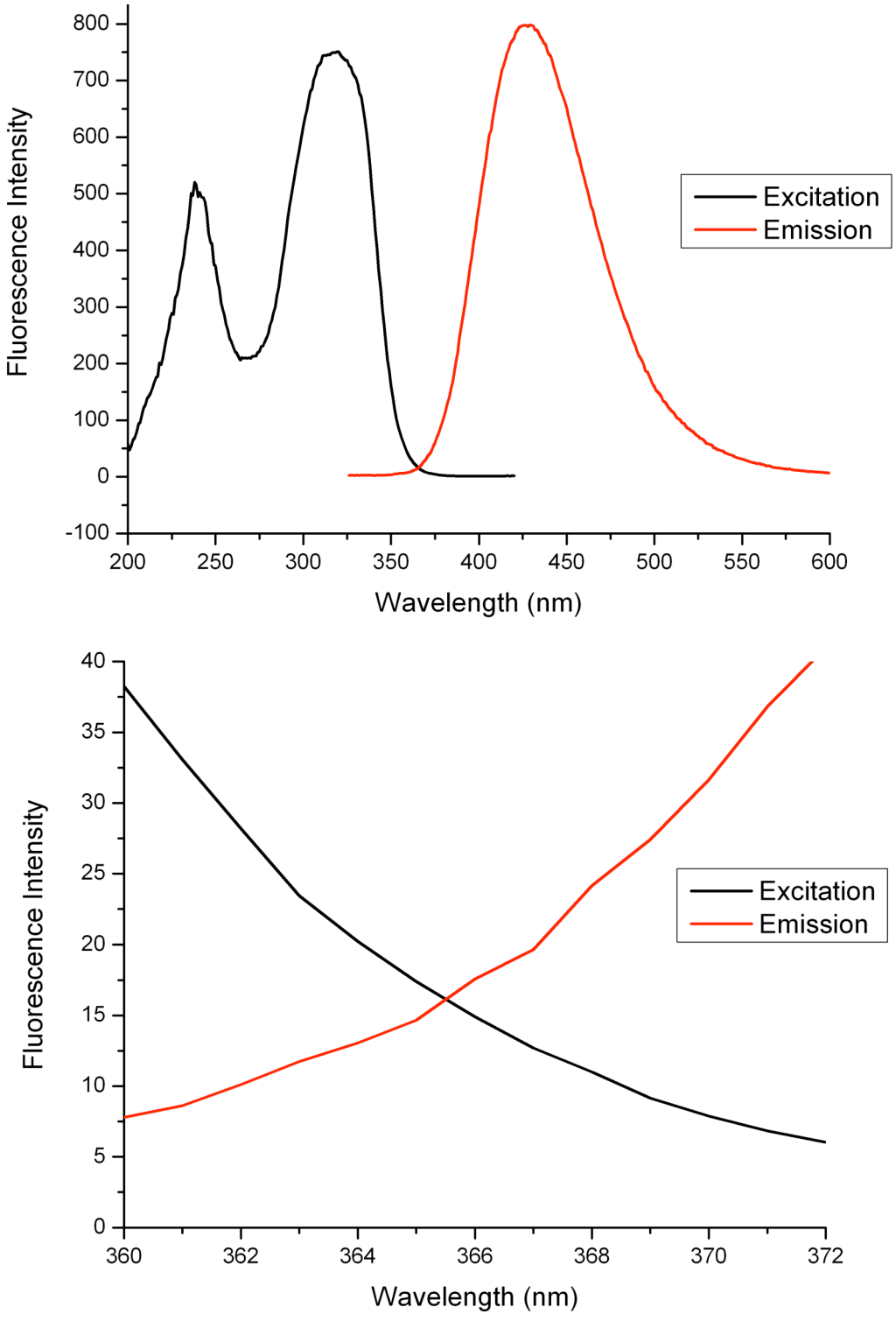

Figure A.3: Determination of E_{00} value for **4** in 100 mM NaCl, 10 mM sodium phosphate pH 7 buffer.

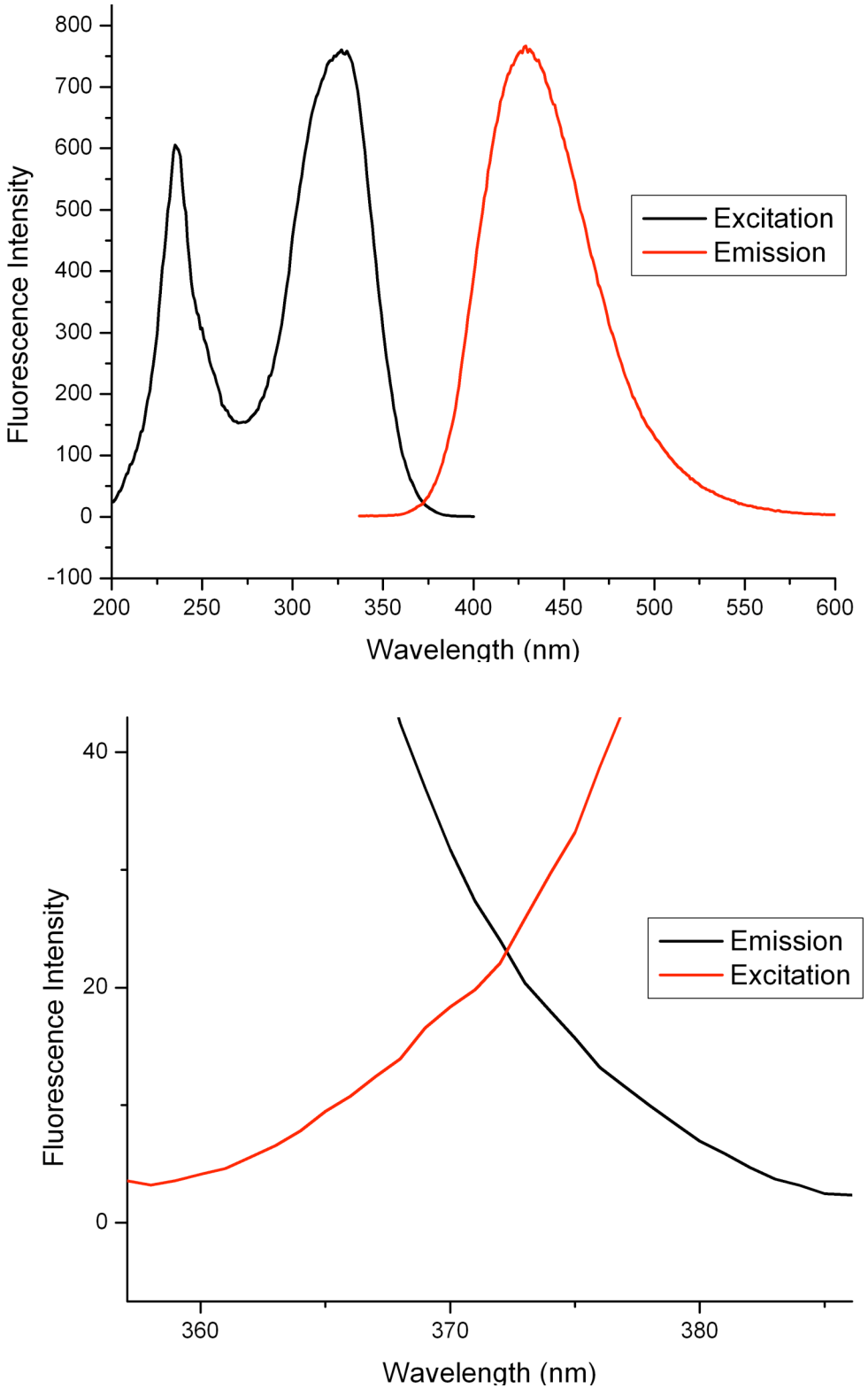

Figure A.4: Determination of E_{00} value for **5** in 100 mM NaCl, 10 mM sodium phosphate pH 7 buffer.

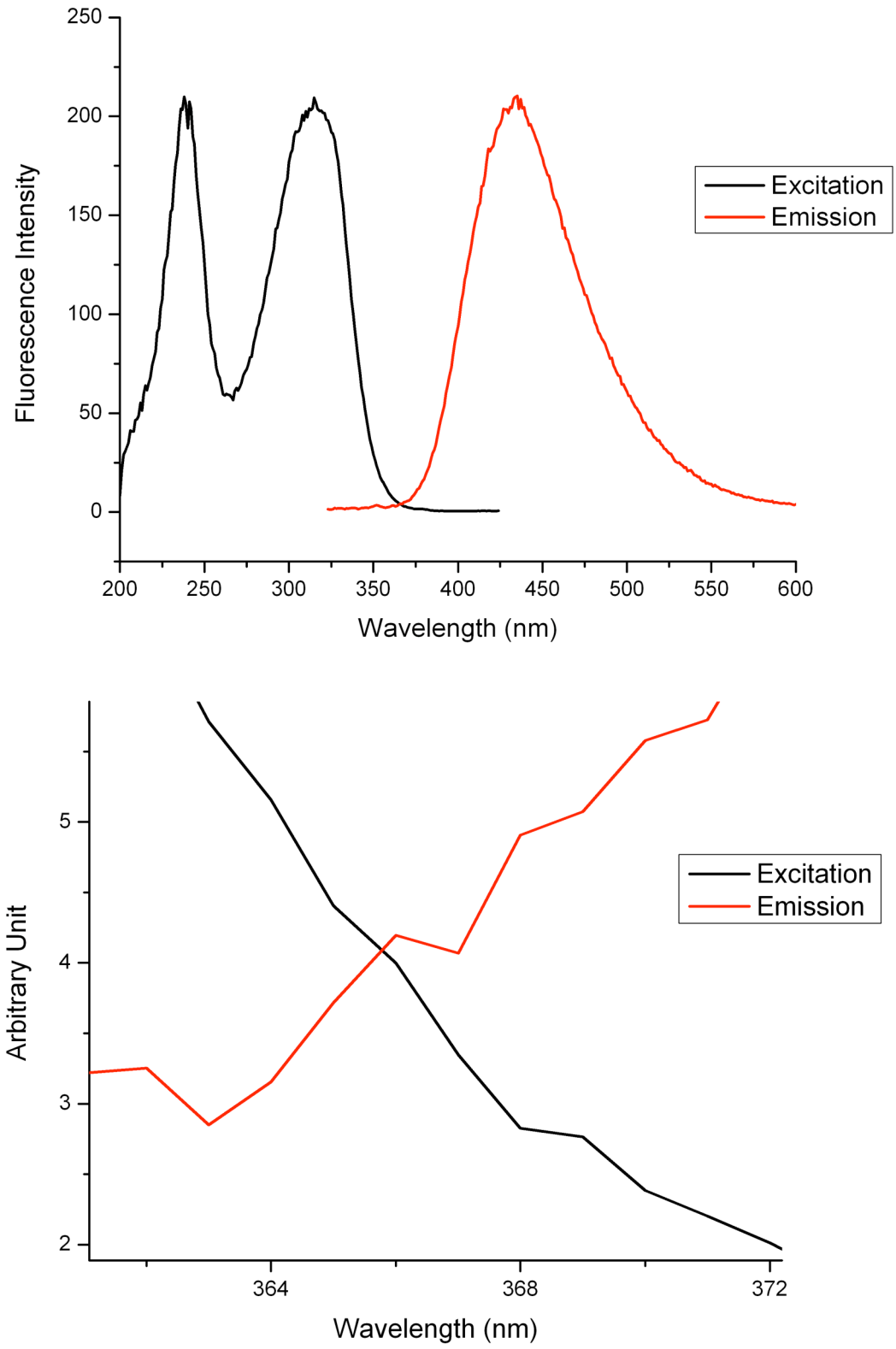

Figure A.5: Determination of E_{00} value for **6** in 100 mM NaCl, 10 mM sodium phosphate pH 7 buffer.

Appendix B
Supporting Information for Chapter 3

B.1 : Sample data analysis of gel electrophoresis of samples

Each lane in represents an individual time point in the photochemical assay. Each lane has a line width set to 12 pixels so that the entirety of the signal can be accurately integrated without overlap from the neighboring lanes

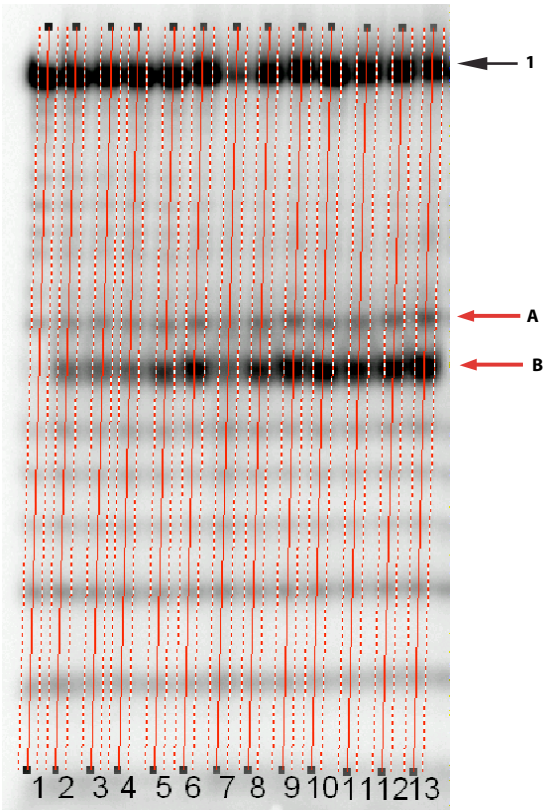

Figure B.1: Example autoradiograph of a 20 % denaturing polyacrylamide gel showing cleavage products of 5′-^{32}P double stranded DNA after photolysis. Lanes were integrated using a line width of 12 pixels. Red arrows (A and B) indicate photocleavage products, while the black arrow indicates starting material.

Analysis of data

Each lane represents a region to be converted into an area graph as shown in using the graph function of ImageQuant.

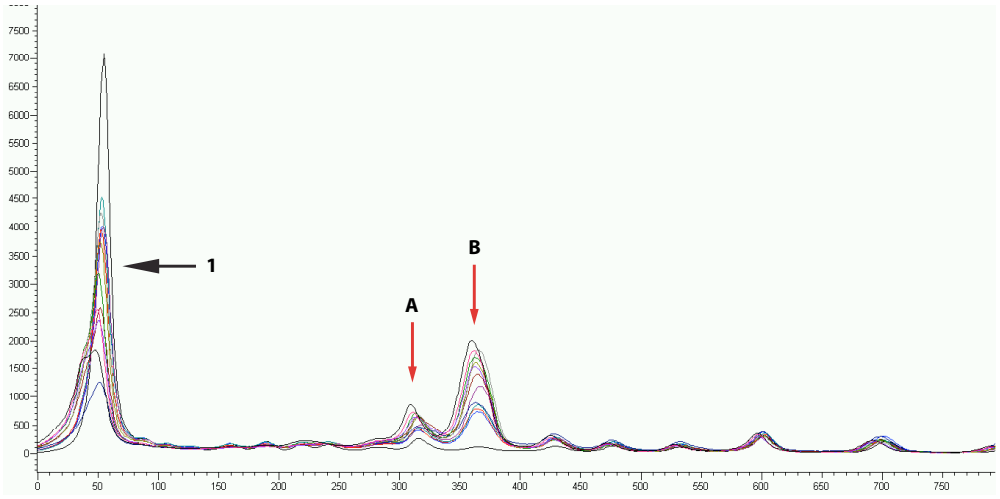

Figure B.2: Overlaid plot of integrated lanes 1-13. Red arrows A and B correspond to photoclevage bands, 1 represents full length DNA in Figure B.1

Using peak finder functionality of ImageQuant, individual peaks can be identified, and the area under each curve can be assigned. All peaks were correlated to the original gel in **Figure B.1** using the Maxam-Gilbert sequencing lane. Peak A and B were chosen for further analysis as they represent cleavage of **ODN2*** 5' to the ^{Br}U (Peak B) and cleavage at the ^{Br}U (Peak A). Once all the graphs had been accurately and completely integrated, an area report was generated yielding the information seen in Table B.1, which was transferred to MicroCal OriginPro v.7.5 for graphical analysis.

(Table B.1)

0 min hν				3.5 min hν			
Peak #	Area	Height	Percent Area	Peak #	Area	Height	Percent Area
1	133424	7064	94.78	1	82329	2551	62.85
A	5363	236	3.30	A	23517	620	13.69
B	3121	94	1.92	B	40280	1370	23.45
0.5 min hν				4.0 min hν			
Peak #	Area	Height	Percent Area	Peak #	Area	Height	Percent Area
1	109917	3995	81.20	1	103048	3168	65.73
A	10827	381	6.18	A	17019	687	8.63
B	22100	711	12.62	B	50535	1690	25.64

1.0 min hν			
Peak #	Area	Height	Percent Area
1	94087	3880	78.43
A	10262	385	6.81
B	22268	736	14.77

1.5 min hν			
Peak #	Area	Height	Percent Area
1	110033	4456	79.47
A	11152	402	6.41
B	24543	808	14.11

2.0 min hν			
Peak #	Area	Height	Percent Area
1	98644	3934	72.83
A	12164	465	7.28
B	33231	1139	19.89

2.5 min hν			
Peak #	Area	Height	Percent Area
1	110699	3724	69.20
A	15528	615	7.86
B	45309	1590	22.94

3.0 min hν			
Peak #	Area	Height	Percent Area
1	54096	1238	65.11
A	19675	450	13.83
B	29957	866	21.06

4.5 min hν			
Peak #	Area	Height	Percent Area
1	121438	4226	69.16
A	15240	642	7.08
B	51198	1818	23.77

5.0 min hν			
Peak #	Area	Height	Percent Area
1	80018	2305	62.87
A	15818	575	9.98
B	43050	1469	27.15

7.0 min hν			
Peak #	Area	Height	Percent Area
1	95503	2531	63.82
A	17744	700	9.21
B	51964	1807	26.97

10.0 min hν			
Peak #	Area	Height	Percent Area
1	88925	1823	59.67
A	21032	829	10.48
B	59896	1982	29.85

Table B.1: Area report generated by ImageQuant once graph in **Figure B.2** had been integrated.

B.2 Initial rate fits of compounds 2-6 under anaerobic conditions

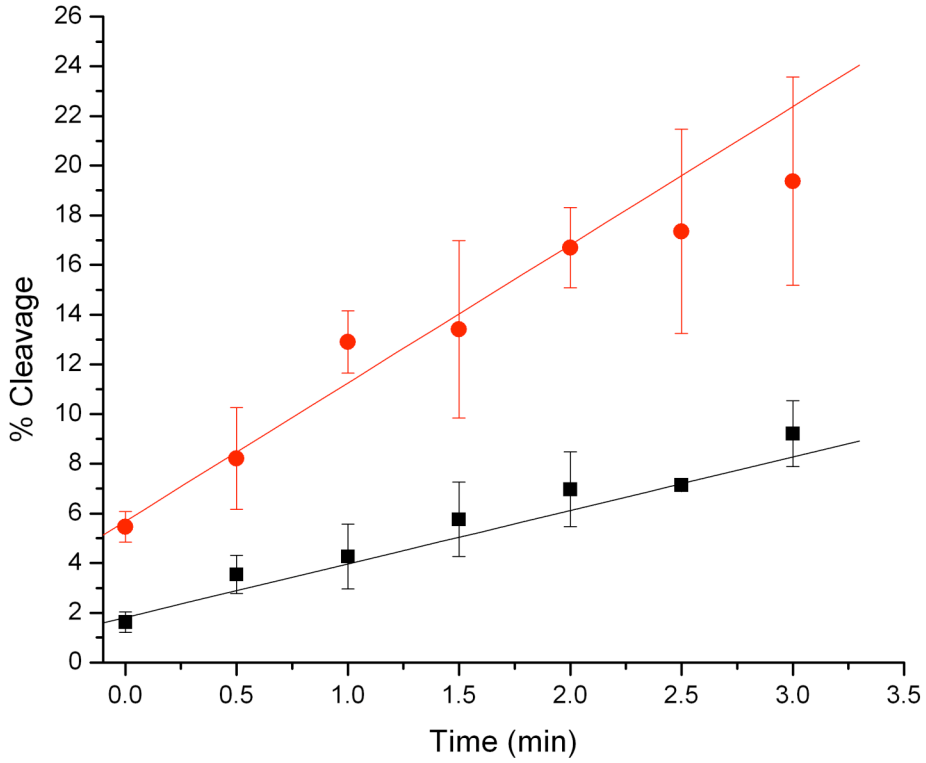

Figure B.3: Initial rate of strand scission induced by EET for **ODN1** (1.5 μM) and **2** (1 mM) under anaerobic conditions in 100 NaCl, 10 mM sodium phosphate buffer. Red=5'-T strand scission, black=scission at ^{Br}U. Lines represent linear fitting using Origin 7.5. Points represent average of two runs, error bars represent range of measurements.

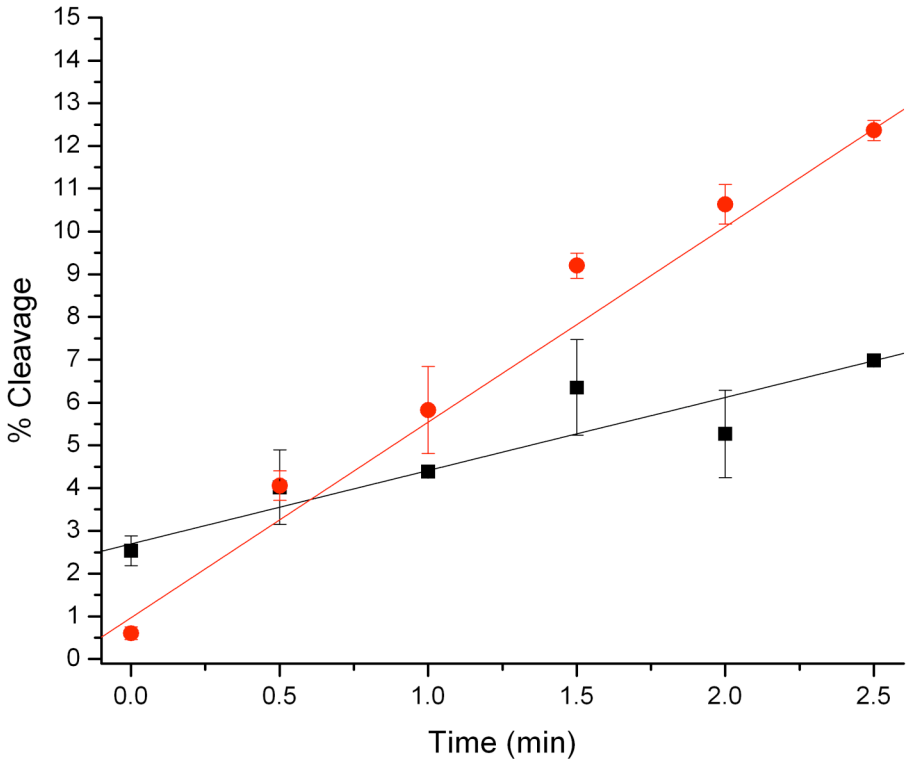

Figure B.4: Initial rate of strand scission induced by EET for **ODN1** (1.5 μM) and **3** (1 mM) under anaerobic conditions in 100 NaCl, 10 mM sodium phosphate buffer. Red=5'-T strand scission, black=scission at ^{Br}U. Lines represent linear fitting using Origin 7.5. Points represent average of two runs, error bars represent range of measurements.

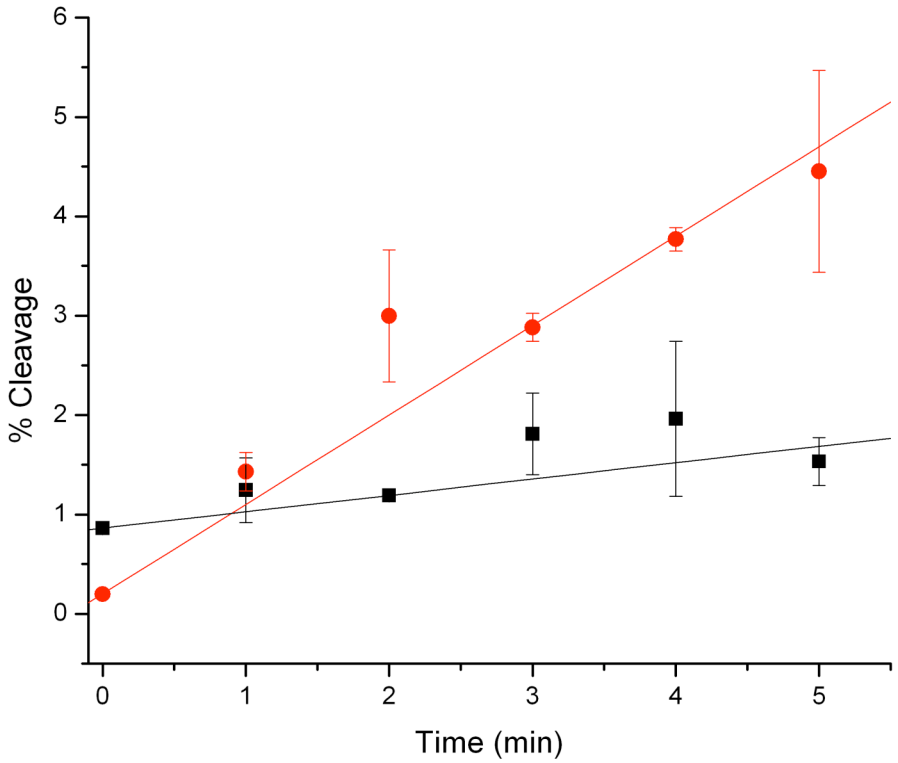

Figure B.5: Initial rate of strand scission induced by EET for **ODN1** (1.5 μM) and **4** (1 mM) under anaerobic conditions in 100 NaCl, 10 mM sodium phosphate buffer. Red=5'-T strand scission, black=scission at ^{Br}U. Lines represent linear fitting using Origin 7.5. Points represent average of two runs, error bars represent range of measurements.

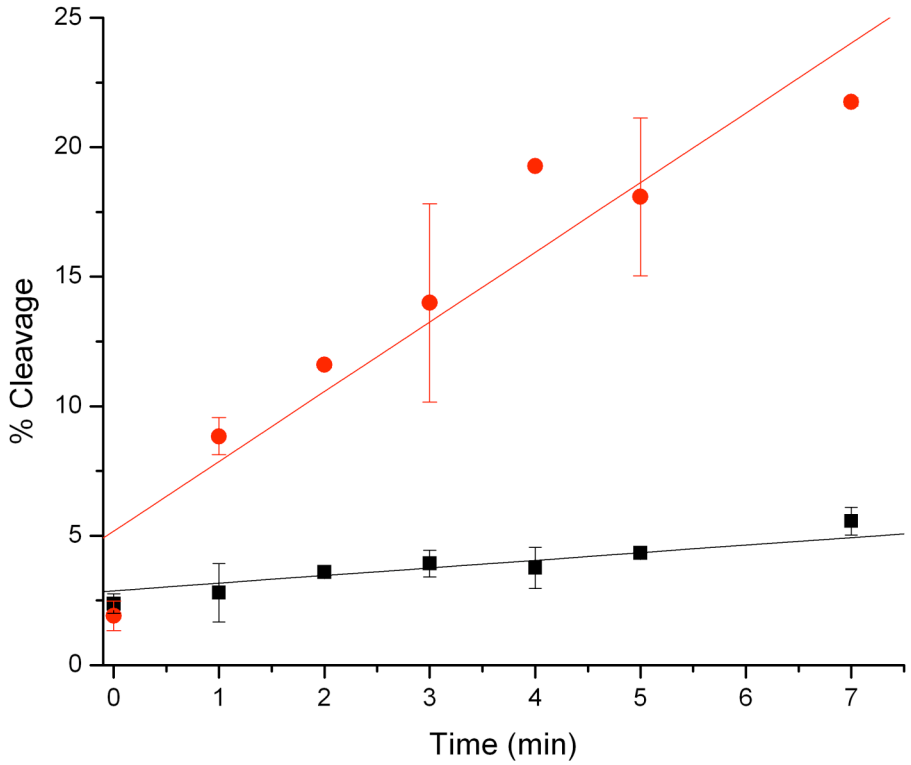

Figure B.6: Initial rate of strand scission induced by EET for **ODN1** (1.5 μM) and **5** (1 mM) under anaerobic conditions in 100 NaCl, 10 mM sodium phosphate buffer. Red=5'-T strand scission, black=scission at ^{Br}U. Lines represent linear fitting using Origin 7.5. Points represent average of two runs, error bars represent range of measurements.

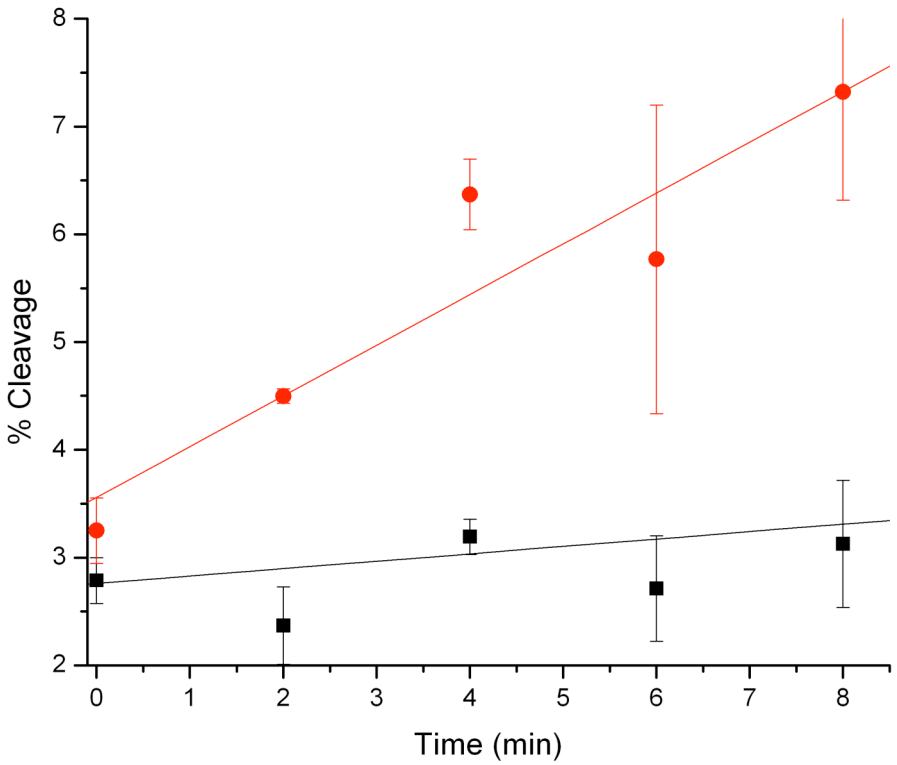

Figure B.7: Initial rate of strand scission induced by EET for **ODN1** (1.5 μM) and **6** (1 mM) under anaerobic conditions in 100 NaCl, 10 mM sodium phosphate buffer. Red=5'-T strand scission, black=scission at ^{Br}U. Lines represent linear fitting using Origin 7.5. Points represent average of two runs, error bars represent range of measurements.

B.3 Fluorescence decay scans of compounds 2-6

All fluorescence decay scans were measured using Hitachi F-4500 spectophotometer with excitation slit width set at 10 nm and emission slit width set at 10 nm. The overlayed spectra represent 10 sucessive scans on the same sample at a scan rate of 240 nm/minute.

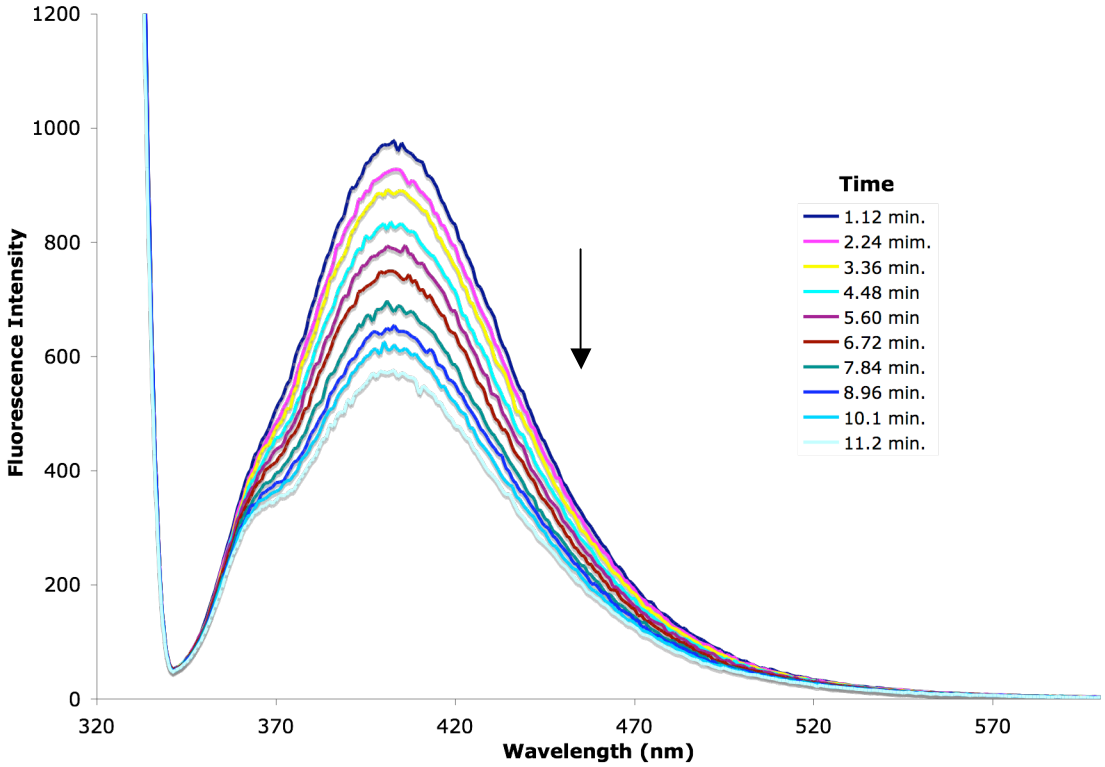

Figure B.8: Fluorescence emission decay scans of 100 nM solution of **1** in 100 mM NaCl, 10 mM sodium phosphate pH 7. Excitation wavelength= 323 nm, emission wavelength = 404 nm, excitation slit width =10 nm, emission slit width = 10 nm.

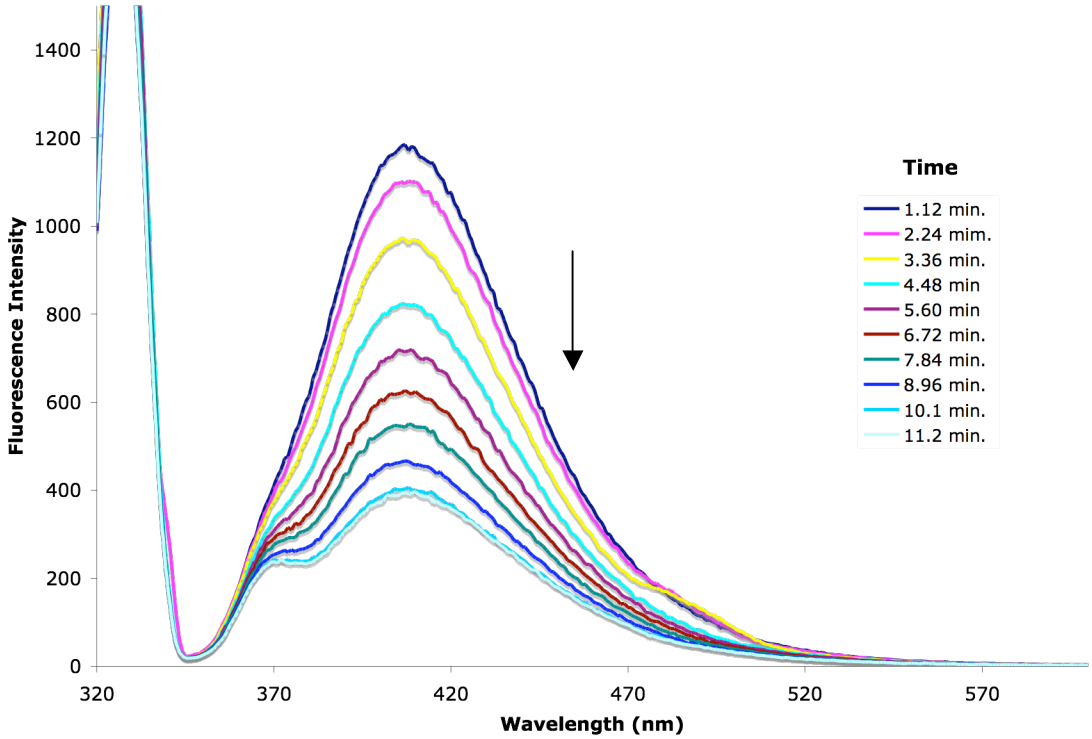

Figure B.9: Emission decay scans of 100 nM solution of **2** in 100 mM NaCl, 10 mM sodium phosphate pH 7. Excitation wavelength= 327 nm, emission wavelength = 409 nm, excitation slit width =10 nm, emission slit width = 10 nm.

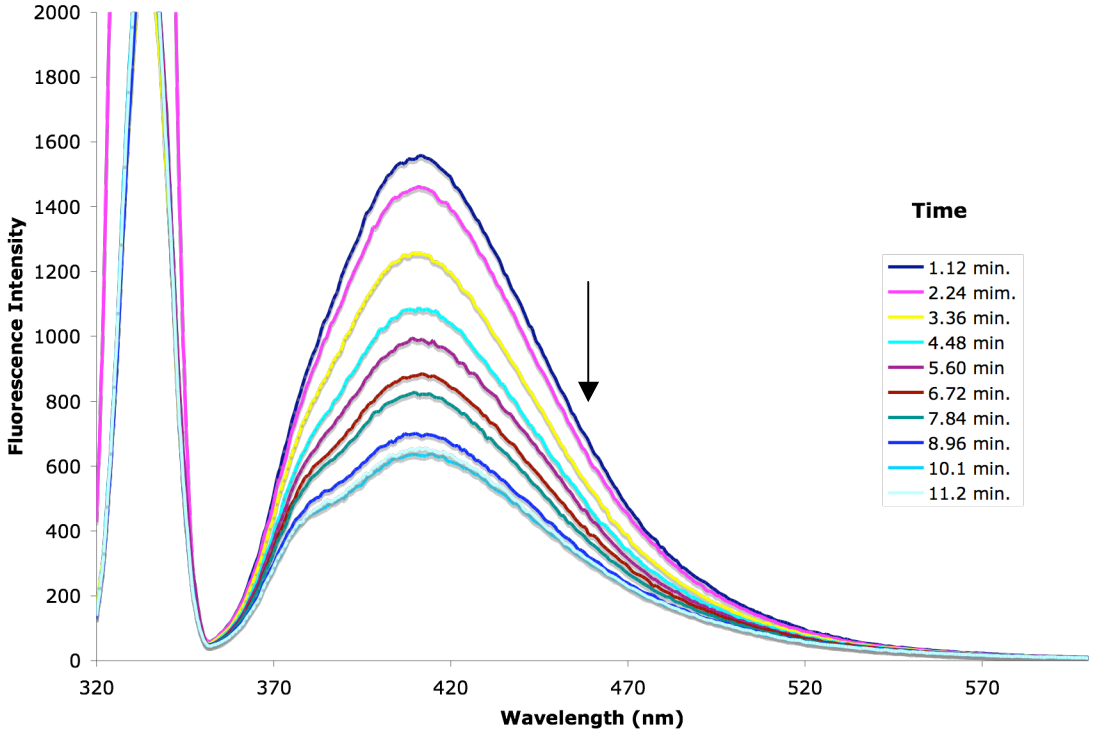

Figure B.10: Emission decay scans of 100 nM solution of **3** in 100 mM NaCl, 10 mM sodium phosphate pH 7. Excitation wavelength= 334 nm, emission wavelength = 414 nm, excitation slit width =10 nm, emission slit width = 10 nm

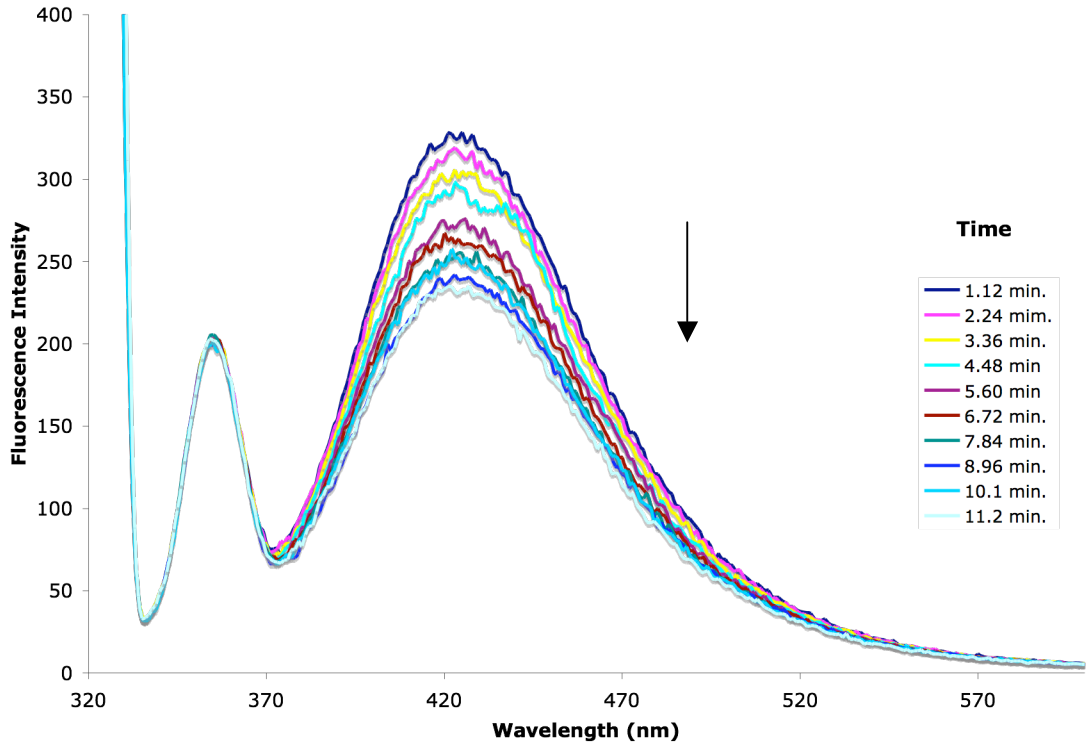

Figure B.11: Emission decay scans of 100 nM solution of **4** in 100 mM NaCl, 10 mM sodium phosphate pH 7. Excitation wavelength= 317 nm, emission wavelength = 427 nm, excitation slit width =10 nm, emission slit width = 10 nm

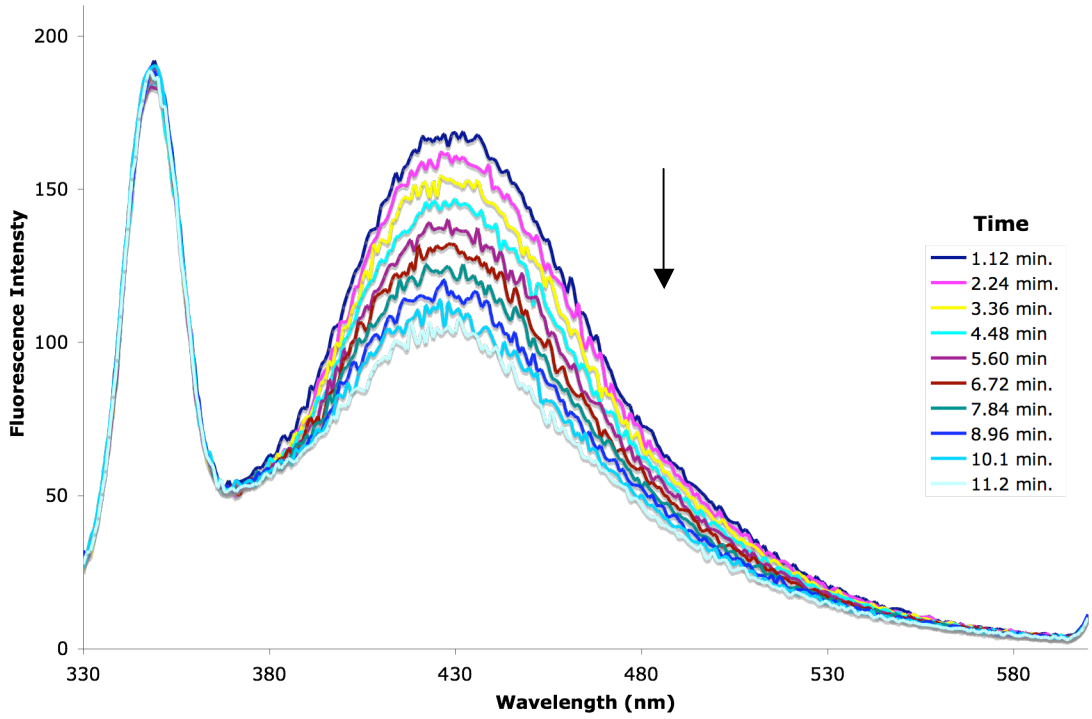

Figure B.12: Emission decay scans of 100 nM solution of **5** in 100 mM NaCl, 10 mM sodium phosphate pH 7. Excitation wavelength= 327 nm, emission wavelength = 429 nm, excitation slit width =10 nm, emission slit width = 10 nm

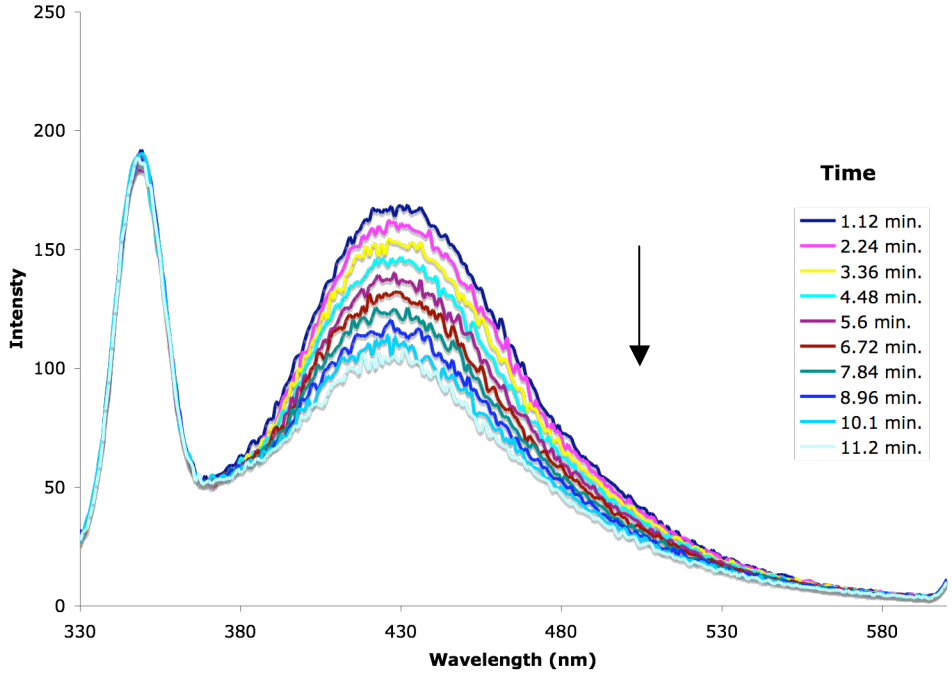

Figure B.13: Emission decay scans of 100 nM solution of **6** in 100 mM NaCl, 10 mM sodium phosphate pH 7. Excitation wavelength= 312 nm, emission wavelength = 433 nm, excitation slit width =10 nm, emission slit width = 10 nm

References

(1) Dahm, R. Friedrich Miescher and the discovery of DNA. *Dev. Biol.* **2005**, *278*, 274-288.

(2) Levene, P. A. The structure of yeast nucleic acid. IV. Ammonia hydrolysis. *J. Biol. Chem.* **2002**, *277*, e1/1-e1/2.

(3) Watson, J. D.; Crick, F. H. C. Molecular structure of nucleic acids. A structure for deoxyribose nucleic acid. *Nature* **1953**, *171*, 737-8.

(4) Grib, N. V.; Berashevich, J. A.; Borisenko, V. E. The Role of Structural Reorganization in Charge Carrier Transfer in a DNA Molecule. *Molecular Biophysics* **2006**, *52*, 537-544.

(5) Teo, Y. N.; Kool, E. T. Studies of oligodeoxyfluorosides (ODFs) as FRET probes for DNA hybridization. *Nucleic Acids Symp. Ser.* **2008**, 233-234.

(6) Wilson, J. N.; Cho, Y.; Tan, S.; Cuppoletti, A.; Kool, E. T. Quenching of fluorescent nucleobases by neighboring DNA: the "insulator" concept. *ChemBioChem* **2008**, *9*, 279-285.

(7) Claus, L.; Vortler, S.; Eckstein, F. Phosphorothioate modification of RNA for stereochemical and interference analyses. *Methods Enzymol.* **2000**, *317*, 74-91.

(8) Eckstein, F. Phosphorothioate oligodeoxynucleotides: what is their origin and what is unique about them? *Antisense Nucleic Acid Drug Dev.* **2000**, *10*, 117-121.

(9) Nielsen, P. E.; Egholm, M.; Berg, R. H.; Buchardt, O. Sequence-selective recognition of DNA by strand displacement with a thymine-substituted polyamide. *Science* **1991**, *254*, 1497-500.

(10) Koshkin, A. A.; Nielsen, P.; Meldgaard, M.; Rajwanshi, V. K.; Singh, S. K.; Wengel, J. LNA (Locked Nucleic Acid): An RNA Mimic Forming Exceedingly Stable LNA:LNA Duplexes. *J. Am. Chem. Soc.* **1998**, *120*, 13252-13253.

(11) Kumar, R.; Singh, S. K.; Koshkin, A. A.; Rajwanshi, V. K.; Meldgaard, M.; Wengel, J. The first analogs of LNA (locked nucleic acids): phosphorothioate-LNA and 2'-thio-LNA. *Bioorg. Med. Chem. Lett.* **1998**, *8*, 2219-2222.

(12) Koshkin, A. A.; Rajwanshi, V. K.; Wengel, J. Novel convenient syntheses of LNA [2.2.1]bicyclo nucleosides. *Tetrahedron Lett.* **1998**, *39*, 4381-4384.

(13) Steffens, R.; Leumann, C. J. Tricyclo-DNA: A Phosphodiester-Backbone Based DNA Analog Exhibiting Strong Complementary Base-Pairing Properties. *J. Am. Chem. Soc.* **1997**, *119*, 11548-11549.

(14) Eley, D. D.; Spivey, D. I. Semiconductivity of organic substances. IX. Nucleic acid in the dry state. *Transactions of the Faraday Society* **1962**, *58*, 411-15.

(15) Davis, W. B.; Ratner, M. A.; Wasielewski, M. R. Conformational Gating of Long Distance Electron Transfer through Wire-like Bridges in Donor-Bridge-Acceptor Molecules. *J. Am. Chem. Soc.* **2001**, *123*, 7877-7886.

(16) Berlin, Y. A.; Burin, A. L.; Ratner, M. A. Charge Hopping in DNA. *J. Am. Chem. Soc.* **2001**, *123*, 260-268.

(17) Turro, N. J.; Barton, J. K. Paradigms, supermolecules, electron transfer and chemistry at a distance. What's the problem? The science or the paradigm? *J. Biol. Inorg. Chem.* **1998**, *3*, 201-209.

(18) Porath, D.; Cuniberti, G.; di Felice, R. Charge transport in DNA-based devices. *Top. Curr. Chem.* **2004**, *237*, 183-227.

(19) Drummond, T. G.; Hill, M. G.; Barton, J. K. Electrochemical DNA sensors. *Nat. Biotechnol.* **2003**, *21*, 1192-1199.

(20) Debije, M. G.; Milano, M. T.; Bernhard, W. A. DNA responds to ionizing radiation as an insulator, not as a "molecular wire". *Angew. Chem., Int. Ed.* **1999**, *38*, 2752-2756.

(21) Fink, H. W. DNA and conducting electrons. *Cell. Mol. Life Sci.* **2001**, *58*, 1-3.

(22) Wagenknecht, H.-A. *Charge transfer in DNA : From mechanism to application*; Wiley: Weinheim, 2005, pgs. 4-26

(23) Murphy, C. J.; Arkin, M. R.; Jenkins, Y.; Ghatlia, N. D.; Bossmann, S. H.; Turro, N. J.; Barton, J. K. Long-range photoinduced electron transfer through a DNA helix. *Science* **1993**, *262*, 1025-9.

(24) Lewis, F. D.; Wu, Y.; Zhang, L.; Zuo, X.; Hayes, R. T.; Wasielewski, M. R. DNA-Mediated Exciton Coupling and Electron Transfer between Donor and Acceptor Stilbenes Separated by a Variable Number of Base Pairs. *J. Am. Chem. Soc.* **2004**, *126*, 8206-8215.

(25) Schuster, G. B. Long-Range Charge Transfer in DNA: Transient Structural Distortions Control the Distance Dependence. *Acc. Chem. Res.* **2000**, *33*, 253-260.

(26) Lewis, F. D.; Kalgutkar, R. S.; Wu, Y.; Liu, X.; Liu, J.; Hayes, R. T.; Miller, S. E.; Wasielewski, M. R. Driving Force Dependence of Electron Transfer Dynamics in Synthetic DNA Hairpins. *J. Am. Chem. Soc.* **2000**, *122*, 12346-12351.

(27) Schuster, G. B. Long-range charge transfer in DNA: transient structural distortions control the distance dependence. *Acc. Chem. Res.* **2000**, *33*, 253-60.

(28) Lewis Frederick, D.; Zhu, H.; Daublain, P.; Fiebig, T.; Raytchev, M.; Wang, Q.; Shafirovich, V. Crossover from superexchange to hopping as the mechanism for photoinduced charge transfer in DNA hairpin conjugates. *J. Am. Chem. Soc.* **2006**, *128*, 791-800.

(29) Bixon, M.; Giese, B.; Wessely, S.; Langenbacher, T.; Michel-Beyerle, M. E.; Jortner, J. Long-range charge hopping in DNA. *Proc. Natl. Acad. Sci. U. S. A.* **1999**, *96*, 11713-11716.

(30) Jortner, J.; Bixon, M.; Voityuk, A. A.; Roesch, N. Superexchange Mediated Charge Hopping in DNA. *J. Phys. Chem. A* **2002**, *106*, 7599-7606.

(31) Conwell, E. M.; Bloch, S. M.; McLaughlin, P. M.; Basko, D. M. Duplex Polarons in DNA. *J. Am. Chem. Soc.* **2007**, *129*, 9175-9181.

(32) Conwell, E. M.; Basko, D. M. Polarons and conduction in DNA. *Synth. Met.* **2003**, *137*, 1381-1383.

(33) Liu, C.-S.; Schuster Gary, B. Base sequence effects in radical cation migration in duplex DNA: support for the polaron-like hopping model. *J. Am. Chem. Soc.* **2003**, *125*, 6098-102.

(34) Lewis Frederick, D. DNA molecular photonics. *Photochem. Photobiol.* **2005**, *81*, 65-72.

(35) Lewis, F. D.; Letsinger, R. L.; Wasielewski, M. R. Dynamics of Photoinduced Charge Transfer and Hole Transport in Synthetic DNA Hairpins. *Acc. Chem. Res.* **2001**, *34*, 159-170.

(36) Boon, E. M.; Barton, J. K. Charge transport in DNA. *Curr. Opin. Struct. Biol.* **2002**, *12*, 320-329.

(37) Henderson, P. T.; Jones, D.; Hampikian, G.; Kan, Y.; Schuster, G. B. Long-distance charge transport in duplex DNA: the phonon-assisted polaron-like hopping mechanism. *Proc. Natl. Acad. Sci. U. S. A.* **1999**, *96*, 8353-8358.

(38) Ly, D.; Sanii, L.; Schuster, G. B. Mechanism of Charge Transport in DNA: Internally-Linked Anthraquinone Conjugates Support Phonon-Assisted Polaron Hopping. *J. Am. Chem. Soc.* **1999**, *121*, 9400-9410.

(39) Nunez, M. E.; Hall, D. B.; Barton, J. K. Long-range oxidative damage to DNA: effects of distance and sequence. *Chem. Biol.* **1999**, *6*, 85-97.

(40) Giese, B. Long-distance electron transfer through DNA. *Annu. Rev. Biochem.* **2002**, *71*, 51-70.

(41) Crespo-Hernandez Carlos, E.; Close David, M.; Gorb, L.; Leszczynski, J. Determination of redox potentials for the Watson-Crick base pairs, DNA nucleosides, and relevant nucleoside analogues. *The Journal of Physical Chemistry B* **2007**, *111*, 5386-95.

(42) Amann, N.; Pandurski, E.; Fiebig, T.; Wagenknecht, H.-A. Electron injection into DNA: Synthesis and spectroscopic properties of pyrenyl-modified oligonucleotides. *Chem.--Eur. J.* **2002**, *8*, 4877-4883.

(43) Ito, T.; Rokita, S. E. Criteria for efficient transport of excess electrons in DNA. *Angew. Chem. Int. Ed.* **2004**, *43*, 1839-18423.

(44) Behrens, C.; Carell, T. Excess electron transfer in flavin-capped, thymine dimer-containing DNA hairpins. *Chemical Communications* **2003**, 1632-1633.

(45) Lewis, F. D.; Liu, X.; Miller, S. E.; Hayes, R. T.; Wasielewski, M. R. Dynamics of Electron Injection in DNA Hairpins. *J. Am. Chem. Soc.* **2002**, *124*, 11280-11281.

(46) Lewis, F. D.; Liu, X.; Wu, Y.; Miller, S. E.; Wasielewski, M. R.; Letsinger, R. L.; Sanishvili, R.; Joachimiak, A.; Tereshko, V.; Egli, M. Structure and Photoinduced Electron Transfer in Exceptionally Stable Synthetic DNA Hairpins with Stilbenediether Linkers. *J. Am. Chem. Soc.* **1999**, *121*, 9905-9906.

(47) Ito, T.; Rokita, S. E. Excess Electron Transfer from an Internally Conjugated Aromatic Amine to 5-Bromo-2'-deoxyuridine in DNA. *J. Am. Chem. Soc.* **2003**, *125*, 11480-11481.

(48) Ito, T.; Rokita, S. E. Reductive Electron Injection into Duplex DNA by Aromatic Amines. *J. Am. Chem. Soc.* **2004**, *126*, 15552-15559.

(49) Behrens, C.; Burgdorf, L. T.; Schwogler, A.; Carell, T. Weak distance dependence of excess electron transfer in DNA. *Angew. Chem., Int. Ed.* **2002**, *41*, 1763-1766.

(50) Wagenknecht, H.-A. *Charge transfer in DNA : From mechanism to application*; Wiley: Weinheim, 2005, 197-224.

(51) Haas, C.; Kraeling, K.; Cichon, M.; Rahe, N.; Carell, T. Excess electron transfer driven DNA repair does not depend on the transfer direction. [Erratum to document cited in CA141:049160]. *Angew. Chem., Int. Ed.* **2004**, *43*, 2321.

(52) Zweig, A.; Maurer, A. H.; Roberts, B. G. Oxidation, reduction, and electrochemiluminescence of donor-substituted polycyclic aromatic hydrocarbons. *J. Org. Chem.* **1967**, *32*, 1322-9.

(53) Marcus, R. A.; Sutin, N. Electron transfers in chemistry and biology. *Biochim. Biophys. Acta* **1985**, *811*, 265-322.

(54) Hartwig, J. F. Carbon-Heteroatom Bond-Forming Reductive Eliminations of Amines, Ethers, and Sulfides. *Acc. Chem. Res.* **1998**, *31*, 852-860.

(55) Surry, D. S.; Buchwald, S. L. Biaryl phosphane ligands in palladium-catalyzed amination. *Angew. Chem., Int. Ed.* **2008**, *47*, 6338-6361.

(56) Gao, X.; Zhang, Y.; Wang, B. Naphthalene-based water-soluble fluorescent boronic acid isomers suitable for ratiometric and off-on sensing of saccharides at physiological pH. *New J. Chem.* **2005**, *29*, 579-586.

(57) Lee, S. J.; Terrazas, M. S.; Pippel, D. J.; Beak, P. Mechanism of electrophilic chlorination: experimental determination of a geometrical requirement for chlorine transfer by the endocyclic restriction test. *J. Am. Chem. Soc.* **2003**, *125*, 7307-7312.

(58) Urgaonkar, S.; Nagarajan, M.; Verkade, J. G. P(i-BuNCH2CH2)3N: an effective ligand in the palladium-catalyzed amination of aryl bromides and iodides. [Erratum to document cited in CA138:187441]. *J. Org. Chem.* **2004**, *69*, 9323.

(59) Wolfe, J. P.; Buchwald, S. L. Scope and limitations of the Pd/BINAP-catalyzed amination of aryl bromides. *J. Org. Chem.* **2000**, *65*, 1144-1157.

(60) Johnson, T. W.; Corey, E. J. Enantiospecific Synthesis of the Proposed Structure of the Antitubercular Marine Diterpenoid Pseudopteroxazole: Revision of Stereochemistry. *J. Am. Chem. Soc.* **2001**, *123*, 4475-4479.

(61) Mendenhall, G. D.; Smith, P. A. S. 2-Nitrocarbazole. (Carbazole, 2-nitro-). *Org. Synth.* **1966**, *46*, 85-9.

(62) Gowda, D. C.; Gowda, S. Formic acid with 10% palladium on carbon: a reagent for selective reduction of aromatic nitro compounds. *Indian J. Chem., Sect. B: Org. Chem. Incl. Med. Chem.* **2000**, *39B*, 709-711.

(63) Cakmak, O.; Demirtas, I.; Balaydin, H. T. Selective bromination of 1-bromonaphthalene: efficient synthesis of bromonaphthalene derivatives. *Tetrahedron* **2002**, *58*, 5603-5609.

(64) Chambers, R. R., Jr.; Collins, C. J.; Maxwell, B. E. Reductive debenzylation of 1-benzylnaphthalene by a sodium-potassium alloy. *J. Org. Chem.* **1985**, *50*, 4960-3.

(65) Rodriguez, J. G.; Tejedor, J. L. Carbon Networks Based on 1,5-Naphthalene Units. Synthesis of 1,5-Naphthalene Nanostructures with Extended p-Conjugation. *J. Org. Chem.* **2002**, *67*, 7631-7640.

(66) Wolfe, J. P.; Wagaw, S.; Marcoux, J.-F.; Buchwald, S. L. Rational Development of Practical Catalysts for Aromatic Carbon-Nitrogen Bond Formation. *Acc. Chem. Res.* **1998**, *31*, 805-818.

(67) Wu, X.; Schmidt, R. R. Solid-phase synthesis of complex oligosaccharides using azidoglucose as a glycosyl acceptor. *Eur. J. Org. Chem.* **2004**, 2826-2832.

(68) Lee, H.-S.; Park, J.-S.; Kim, B. M.; Gellman, S. H. Efficient Synthesis of Enantiomerically Pure b2-Amino Acids via Chiral Isoxazolidinones. *J. Org. Chem.* **2003**, *68*, 1575-1578.

(69) Danner, P.; Bauer, M.; Phukan, P.; Maier, M. E. Total synthesis of cryptophycin 3. *Eur. J. Org. Chem.* **2005**, 317-325.

(70) Chinchilla, R.; Dodsworth, D. J.; Najera, C.; Soriano, J. M. 2,7-di-tert-butyl-Fmoc-P-OSu: a new polymer-supported reagent for the protection of the amino group. *Bioorg. Med. Chem. Lett.* **2002**, *12*, 1817-1820.

(71) Chen, Q.; Sowa, D. A.; Gabathuler, R. Synthesis of Doxorubicin Conjugates Through 14-Hydroxy Group to Melanotransferrin P97. *Synth. Commun.* **2003**, *33*, 2391-2400.

(72) Carpino, L. A.; Han, G. Y. 9-Fluorenylmethoxycarbonyl amino-protecting group. *J. Org. Chem.* **1972**, *37*, 3404-9.

(73) Li, F.; Sarkhel, S.; Wilds, C. J.; Wawrzak, Z.; Prakash, T. P.; Manoharan, O. M.; Egli, M. 2'-Fluoroarabino- and Arabinonucleic Acid Show Different Conformations, Resulting in Deviating RNA Affinities and Processing of Their Heteroduplexes with RNA by RNase H. *Biochemistry* **2006**, *45*, 4141-4152.

(74) Gannett, P. M.; Johnson, E. M., II; Grimes, M. A.; Myers, A. L.; Deavers, R. E., III; Tracy, T. S. Synthesis of deuterated 4,4'-diaminodiphenylsulfone (Dapsone) and related analogs. *J. Labelled Compd. Radiopharm.* **2003**, *46*, 107-114.

(75) Sorokin, V. I.; Ozeryanskii, V. A.; Pozharskii, A. F. A simple and effective procedure for the N-permethylation of amino-substituted naphthalenes. *Eur. J. Org. Chem.* **2003**, 496-498.

(76) Keith, D. D.; Tortora, J. A.; Yang, R. Synthesis of L-2-amino-4-methoxy-trans-but-3-enoic acid. *J. Org. Chem.* **1978**, *43*, 3711-13.

(77) Dilbeck, G. A.; Field, L.; Gallo, A. A.; Gargiulo, R. J. Biologically oriented organic sulfur chemistry. 19. Synthesis and properties of 2-amino-5-mercapto-5-methylhexanoic acid, a bishomolog of penicillamine. Use of boron trifluoride

etherate for catalyzing Markovnikov addition of a thiol to an olefin. *J. Org. Chem.* **1978**, *43*, 4593-6.

(78) Birks, J. B. *Photophysics of Aromatic Molecules*; Wiley-Interscience: London, 1970, 85-87

(79) Yousef, U. S.; Abdel-Azzem, M. A cyclic voltammetric and coulometric study of a modified electrode prepared by electrooxidative polymerization of nickel complex of 1,5-diaminonaphthalene in acetonitrile. *Pol. J. Chem.* **1998**, *72*, 2583-2597.

(80) Abdel-Azzem, M.; Yousef, U. S.; Pierre, G. A cyclic voltammetric and coulometric study of a modified electrode prepared by electrooxidative polymerization of 1,5-diaminonaphthalene in aqueous acidic medium. *Eur. Polym. J.* **1998**, *34*, 819-826.

(81) Abdel Azzem, M. Electrooxidative oligomerization of 1,5-diaminonaphthalene in acetonitrile medium. *J. Electroanal. Chem.* **1996**, *417*, 163-173.

(82) Finch, A. S., University of Maryland at College Park, 2008.

(83) Grigg, G. W. Selective breakage of DNA alongside 5-bromodeoxyuridine nucleotide residues by high temperature hydrolysis. *Nucleic Acids Res.* **1977**, *4*, 969-87.

(84) Cook, G. P.; Chen, T.; Koppisch, A. T.; Greenberg, M. M. The effects of secondary structure and O2 on the formation of direct strand breaks upon irradiation of 5-bromodeoxy-uridine-containing oligonucleotides. *Chemistry and Biology* **1999**, *6*, 451-459.

(85) Cook, G. P.; Greenberg, M. M. A Novel Mechanism for the Formation of Direct Strand Breaks upon Anaerobic Photolysis of Duplex DNA Containing 5-Bromodeoxyuridine. *J. Am. Chem. Soc.* **1996**, *118*, 10025-10030.

(86) Grigg, G. W. Selective breakage of DNA alongside 5-bromodeoxyuridine nucleotide residues by high temperature hydrolysis. *Nucleic Acids Res. FIELD Full Journal Title:Nucleic Acids Research* **1977**, *4*, 969-87.

(87) Ren, J.; Chaires, J. B. Rapid Screening of Structurally Selective Ligand Binding to Nucleic Acids. *Mehtods in Enzymology* **2001**, *340*, 99-108.

(88) Hey, T.; Lipps, G.; Krauss, G. Binding of XPA and RPA to Damaged DNA Investigated by Fluorescence Anisotropy. *Biochemistry* **2001**, *40*, 2901-2910.

(89) Callaway, K.; Rainey Mark, A.; Dalby Kevin, N. Quantifying ERK2-protein interactions by fluorescence anisotropy: PEA-15 inhibits ERK2 by blocking the binding of DEJL domains. *Biochim. Biophys. Acta* **2005**, *1754*, 316-23.

(90) Lee, N.; Gorelick Robert, J.; Musier-Forsyth, K. Zinc finger-dependent HIV-1 nucleocapsid protein-TAR RNA interactions. *Nucleic Acids Res.* **2003**, *31*, 4847-55.

(91) Bahr, M.; Valis, L.; Wagenknecht, H.-A.; Weinhold, E. DNA Labeling Topologies for Monitoring DNA-Protein Complex Formation by Fluorescence Anisotropy. *Nucleosides, Nucleotides Nucleic Acids* **2007**, *26*, 1581-1584.

(92) Wybranowski, T.; Cyrankiewicz, M.; Ziomkowska, B.; Kruszewski, S. The HSA affinity of warfarin and flurbiprofen determined by fluorescence anisotropy measurements of camptothecin. *BioSystems* **2008**, *94*, 258-262.

(93) Sarkar, D.; Das, P.; Basak, S.; Chattopadhyay, N. Binding Interaction of Cationic Phenazinium Dyes with Calf Thymus DNA: A Comparative Study. *J. Phys. Chem. B* **2008**, *112*, 9243-9249.

(94) Qi, Z.-d.; Zhang, Y.; Liao, F.-l.; Ou-Yang, Y.-w.; Liu, Y.; Yang, X. Probing the binding of morin to human serum albumin by optical spectroscopy. *J. Pharm. Biomed. Anal.* **2008**, *46*, 699-706.

(95) Ingersoll, C. M.; Strollo, C. M. Steady-state fluorescence anisotropy to investigate flavonoids binding to proteins. *J. Chem. Educ.* **2007**, *84*, 1313-1315.

(96) Ausebel, F. M.; Brent, R.; Kingston, R. E.; Moore, D. D.; Seidman, J. G. *Short Protocols in Molecular Biology*; 5th ed.; Wiley: New York, 2002,